
THE DISTRIBUTED SPACECRAFT ATTITUDE CONTROL SYSTEM SIMULATOR: FROM DESIGN CONCEPT TO DECENTRALIZED CONTROL

Jana L. Schwartz

Dissertation submitted to the Faculty of the
Virginia Polytechnic Institute and State University
in partial fulfillment of the requirements for the degree of

Doctor of Philosophy
in
Aerospace Engineering

Dr. Christopher D. Hall, Committee Chair
Dr. Mary E. Kasarda, Committee Member
Dr. Hanspeter Schaub, Committee Member
Dr. Daniel J. Stilwell, Committee Member
Dr. Craig A. Woolsey, Committee Member

July 7, 2004
Blacksburg, Virginia

Keywords: Air Bearing Table, Spacecraft Simulator,
Formation Flying, Attitude Estimation, Parameter Estimation

©2004, Jana L. Schwartz

THE DISTRIBUTED SPACECRAFT ATTITUDE CONTROL SYSTEM SIMULATOR: FROM DESIGN CONCEPT TO DECENTRALIZED CONTROL

Jana L. Schwartz

(ABSTRACT)

A spacecraft formation possesses several benefits over a single-satellite mission. However, launching a fleet of satellites is a high-cost, high-risk venture. One way to mitigate much of this risk is to demonstrate hardware and algorithm performance in ground-based testbeds. It is typically difficult to experimentally replicate satellite dynamics in an Earth-bound laboratory because of the influences of gravity and friction. An air bearing provides a very low-torque environment for experimentation, thereby recapturing the freedom of the space environment as effectively as possible. Depending upon configuration, air-bearing systems provide some combination of translational and rotational freedom; the three degrees of rotational freedom provided by a spherical air bearing are ideal for investigation of spacecraft attitude dynamics and control problems.

An interest in experimental demonstration of formation flying led directly to the development of the Distributed Spacecraft Attitude Control System Simulator (DSACSS). The DSACSS is a unique facility, as it uses two air-bearing platforms working in concert. Thus DSACSS provides a pair of ‘spacecraft’ three degrees of attitude freedom each. Through use of the DSACSS we are able to replicate the relative attitude dynamics between nodes of a formation such as might be required for co-observation of a terrestrial target.

Many dissertations present a new mathematical technique or prove a new theory. This dissertation presents the design and development of a new experimental system. Although the DSACSS is not yet fully operational, a great deal of work has gone into its development thus far. This work has ranged from configuration design to nonlinear analysis to structural and electrical manufacturing. In this dissertation we focus on the development of the attitude determination subsystem. This work includes development of the equations of motion and analysis of the sensor suite dynamics. We develop nonlinear filtering techniques for data fusion and attitude estimation, and extend this problem to include estimation of the mass properties of the system. We include recommendations for system modifications and improvements.

In Memory of Dr. Frederick H. Lutze, Jr.

Acknowledgments

This is not a one-person dissertation.

None of this work could have been completed without the dedicated work of the entire Space Systems Simulation Laboratory team. I am proud to have led and learned from such a fantastic group of students.

Thanks to Christopher Hall, who has been my advisor since 1998. I've gotten six years of great advice, opportunity, education, and conversation. Also thanks to each of the members of my committee for their help, patience, and encouragement.

A special thank you to my parents, who never said I couldn't do anything. To my friends, who made it much more than simply 'enjoyable.' To everyone who has ever gone out of their way for my sake. To anyone left who remembers VT-ISMM, and to everyone who was involved.

Finally, I must acknowledge the funding agencies who, in part, made my graduate career possible: the National Science Foundation, NASA Goddard Space Flight Center, P.E.O. International and Zonta International. And PK's, who provided a great deal of free pizza and a good reason to go out on Thursday nights.

"It's not the size of the diploma that matters,
it's the quality of the degree."
— Dr. Roger Avery, Senior Associate Dean

Contents

List of Figures	viii
List of Tables	x
1 Introduction	1
1.1 Distributed Systems in Space	2
1.2 Formation Flying in the Laboratory	3
1.3 Dissertation Overview	4
2 Satellite Dynamics and Formation Flying	5
2.1 Equations of Motion	6
2.1.1 Two-Body Orbital Dynamics	6
2.1.2 Unperturbed Nonlinear Dynamics in a Rotating Reference Frame	7
2.1.3 The Hill–Clohessy-Wiltshire Equations	9
2.1.4 Orbital Element Formulations	14
2.2 Formation Design	16
2.3 Coupled Attitude and Orbit Equations	17
2.4 Distributed System Dynamics and Control	19
3 Survey of Spacecraft Simulators	21
3.1 Planar Motion	23
3.2 Rotational Systems	26
3.2.1 Tabletops and Umbrellas: Freedom in Yaw	27

3.2.2	Dumbbells: Freedom in Yaw and Roll	35
3.3	Combination Systems	37
3.4	Manned Space Flight	39
3.5	Facility Enhancements	40
3.6	Summary of Air-Bearing Spacecraft Simulators	42
3.7	GPS Testbeds	45
4	The Distributed Spacecraft Attitude Control System Simulator	46
4.1	Design and Development	46
4.1.1	Whorl-I Hardware	47
4.1.2	Whorl-II Hardware	50
4.1.3	DSACSS Software	52
4.2	Experimental Equations of Motion	53
4.2.1	Kinematic Equations	53
4.2.2	Rigid Body and Gyrostat Dynamics	55
4.3	Perturbations	57
4.3.1	Rotating Earth Perturbation, Newtonian Derivation	57
4.3.2	Rotating Earth Perturbation, Lagrangian Derivation	60
4.3.3	Drag Perturbations	61
4.4	Whorl Sensor Equations	63
4.5	Extended Kalman Filter	68
4.5.1	Extended Kalman Filter Equations	68
4.5.2	Quaternion / Angular Velocity Filter	69
4.5.3	Attitude Error / Angular Velocity Filter	70
4.5.4	Attitude Error / Rate Gyro Bias Filter	72
4.5.5	Experimental Filter Performance	79
4.6	Parameter Estimation	82
4.6.1	Equations of Motion	83
4.6.2	<i>A Priori</i> Estimates	84

4.6.3	Batch Least-Squares Parameter Estimation	85
4.6.4	Least-Squares Estimation Performance	88
4.6.5	Sequential Parameter Estimation	91
5	Conclusions and Recommendations	96
5.1	Summary	96
5.2	Recommendations	97
A	Lessons in Management from the Space Systems Simulation Laboratory	99
References		103
Vita		124

List of Figures

2.1	The Coupled Orbit and Attitude Formation Flying Problem	18
3.1	The Two-Link Manipulator Arm in Stanford University's Aerospace Robotics Laboratory ¹	24
3.2	One of MIT's SPHERES During a Planar Test ²	26
3.3	'Tabletop' (a) and 'Umbrella' (b) styles: full freedom in yaw	27
3.4	'Dumbbell' style: full freedom in yaw and roll	27
3.5	NASA Marshall Space Flight Center's Air Bearing, circa 1960 ³	28
3.6	Naval Postgraduate School's Three Axis Attitude Dynamics and Control Simulator ⁴	30
3.7	Air Force Research Laboratory's ASTREX Testbed ⁵	32
3.8	Honeywell Space Systems's Momentum Control System and Line of Sight Testbed ⁶	34
3.9	University of Michigan's Triaxial Air Bearing Testbed ⁷	36
3.10	The UCLA / Cal Tech Model Spacecraft Spheres ⁸	37
3.11	Lawrence Livermore National Laboratory's Dynamic Air Table host ⁹ . .	38
3.12	Lawrence Livermore National Laboratory's Dynamic Air Rail Concept ⁹ .	38
3.13	The ALFA Mercury Astronaut Trainer ¹⁰	40
3.14	An Overview of Air-Bearing Testbed Capabilities: Payload Weight [lb] .	43
3.15	An Overview of Air-Bearing Testbed Capabilities: Tilt [deg ±]	43
4.1	Whorl-I	48
4.2	Whorl-II	51

4.3	The Spinning Top	56
4.4	Magnitude of Perturbation Torques	62
4.5	MotionPak II Test Setup for Accelerometer Calibration	64
4.6	MotionPak II Test Setup for Rate Gyro Calibration	65
4.7	MotionPak II Acceleration Calibration Data	66
4.8	MotionPak II Rate Gyro Calibration Data	67
4.9	Histogram of MotionPak II Data and Ideal Gaussian Distribution	67
4.10	Estimated Attitude and Angular Velocity, $\hat{\mathbf{x}}^{bi}$, for Nominal Whorl-I Maneuver	75
4.11	Filter Error and Covariance Envelope, $\mathbf{x}^{\hat{bb}}$, for Nominal Whorl-I Maneuver	75
4.12	Definition of Two-Angle Parameterization	76
4.13	True and Estimated Two-Angle Attitude for Nominal Whorl-I Maneuver	77
4.14	Two-Angle Attitude Error for Nominal Whorl-I Maneuver	77
4.15	Two-Angle Attitude Error for Nominal Whorl-I Maneuver. (a) Low-Quality Vector Sensor; (b) No Vector Sensor	78
4.16	Effect of Spin Rate on Two-Angle Attitude Error, No Vector Sensor. (a) π rad/s Flat Spin; (b) 2π rad/s Flat Spin	78
4.17	Effect of Out-of-Plane Motion on Two-Angle Attitude Error, No Vector Sensor. (a) Angle Estimates; (b) Angle Errors	80
4.18	Two-Angle Attitude Estimation for Out-of-Plane Maneuver. (a) Whorl-I; (b) Whorl-II	80
4.19	Experimental Performance, Non-moving Platform. (a) Full-State Estimates; (b) Two-Angle Estimates	81
4.20	Experimental Performance, Small-Amplitude x -Rotation. (a) Full-State Estimates; (b) Two-Angle Estimates	81
4.21	Torque Method LSE Performance in Natural and Integrated Forms [% Median Error]	90

List of Tables

3.1	Torques Acting on Air-Bearing Systems	41
4.1	Parameter Estimates From CAD Model	85
4.2	Parameter Estimates Obtained Using Perfect Data	91
4.3	Parameter Estimates Obtained Using Filtered Data, Two Vector Sensors	92
4.4	Parameter Estimates Obtained Using Filtered Data, Accelerometer-Only Sensor Suite	93

Chapter 1

Introduction

In the past decade, advances in computer size, speed, and networking have fostered a shift in the design of a variety of systems. When attempting to build a top-ten supercomputer, Virginia Tech’s “System X” team did not make use of the fastest, most cutting-edge computing technology. Rather, they created a system of 1,100 Apple G5 PowerMac desktop computers working together — rated in November 2003 as the third fastest system in the world, with a speed of 10.3 trillion operations-per-second.* When Dr. Robert Ballard and director James Cameron sent expeditions to the Titanic, they did not use a lone manned underwater vehicle. Instead, they used teams of custom-designed, remotely-operated vehicles to explore the area quickly and completely with minimal risk. These missions included excursions into the ship that would not have been possible with larger vehicles.[†] Some applications cannot be accomplished by a monolithic system; it would be impractical (perhaps impossible) to have a single robot simultaneously play every position on a soccer team. The ultimate goal of the RoboCup project is to develop a team of fully autonomous humanoid robots that can win against the human world championship team by 2050.[‡] Other distributed system applications include disaster search and rescue, multi-point scientific data collection, passive surveillance, and reconnaissance missions.

* <http://www.tcf.vt.edu/>

† <http://www.titanic-titanic.com/>

‡ <http://www.robocup.org/>

1.1 Distributed Systems in Space

Spacecraft formation flying is yet another application of distributed technology. Just as teams of unmanned aerial and ground vehicles have been proposed for battlefield scenario awareness, teams of spacecraft have been suggested for a variety of scientific and strategic missions. These missions require higher levels of autonomy and communication between nodes than some of the programs described above, but all benefit from the same core technologies.

A spacecraft formation possesses several benefits over a single-satellite mission. Certainly there is less launch risk if the system is distributed across several launch platforms. Further, a greater range of structural configurability may offer lower launch costs for many small vehicles than for a single, large spacecraft. Although the initial cost of a fleet of vehicles may be higher than in a single-spacecraft design, the benefits of mass-production can eventually be used to lower per-vehicle cost — a manufacturing phenomenon rarely seen in the space industry, wherein most designs are highly tailored to unique mission goals. Use of a group of spacecraft provides a level of redundancy in a notably high-risk environment. If, as in the case of the Hubble Space Telescope,[§] there is a flaw with one spacecraft in a formation, the mission will not be entirely compromised. Rather, the rest of the formation will be able to operate (perhaps in some reduced capacity ‘fault tolerant’ mode) until the malfunctioning spacecraft is repaired or replaced. This reconfigurability is also beneficial for technology upgrades, allowing new formation nodes to be dynamically introduced to the system as updated vehicles are placed in orbit. Moreover, the inherent redundancy in the system allows each vehicle’s design to be less robust — and thereby less expensive — with less risk to the mission.

With all of these benefits at hand, spacecraft formation flying has become an exciting area of research. Of course, the problem of relative orbital dynamics is not a new one; the spacecraft rendezvous problem was a major focus of the Gemini program.[¶] However, spacecraft formation flying differs from rendezvous in several key ways. An orbit transfer culminating in rendezvous typically takes place over only a few hours, and high fuel-consumption is expected during the duration of the maneuver. The orientation of the two spacecraft with respect to one another is only important for a relatively brief portion of the mission. Docking is highly assisted by well-engineered grappling devices that allow the two vehicles to interface regardless of small relative attitude errors. Further, docking maneuvers are often performed by an astronaut. Optimally, a spacecraft formation would

[§] <http://hubble.nasa.gov/>

[¶] <http://spacelink.nasa.gov/NASA.Projects/Human.Exploration.and.Development.of.Space/>
Human.Space.Flight/Gemini.Missions/

be able to maintain configuration without a person-in-the-loop. The useful lifetime of the mission is dictated by the available fuel; therefore efficient orbit control is imperative. However, perhaps the most important distinction between rendezvous and formation flying is the purpose of the mission. During rendezvous operations the primary mission objective is to approach and dock with the target spacecraft. In contrast, the mission during formation flying operations is based on scientific or strategic goals: formation flying is the means to perform the mission, not the mission itself.

1.2 Formation Flying in the Laboratory

This ‘secondary’ status places a great deal of emphasis on a set of new, unproven techniques and technologies. Obviously, the benefits of formation flying are minimal if the spacecraft are unable to communicate or otherwise work together after launch. It is risky to demonstrate new space technologies because launch costs are so expensive; this risk explains why the Nickel-Cadmium (NiCad) rechargeable battery chemistry is still so widely used in space despite major improvements in power and energy density available in newer cell types. Another example of the space industry’s reticence towards change are the flight computers in the Space Shuttle Orbiter: the five-unit IBM AP-101S system was upgraded from the original AP-101B processors in 1991, providing the Shuttle with a flight computer with processing speeds on the order of an Intel 386 and the memory to store 524,288 16-bit words.^{||}

One way to mitigate much of this risk is to demonstrate hardware and algorithm performance in ground-based testbeds. However, it is difficult to experimentally replicate satellite dynamics in an Earth-bound laboratory because of the influences of gravity and friction. An air bearing provides a low-torque environment for experimentation, thereby replicating the freedom of the space environment as effectively as possible. Depending upon configuration, air-bearing systems provide some combination of translational and rotational freedom; the three degrees of rotational freedom provided by a spherical air bearing are ideal for investigation of spacecraft attitude dynamics and control problems.

^{||} [http://spacelink.nasa.gov/NASA.Projects/Human.Exploration.and.Development.of.Space/
Human.Space.Flight/Shuttle/Shuttle.Frequently.Asked.Questions/Second.Generation.Computers.FAQ](http://spacelink.nasa.gov/NASA.Projects/Human.Exploration.and.Development.of.Space/Human.Space.Flight/Shuttle/Shuttle.Frequently.Asked.Questions/Second.Generation.Computers.FAQ)

Interestingly, even the upgraded computers are now so obsolete that NASA looks for sources of replacement parts by browsing eBay auctions! (NASA does not purchase flight computers on eBay.)
<http://www.computerworld.com/hardwaretopics/hardware/story/0,10801,71140,00.html>

1.3 Dissertation Overview

An interest in experimental demonstration of formation flying led directly to the development of the DSACSS. The DSACSS is a unique facility, as it provides a pair of ‘spacecraft’ three degrees of attitude freedom by coordinating the behaviors of two spherical air bearings. Through use of the DSACSS we are able to replicate the relative attitude dynamics between nodes of a formation such as might be required for co-observation of a terrestrial target. Initial planning and hardware procurement for this project began in 1998, but the main development emphasis did not start until 2002.

Many dissertations present a new mathematical technique or prove a new theory. This dissertation presents the design and development of a new experimental system. Although the DSACSS is not yet fully operational, a great deal of work has gone into its development thus far. This work has ranged from configuration design to nonlinear analysis to structural and electrical manufacturing. In Chapter 2 we present the equations of motion for a formation of spacecraft, including both orbital and attitude dynamics. In Chapter 3 we provide a review of air-bearing spacecraft simulators. We also give an introduction into a new technique for including orbital dynamics in the experiment: the use of GPS simulators. Chapter 4 documents the bulk of the work in this dissertation. We begin with information on the design, development, and current status of the DSACSS system. We derive the specific equations of motion for the DSACSS air bearings. We present the sensor suite in detail and derive algorithms for nonlinear filtering of the sensor information. In Chapter 5 we summarize this text, provide some concluding thoughts, and offer suggestions for future work.

Chapter 2

Satellite Dynamics and Formation Flying

The earliest formation flying problems were, in truth, rendezvous problems. Most analysis of the rendezvous problem neglects the terminal attraction between vehicles, making it somewhat relevant to the formation flying problem. However, there are key differences between these two classes of problems. First, spacecraft rendezvous is typically controlled by a pilot whereas the ultimate goal of formation flying is to have the fleet of spacecraft operating autonomously. These two control approaches require very different sensor suites and communication requirements between the vehicles. Next, only one vehicle is actively maneuvered during rendezvous — a very inefficient technique for controlling a formation of spacecraft. Perhaps most importantly, rendezvous problems take place over relative short time frames, normally only a few orbital periods. A spacecraft formation has a much longer mission timeline. This difference in time scale causes the linearized equations of motion — which work quite well in the short term — to be less applicable for analysis of formation dynamics. We consider the most interesting spacecraft formations to be long term, autonomous missions wherein each satellite plays an active role in formation maintenance.

The Landsat-7 / Earth Observing-1 (EO-1) mission is often called out as the first on-orbit demonstration of formation flying. However, it does not meet all of the criteria proposed above. EO-1's orbit is controlled relative to Landsat-7's orbit, but the control is commanded from the ground. The two spacecraft do not communicate, and Landsat-7 does not maneuver to maintain the formation.¹¹ Further, the two satellites are much farther apart than most proposed formation flying missions; EO-1 is 60 s (approximately 450 km) behind Landsat-7 in a same-ground-track orbit. This spacing is dictated by

the science mission, but it causes the relative dynamics of this two-satellite cluster to be dissimilar to formations with only a few meters of separation between nodes. Also dictated by the science mission, both spacecraft are nadir pointing; the dynamics of a formation become much more interesting when precision pointing requirements are introduced.

Thus spacecraft formation flying is an exciting area of research with a great deal of technology demonstration yet to be performed. In this chapter, we develop the equations of motion for spacecraft formation flying. We begin with the orbital dynamics, proceed to the attitude dynamics, and finally formulate the coupled problem of precision pointing — coupled orbit and attitude control. Throughout this development we make reference to analysis of this problem in the literature, and we conclude with a brief discussion of the distributed control problem as applied to a spacecraft formation.

2.1 Equations of Motion

An understanding of the formation flying problem begins with an understanding of the equations that govern single-vehicle orbital dynamics. Using these tools, we can then develop the equations that govern the relative motion between elements of a formation. We begin with the general, nonlinear equations of motion for a single orbiting spacecraft. These equations are easily extended for the relative motion problem, as we show. In doing so, we find that it is convenient to introduce the concept of ‘chief’ and ‘deputy’ spacecraft. However, it is important to keep in mind that this notation has no bearing on the ultimate implementation of any distributed control logic. Rather, the orbit defined by the chief satellite need not be inhabited by an actual spacecraft in the formation; it may simply be a convenient reference trajectory for the formation to track.

2.1.1 Two-Body Orbital Dynamics

The motion of a spacecraft orbiting a central body in the presence of no perturbations — that is, the two-body problem — is governed by

$$\ddot{\mathbf{r}} = -\frac{G(M+m)}{r^3} \mathbf{r} \quad (2.1)$$

where G is the gravitational constant, M is the mass of the central body, m is the mass of the spacecraft, and \mathbf{r} is the position vector of the spacecraft.

If we include the effects of external forces, the equation becomes

$$\ddot{\mathbf{r}} = -\frac{G(M+m)}{r^3}\mathbf{r} + \mathbf{f}_{\text{ext}}/m \quad (2.2)$$

For a two satellite formation including a chief spacecraft and one deputy, we have two such equations

$$\ddot{\mathbf{r}}_c = -\frac{\mu}{r_c^3}\mathbf{r}_c + \mathbf{f}_{c\text{ext}}/m_c \quad (2.3)$$

$$\ddot{\mathbf{r}}_d = -\frac{\mu}{r_d^3}\mathbf{r}_d + \mathbf{f}_{d\text{ext}}/m_d \quad (2.4)$$

where we have defined the gravitational parameter $\mu \approx GM$, which is a good approximation for $m \ll M$. We define the position of the deputy with respect to the chief spacecraft as $\boldsymbol{\rho} \triangleq \mathbf{r}_d - \mathbf{r}_c$ and obtain the relative motion equation

$$\ddot{\boldsymbol{\rho}} = -\frac{\mu}{\rho^3}\boldsymbol{\rho} + \mathbf{a}_{(d-c)\text{ext}} \quad (2.5)$$

where $\mathbf{a}_{(d-c)\text{ext}}$ is the differential disturbance acceleration (relative acceleration is a convenient quantity when coordinating spacecraft with different masses).

Equation 2.5 is the most basic relative motion equation for orbital dynamics. However, although this equation is exact, it is not particularly useful. In the remainder of this section we develop alternative, approximate representations of the relative motion. In doing so, we exchange generality for usability.

2.1.2 Unperturbed Nonlinear Dynamics in a Rotating Reference Frame

Following the development by Schaub and Junkins, we note that it is convenient to express the relative motion equations in a rotating reference frame defined by a circular reference orbit with radius r_c .¹² The rotating reference frame, termed the Hill frame, rotates once per orbit with respect to inertial space. The axes of the Hill frame, $\hat{\mathbf{o}}_r$, $\hat{\mathbf{o}}_\theta$ and $\hat{\mathbf{o}}_h$ are defined (like most orbit-fixed coordinate systems) in the radial, near-velocity, and orbit-normal directions, respectively. Thus the reference frame has an angular velocity of

$$\boldsymbol{\omega}^{H_i} = \dot{\nu}\hat{\mathbf{o}}_h \quad (2.6)$$

where ν is the true anomaly of the chief satellite's orbit.

The position vector of the deputy spacecraft can be expressed as

$$\mathbf{r}_d = \mathbf{r}_c + \boldsymbol{\rho} \quad (2.7)$$

$$= (r_c + x) \hat{\mathbf{o}}_r + y \hat{\mathbf{o}}_\theta + z \hat{\mathbf{o}}_h \quad (2.8)$$

where x , y and z are the components of $\boldsymbol{\rho}$ in the Hill frame.

Taking two time derivatives of this equation yields

$$\begin{aligned} \ddot{\mathbf{r}}_d &= (\ddot{r}_c + \ddot{x} - 2\dot{y}\dot{\nu} - \ddot{y}\nu - \dot{\nu}^2(r_c + x)) \hat{\mathbf{o}}_r \\ &\quad + (\ddot{y} + 2\dot{\nu}(\dot{r}_c + \dot{x}) + \ddot{\nu}(r_c + x) - \dot{\nu}^2y) \hat{\mathbf{o}}_\theta + \ddot{z} \hat{\mathbf{o}}_h \end{aligned} \quad (2.9)$$

Recall that the magnitude of the orbital angular momentum of the chief satellite is $h = r_c^2\dot{\nu}$. This quantity is a first integral of two-body motion, thus

$$\dot{h} = 2r_c\dot{r}_c\dot{\nu} + r_c^2\ddot{\nu} \quad (2.10)$$

$$= 0 \quad (2.11)$$

providing a constraint on the second derivative of the true anomaly of the chief satellite's orbit,

$$\ddot{\nu} = -2\frac{\dot{r}_c}{r_c}\dot{\nu} \quad (2.12)$$

This constraint simplifies the chief satellite's acceleration equation by canceling terms in the in-track direction

$$\ddot{\mathbf{r}}_c = (\ddot{r}_c - r_c\dot{\nu}^2) \hat{\mathbf{o}}_r + (2\dot{r}_c\dot{\nu} + r_c\ddot{\nu}) \hat{\mathbf{o}}_\theta \quad (2.13)$$

$$= (\ddot{r}_c - r_c\dot{\nu}^2) \hat{\mathbf{o}}_r \quad (2.14)$$

We have assumed that there are no perturbations in the development of Equation 2.10. Maintaining that assumption, we relate Equations 2.3 and 2.14 to obtain a scalar equation for the acceleration of the chief satellite:

$$\ddot{r}_c = r_c\dot{\nu}^2 - \frac{\mu}{r_c^2} \quad (2.15)$$

We make use of Equations 2.4 and 2.15 to develop a final vector expression for the motion of the deputy:

$$\ddot{\mathbf{r}}_d = \left(\ddot{x} - 2\dot{\nu} \left(\dot{y} - y \frac{\dot{r}_c}{r_c} \right) - x\dot{\nu}^2 - \frac{\mu}{r_c^2} \right) \hat{\mathbf{o}}_r \quad (2.16)$$

$$\begin{aligned} &\quad + \left(\ddot{y} + 2\dot{\nu} \left(\dot{x} - x \frac{\dot{r}_c}{r_c} \right) - y\dot{\nu}^2 \right) \hat{\mathbf{o}}_\theta + \ddot{z} \hat{\mathbf{o}}_h \\ &= -\frac{\mu}{r_d^3} \mathbf{r}_d \end{aligned} \quad (2.17)$$

This vector expression can be written as three scalar equations:

$$\ddot{x} - 2\dot{\nu} \left(\dot{y} - y \frac{\dot{r}_c}{r_c} \right) - x\dot{\nu}^2 - \frac{\mu}{r_c^2} = -\frac{\mu}{r_d^3} (r_c + x) \quad (2.18)$$

$$\ddot{y} + 2\dot{\nu} \left(\dot{x} - x \frac{\dot{r}_c}{r_c} \right) - y\dot{\nu}^2 = -\frac{\mu}{r_d^3} y \quad (2.19)$$

$$\ddot{z} = -\frac{\mu}{r_d^3} z \quad (2.20)$$

These are the full, nonlinear equations of relative motion for a deputy spacecraft with respect to a chief spacecraft in an arbitrary, unperturbed orbit. Note that the cross-track equation is only loosely coupled with the others via the r_d term.

$$r_d = \sqrt{(r_c + x)^2 + y^2 + z^2} \quad (2.21)$$

$$= r_c \sqrt{1 + 2\frac{x}{r_c} + \frac{x^2 + y^2 + z^2}{r_c^2}} \quad (2.22)$$

$$\approx r_c \sqrt{1 + 2\frac{x}{r_c}} \quad (2.23)$$

Upon first inspection, Equation 2.23 seems much more useful than Equation 2.5. In practice, however, the full nonlinear equations are rarely used. When this set of equations is invoked, it is common to immediately simplify the bounds of the problem by assuming constant mass and external forces, for example. The work of de Queiroz, Kapila and Yan begins with the nonlinear relative motion equations but assumes the mass and disturbance accelerations to be slowly varying.¹³ Thus, although their formulation begins with the premise of complete nonlinearity, it is unclear that the globally asymptotically stable Lyapunov control law which they derive is any more general than those presented later in this review.

2.1.3 The Hill–Clohessy-Wiltshire Equations

Recall from basic orbital dynamics that

$$\frac{\mu}{r_c^3} = \frac{\dot{\nu}^2}{1 + e \cos \nu} \quad (2.24)$$

where e is the eccentricity of the chief satellite's orbit.¹²

If we assume the chief's orbit to be circular the change-in-radius (\dot{r}_c) and eccentricity terms drop out, and the derivative of the true anomaly can be replaced by the mean

motion, n . Making use of these substitutions in Equations 2.18–2.20 we obtain the classic Hill–Clohessy–Wiltshire (HCW) equations:

$$\ddot{x} - 2n\dot{y} - 3n^2x = 0 \quad (2.25)$$

$$\ddot{y} + 2n\dot{x} = 0 \quad (2.26)$$

$$\ddot{z} + n^2z = 0 \quad (2.27)$$

The first documentation of these equations comes from Hill in 1878.^{14,15,16} In these works, Hill described the motion of the Moon relative to the Earth. Hill’s original derivation of the relative motion equations includes a term μ/r^3 that, when removed, yields the linear equations presented by Clohessy and Wiltshire in 1960.¹⁷ The HCW equations were then published nearly simultaneously by several groups, including conference and journal papers by Clohessy and Wiltshire,¹⁸ a book on space technology edited by Seifert,¹⁹ and in individual journal publications by Spradlin,²⁰ Eggleston,²¹ and Geyling,²² several of which cite Clohessy and Wiltshire’s 1959 conference publication.¹⁸ These linearized equations of motion, although first derived for investigation of orbital rendezvous problems, are useful in describing the relative orbital dynamics in spacecraft formation flight. However, one must recall an important difference between formation flying and rendezvous problems: duration. Rendezvous missions are relatively brief: typically, one spacecraft executes a series of large maneuvers during the course of just a few orbits. As such, rendezvous missions are not grossly affected by the perturbative effects that cause satellites in a formation to drift apart. Similarly, errors that arise from the use of this linearized model do not have sufficient time to amass in the duration of a rendezvous mission.

The unperturbed version of the HCW equations, shown in Equations 2.25–2.27 can be solved analytically:

$$x(t) = (\dot{x}_0/n) \sin nt - (3x_0 + 2\dot{y}_0/n) \cos nt + 4x_0 + 2\dot{y}_0/n \quad (2.28)$$

$$y(t) = (2\dot{x}_0/n) \cos nt + (6x_0 + 4\dot{y}_0/n) \sin nt - (6nx_0 + 3\dot{y}_0)t - 2\dot{x}_0/n + y_0 \quad (2.29)$$

$$z(t) = (\dot{z}_0/n) \sin nt + z_0 \cos nt \quad (2.30)$$

Note that Equation 2.29 includes a secular term — that is, a term that increases linearly in time. We can enforce an additional constraint to eliminate the secular drift by choosing

$$\dot{y}_0 = -2x_0n \quad (2.31)$$

Invoking this constraint results in a relative orbit that is displaced from, but has the same energy — and thus the same semimajor axis — as the (circular) reference orbit,

leading to

$$x(t) = (\dot{x}_0/n) \sin nt + x_0 \cos nt \quad (2.32)$$

$$y(t) = (2\dot{x}_0/n) \cos nt - 2x_0 \sin nt - 2\dot{x}_0/n + y_0 \quad (2.33)$$

$$z(t) = (\dot{z}_0/n) \sin nt + z_0 \cos nt \quad (2.34)$$

These equations have been used as the basis for analysis of rendezvous and formation flying missions since 1960. By inspection, we observe that the relative motion in the cross-track direction, z , is decoupled from the radial, x , and along-track, y , components. Specifically, the cross-track relative motion behaves as an harmonic oscillator. This separation in the linearized system is reasonable, as the cross-track relative motion is only weakly coupled in the complete nonlinear solution. In the linearized system the radial / along-track motion always follows a 2:1 ellipse.

The simple nature of these equations has led to their application in an abundance of papers. Some of this work has led to valuable insights. Other contributions have, debatably, served only to obfuscate the objective at hand. Due to their simplicity, the HCW equations have been seized upon by the mathematically-minded research community, in the quest for simple, elegant solutions to esoteric control problems. However, they do not necessarily provide the best engineering solutions to the formation flying problem. Rather, these equations are perhaps so simple that they can distract from the true problem at hand.

Mathematicians are attracted to the HCW equations in part because they yield several linearly stable solutions: in-plane, in-track, circular, and projected circular relative orbits. The in-plane formation is perhaps the simplest of all formation designs: the spacecraft are in the same orbital plane and are separated only by a difference in anomaly (time). This formation is initialized by setting all conditions to zero except for the y displacement, which yields a constant, nonzero offset in the along-track direction. The along-track initial condition is related to the mean anomaly separation.

Just as the in-plane formation provides context for a formation of satellites to maintain the same orbital plane, the in-track configuration sets a formation up to have each vehicle trace out the same ground track. The circular formation maintains the three-dimensional distance among spacecraft. The projected circular formation maintains this constraint only in the along-track / cross-track plane. Sabol, Burns and McLaughlin provide an analysis of the natural stability of these linearly stable formations in the presence of perturbative forces.²³ The formations are initialized based on the HCW equilibria and the exact solution is calculated by propagating mean elements are through the Draper Semianalytic Satellite Theory.²³ The authors consider two cases of in-plane formations,

one with a 100-revolution-per-seven-nodal-day repeat ground track cycle, and one with a 14-revolution-per-nodal-day cycle. The 100:7 cycle is a short repeat ground-track orbit; such orbits are relatively stable in the presence of gravitational perturbations. The 14:1 cycle is a daily repeat ground-track orbit; these smaller ratio orbits are sensitive to tesseral resonances, causing periodic variation in the along-track separation of the formation.²³

The authors considered the same two cases for the in-track formation configuration. Because the spacecraft cross the same points on the Earth in an in-track formation, they encounter identical gravitational perturbative forces. However, because the spacecraft are in different orbital planes atmospheric drag causes an along-track drift. This drift causes an unbounded along-track separation in the formation for both cycles.²³ The circular and projected-circular formations are unstable, primarily due to Earth-oblateness effects.²³

Despite these shortcomings, not all applications of the HCW equations should be considered inappropriate. Certainly linearized equations of motion provide an unrivaled system for initial analyses. A 1985 publication by Vassar and Sherwood is an early use of the HCW equations for a simple satellite cluster, much like the Landsat-7 / EO-1 mission. The authors derived a “practical control scheme” from the linearized system for a two satellite leader-follower formation.²⁴ Their formation of interest is a terrestrial laser communication system. The chief satellite is in geosynchronous orbit; outfitted with a mirror, it is used to relay laser signals from one ground station to another. The deputy satellite must lead the chief in order to provide atmospheric calibration data to the transmitting ground station. The only specification on the deputy’s orbit is an in-track separation from the chief of 700 m $\pm 3\%$. The authors determined that the primary perturbative force on this formation would be differential solar radiation pressure; this disturbance would cause the in-plane separation to grow without bound.* Assuming the deputy spacecraft to be equipped with chemical propulsion, the authors proposed a closed-loop optimal digital control law for formation-keeping based on similar controllers derived for stationkeeping.

Similarly, Howard, Lovell and Horneman make use of the HCW equations in preliminary analysis of the collision avoidance problem for satellites flying in close formation.²⁵ Perhaps surprisingly, use of the linear equations in this case is valid for two reasons. First, assuming the formation is composed of several of the same spacecraft, the perturbing forces such as drag and solar radiation pressure should be comparable for each vehicle. Similarly, in a tight formation we can expect the spacecraft to be in sufficiently close proximity so as to experience the same gravitational perturbations. Secondly — and most

*Intriguingly, the authors considered the engineering option of choosing the reflectivities of the two satellites to mitigate the effects of this perturbation passively. They concluded that this option is impractical for two reasons: varying spacecraft reflectivity while on orbit is not a clear-cut task; moreover, the interests of the formation-keeping engineer and the thermal engineer would be at odds.

importantly — this work is proposed as preliminary analysis, and the authors intend to expand their work to include perturbations and general elliptical orbits.

In contrast, misapplication of the HCW equations can lead to rigorous mathematical analysis of a non-physical system. Kapila, Sparks, *et al.* make use of the HCW equations in their development of linear, pulse-based, discrete-time feedback controllers.²⁶ Through use of full-state feedback, the authors demonstrate closed-loop stability of the linear system using standard LQ regulation techniques. They claim to have developed “a mathematically rigorous control design framework for linear control of spacecraft relative position dynamics with guaranteed close-loop stability... that can potentially lower the fuel consumption in multiple spacecraft formation flying.” It is unclear to this author that they have accomplished any such thing, as fuel potentially saved through their novel control scheme will be wasted attempting to maintain a false equilibrium condition. Veres and Gabriel also make use of the HCW equations to begin to solve a challenging nonlinear control problem. Specifically, they note that there are few methods for achieving constrained control in the formation flying class of problems because of the complexity of calculating robust controllability sets. They use the linearized system to find approximations to the controllability sets, and demonstrate the effectiveness of these approximations in a nonlinear simulation.²⁷ Again, constrained control around an artificially stable equilibrium motion is prohibitively expensive for a practical distributed spacecraft system. Similarly, Yeh, Nelson and Sparks derive a second-order sliding mode controller based on the HCW equilibria specifically designed to cancel out the perturbative forces.²⁸ In general, this linearization of the relative motion should not be used in the design of autonomous closed-loop control laws: the formation will quickly deplete its available fuel.

The HCW equations can be improved upon to form augmented (though still linear) systems of equations that include select perturbative forces. By doing so, these dynamic effects can be recognized (and perhaps made) of use rather than countered. The most common terms to be reintroduced are the gravitational and drag perturbations. Schweighart and Sedwick developed one of the more commonly referenced J_2 extensions,²⁹ which has been extended by Roberts and Roberts.³⁰ Ross developed another form for the J_2 gravity perturbation.³¹ Lovell, Horneman, *et al.* include the J_2 gravity perturbation and a simple drag model in their work on formation reconfiguration and maintenance.³² Many other authors have investigated the drag perturbation, a difficult problem to model.^{33,34,35} Wiesel models both a simple drag force and gravitational perturbations through order 14 by combining periodic orbit, Floquet, and modal-perturbation theories for a restricted class of nearly circular reference orbits.³⁶

The relative orbit equations can be linearized in many different ways.³⁷ At this point,

we have discussed only inertial and orthogonal rotating reference frames. We could also develop the equations in a rotating reference frame with non-orthogonal axes. Further, we have linearized about a circular orbit. The Tschauner-Hempel equations generalize the relative motion equations to a chief satellite in any elliptical orbit. The Brumberg-Kelly equations provide this same generality for elliptic reference orbits via a different parameterization. Alternatively, Battin presents a linearization of the gravitational force itself, rather than the relative state information.³⁸ We mention these other options in order to provide some perspective on the number of ways in which the formation flying problem can be approached. We focus on only one other formulation: the very useful relative orbital element technique.

2.1.4 Orbital Element Formulations

The HCW equations can easily be solved analytically in the case of an unperturbed, circular chief orbit. Analytic solutions for more realistic orbit conditions, although achievable in Cartesian coordinates, are much more challenging to obtain. Moreover, the initial Cartesian coordinates no longer provide intuition into the dynamics of the system. In these cases, a relative orbital element formulation of the equations can be much more useful.

A relative orbit motion formulation based on an orbital element error expansion yields far superior performance without losing the the simplicity and elegant functionality inherent in a linear system. For example, Alfriend, Schaub and Gim demonstrate the effect of the simplifying assumptions in the HCW equations (that is, that the chief satellite is in a circular orbit, the Earth is spherically symmetric, and the nonlinear terms in the relative motion variables can be neglected) on the required fuel for establishing and maintaining a relative motion orbit.³⁹ Specifically, linearizing the equations in terms of small orbital element differences provides more accurate results than either rectilinear or curvilinear Cartesian coordinates.⁴⁰ Schaub, Vadali, Junkins and Alfriend have developed control laws that incorporate linear feedback of the relative orbital elements or nonlinear feedback of the relative Cartesian coordinates.⁴¹ Moreover, there are multiple sets of orbital elements to choose from; we can select a representation that best fits each particular problem. For example, we would choose to use different coordinates when solving for relative motion with respect to general elliptic chief orbits versus those with small eccentricity, or near-circular chief orbits in order to avoid mathematical singularities. Further, the relative orbital element forms provide an intuitive set of coordinates for formation design, even in the presence of perturbative forces. This usefulness is partly due to the fact that we can choose sets of orbital elements such that some of the elements are unaffected

by the perturbations, while the others are governed by simple additive terms. Finally, obtaining a solution using the Cartesian representation requires integration of all six differential equations; orbital element forms only require the integration of the current value of the anomaly (which can be obtained algebraically in the absence of perturbations).

There are many sets of orbital elements from which we can choose to define the relative motion equations.¹² Recall that the classical orbital elements are

$$\mathbf{e} = [a, e, i, \Omega, \omega, \nu]^T \quad (2.35)$$

Just as this set of coordinates can be ill-defined in the two-body problem (*e.g.*, the periapsis direction is undefined for a circular orbit, and the line of nodes is undefined for an equatorial orbit), so too can it cause singularities in the relative orbit problem.

A better choice of relative coordinates based on the classical elements is

$$\delta\mathbf{e} = [\delta a, \delta\theta, \delta i, \delta q_1, \delta q_2, \delta\Omega]^T \quad (2.36)$$

where θ is the true latitude, $\theta \triangleq \omega + \nu$, $q_1 = e \cos \omega$, and $q_2 = e \sin \omega$; this form mitigates the singularities for near-circular orbits.⁴²

This choice of coordinates is also convenient because, for small formations, the relative orbital elements can be mapped linearly to and from the HCW Cartesian coordinates.^{42,43} This mapping can be used to derive convenient hybrid-representation feedback control laws: the relative orbit can be specified through orbital element differences while the absolute orbit is expressed in Cartesian coordinates.⁴⁴

However, using the true latitude and true anomaly is not ideal for elliptic chief orbits, as the relative true anomaly will vary in time. Instead, we can make use of the mean anomaly, M_0 , with relative orbital elements

$$\delta\mathbf{e} = [\delta a, \delta M_0, \delta i, \delta\omega, \delta e, \delta\Omega]^T \quad (2.37)$$

The mean anomaly remains constant for unperturbed motion with an elliptical chief satellite.⁴² We can, of course, convert between orbital element coordinate sets as necessary.

There are many additional relative orbital element sets to choose from. When dealing with secular perturbation it is convenient to switch to a mean orbital element formulation rather than a set of osculating elements. These dynamics are easily represented by either Lagrange's planetary equations or Gauss' variational equations, both of which are well documented in orbital dynamics texts.^{38,45,12} Although this body of work is very

interesting, it is beyond the scope of this text. We refer the reader to the textbook derivations of the equations of motion and review only a few key sources below.

Schaub and Alfriend have worked to define a family of J_2 -invariant orbits and to design controllers that work within the context of this natural motion.^{41,44,46,47,48} Impulsive feedback control based on Gauss' variational equations of motion allows specific orbital elements to be controlled with minimal impact on the remaining osculating elements.⁴⁹ Vadali, Schaub and Alfriend⁴⁸ and Vaddi, Alfriend and Vadali⁵⁰ have derived sub-optimal controllers for formation establishment and reconfiguration. Gim and Alfriend develop the state transition matrix of the relative motion of the deputy for a non-circular chief orbit under the effect of perturbations.⁵¹

2.2 Formation Design

Up to this point we have discussed the equations of a single deputy spacecraft with respect to the chief. Although those equations are easily generalized for multiple deputies, analysis of an entire formation requires a more well-rounded approach. Of critical importance for a formation flying mission is the balance between fuel conservation and even fuel consumption among the satellites in the formation. Campbell has developed a formation planner intended for large clusters that provides a context for calculation of minimum-time and minimum-fuel maneuvers while maintaining a constraint for collision avoidance. However, these maneuvers are optimized on a per-spacecraft basis, not for the formation as a whole.⁵² If, for example, the chief satellite's orbit was allowed to evolve freely and all deputy spacecraft were controlled to track this drift the lifetime of the formation would be determined by the fuel consumption of the most-controlled deputy. However, when this spacecraft ran out of fuel the chief spacecraft would still have its full amount of fuel remaining. Obviously managing a distributed system effectively requires more than managing each node independently.

Vadali, Vaddi and Alfriend made use of their thorough understanding of the J_2 perturbation to derive a “drifting formation” control scheme to evenly distribute fuel consumption about each of the spacecraft in a formation. Remarkably, their control concept requires one-third of the fuel per vehicle than does a naively designed individual-spacecraft station-keeping controller.⁵³ Beard and Hadaegh create a cost function composed of two parts to help mitigate fuel usage. The first part represents the total fuel required by the entire formation in order to perform some maneuver. The second part is motivated by the negative entropy of a probability distribution; this term is minimized in the case of uniform distribution. Thus they find the solution for a maneuver that uses the least total fuel

possible while distributing the expenditure as evenly as possible.⁵⁴ These two papers represent very different views of how to approach this problem: one with a solid knowledge of the nonlinear dynamics of the system, and one with the logic of a mathematician.

It is important to keep in mind that formation flying is not a mission in and of itself, it is rather a forum for scientific investigation. Therefore, it is important to understand the needs of the science mission and address them in an efficient manner. Hughes and Hall derived an algorithm to distribute the nodes of a constant shape formation equally in time for an arbitrary elliptical chief orbit.⁵⁵ Such an arrangement is important in virtual aperture and coordinated remote sensing missions. Moreover, the authors define additional mission performance metrics by extending those already developed for single-satellite remote sensing missions.⁵⁶ Inalhan, Tillerson and How derive solutions for the necessary conditions on the initial states that produce T -periodic solutions that have the vehicles returning to the initial relative states at the end of each orbit.⁵⁷ Such a formation might be useful for specific Earth-observing objectives. Bailey, McLain and Beard determine that complex scientific arrangements can provide substantial improvements in fuel consumption by combining the retargeting and imaging maneuvers required to image multiple stellar sources.⁵⁸ However, it is unclear to this author if such a scheme could be practical scientifically.

2.3 Coupled Attitude and Orbit Equations

Some of the work described in Section 2.2 alludes to the important coupling between the orbital and attitude dynamics of spacecraft flying in formation. The two sets of equations are often considered distinctly under the assumption that the attitude dynamics occurs at a much faster rate than the orbital dynamics — this assumption is often true. However, in the case of a close formation with limited thrust control, inaccurate modeling of the attitude dynamics could lead to spacecraft collisions. Collision avoidance is beyond the scope of this text; it is mentioned only to help motivate the problem. The two sets of equations are coupled by the science mission of the formation, too: it does little good to have a distributed aperture if the individual nodes are not pointed at the same target.

For example, consider the two-satellite formation shown in Figure 2.1a. The two spacecraft are in different orbits, and have different sub-satellite points as indicated by the colored dots. The grey lines trace the ground tracks of the two vehicles. One possible co-observation mission would have the two satellites pointing at the centroid of the sub-satellite points, indicated by the center dot in Figure 2.1b. Figure 2.1c shows the operational requirements for one of the two spacecraft. The vehicle must point its bore-

sight axis along the vector from the spacecraft to the target, $\mathbf{r}_{T/S}$. Further, it must orient its thruster opposite from the desired delta-vee direction, $-\Delta\mathbf{v}$.

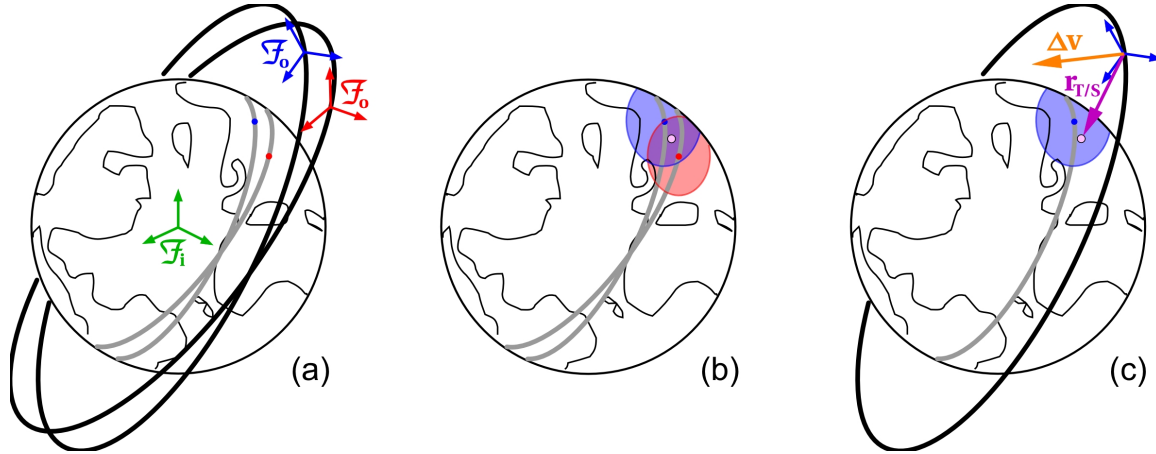


Figure 2.1: The Coupled Orbit and Attitude Formation Flying Problem

Consider a spacecraft with a single non-vectored thruster and a fixed camera angle. The orientations of these hardware components are separated by an angle θ_{config} , a constant known value. The above mission parameters also define a separation angle, θ_{mission} . This value changes in time as the formation evolves

$$\theta_{\text{mission}} = \arccos \left(\frac{\Delta\mathbf{v}^T \mathbf{r}_{T/S}}{\|\Delta\mathbf{v}\| \|\mathbf{r}_{T/S}\|} \right) \quad (2.38)$$

Only if θ_{mission} coincides with θ_{config} can these requirements be resolved exactly. Thus, except in mathematical point-solutions, the desired attitude for either the scientific mission or the formation maintenance requirement will not be maintained. Even in this simple example, neglecting the attitude dynamics would result, minimally, in impaired system performance.

Most of the literature in this area is very basic. It is common to ‘couple’ the equations but then assume perfect orbit control, or to neglect the orbital dynamics entirely, thereby implying the same assumption.^{8, 59, 60, 61, 62, 63, 64} Wang and Hadaegh present the most impressive of these works; they include a partially decentralized control scheme.⁶⁵ However, they also decouple orbit control errors from their attitude controller. They are able to effectively avoid the question of orbit perturbations by only considering J_2 -invariant relative orbits.

Philip and Ananthasayanam perform coupled analysis for the rendezvous and docking problem, but are motivated by the vision system rather than mission dynamics.⁶⁶ Fragopoulos and Innocenti decouple the motions in their analysis, but then recombine

them into a coupled H-infinity controller for rendezvous with a space station.⁶⁷ Redding, Persson and Bergmann derive a simultaneous solution of open-loop attitude and orbital maneuvers as applied to the Space Shuttle in order to account for jet coupling in all six control axes. They form the open-loop part of a feed-forward, feed-back rotational / translation maneuver controller.⁶⁸ Again we see that the problem of rendezvous is related to formation flying, but takes place on a much shorter time scale.

In contrast, Naasz *et.al* present a thorough single-satellite analysis for a spacecraft with limited thruster configurations.⁶⁹ Moreover, the spacecraft can only fire thrusters when above a certain power threshold. Yamanaka provides a similar level of analysis into a large-scale formation reconfiguration problem.⁷⁰ It is unclear to this author whether the proposed formation is physically valid, but it does maintain a coupling between the orbit and attitude dynamics throughout. Regardless, these papers represent the direction that formation flying analysis must follow in order to produce physically valid relative motions that can complete the intended mission.

2.4 Distributed System Dynamics and Control

Real time demonstration of distributed control of the DSACSS is beyond the scope of this dissertation. However, it is important to mention the distributed nature of the testbed in order to motivate some assumptions. A formation of satellites is a distributed system, and as such has two control options: centralized or decentralized control. Further, the observation problem can be equally split into centralized or decentralized navigation. In centralized control, one node receives information from the rest of the system and determines the actions of the entire group. Such a technique requires a simplistic communications scheme but has a single point of failure. Fully decentralized control architectures require each node to communicate with every other node: the system is wholly redundant, but has communication requirements that are typically prohibitively high.^{71,72} Partially decentralized schemes attempt to find some balance between these two schemes, trading communication load for risk.⁷³ Carpenter has proposed several distributed and partially distributed formation control techniques.^{71,72,73} Again, most research has focused on the orbital dynamics aspect of this problem, although these choices apply to both the orbital and the attitude estimation and control schemes.

Perhaps the most simple distributed control methodology is the leader-follower approach. In a leader-follower formation, one of the spacecraft is designated as the the leader. The other spacecraft in the formation track the state of the leader with some prescribed offset. There are numerous variations on leader-follower approaches, including designating

multiple parallel lead spacecraft, recursive following (spacecraft_{i-1} follows spacecraft_i), and other tree structures.^{74,75,76}

In the virtual-structure approach, the formation is treated as a single unit with functional nodes rather than as a collection of individual vehicles. The formation is based on a reference state and the motion of the components of the virtual structure are defined with respect to that reference. Through this representation it is clear how to maintain constraints within the distribution of the formation. Ren and Beard demonstrate that incorporating feedback control into a virtual-structure approach provides improved performance over an open-loop controller.⁷⁵

The main idea in the behavioral approach is to prescribe several desired, (often competing) behaviors for each spacecraft. The dynamics of the formation are then determined through a weighted average of the inputs from each behavior. Typical behaviors include collision avoidance, goal seeking, and formation keeping. Fundamentally, these behaviors are functions of the relative states of a spacecraft and its neighbors.

The perceptive frame can be thought of as a conglomeration of the above techniques. It has been used to integrate the decentralized feedback of each satellite with on-line sensor information to achieve the goal of formationkeeping and intersatellite coordination.⁷⁷ It has also been used to coordinate sliding mode tracking control laws for individual satellites.⁷⁸

Chapter 3

Survey of Spacecraft Simulators

Air bearings have been used for spacecraft attitude determination and control hardware verification and software development for nearly 45 years, virtually coincident with the beginnings of the Space Race. Facilities vary widely, ranging from prodigious government laboratories to simple university testbeds. In this chapter, we present the results of our investigation into the historical development of these facilities, including what technologies have been incorporated into spacecraft simulators, what capabilities have been developed, and what functionality current systems provide. This information can serve as a benchmark for the development and use of future testbeds.*

There are many solutions to the problem of simulating the functional space environment. Air bearings offer only one of the possibilities. Particular techniques may be more applicable in one situation than another: whereas the underwater test tank provides an invaluable part of an astronaut's training, the usefulness of submerging a satellite is obviously limited. Certainly air bearings cannot provide the full experience of microgravity; however, they do allow for the manipulation of hardware in a minimal-torque environment. A low-torque environment is often central to the success of high-precision systems, but duplicating it on the ground to validate controls concepts is difficult. Programs that might benefit from hardware demonstration and testing often forego these stages because the influence of gravity and friction render Earth-based behavior unrealistic. An air bearing offers a nearly torque-free environment, perhaps as close as possible to that of space, and for this reason it is the preferred technology for ground-based research in spacecraft dynamics and control. Depending on the type of air bearing, some combination of virtually torque-free rotational motion and force-free translational motion can

*An earlier version of Sections 0–6 of this chapter was previously published as Schwartz et al.;⁷⁹ reprinted by permission of the American Institute of Aeronautics and Astronautics, Inc.

be achieved. Magnetic suspension systems and gravity offload devices can also produce low-torque dynamic environments, but such systems typically offer a smaller range of motion than that provided by an air bearing.

Test facilities supported by air bearings are intended to enable payloads to experience some level of rotational and translational freedom. Pressurized air passes through small holes in the grounded section of the bearing and establishes a thin film that supports the weight of the moving section. This slow-moving air imparts virtually no shear between the two sections of the bearing. Thus, the air film is an effective lubricant. An air bearing that can support a payload weighing several thousand pounds may require air pressurized to only about 100 psi with a flow rate of only a few cubic feet per minute. A familiar example of such a device is an air-hockey table. These planar air-bearing systems provide one rotational and two translational degrees-of-freedom for a plastic puck.

Spherical air bearings are one of the most common devices used in spacecraft attitude dynamics research because (ideally) they provide unconstrained rotational motion. As the name implies, the two sections of the bearing are portions of concentric spheres, machined and lapped to small tolerances. One spherical section rotates on an air film bounded by the other section in three degrees-of-freedom. The rotating surface is rarely a 4π steradian sphere, as equipment affixed to the bearing limits the range of motion. Of course, other mechanical arrangements can serve a similar purpose — ball-and-socket joints, for example — but air bearings yield much lower friction. Systems of multiple gimbals can be used for this purpose, but such arrangements introduce the problem of gimbal lock. Even if rotational freedom is constrained to avoid this situation, the gimbal dynamics will still interact with the payload dynamics through some nonlinear function of gimbal angle, making realistic simulation much more difficult. Spherical air bearings provide a payload rotational freedom without the friction or the singularities inherent in these other mechanical examples while enforcing an analogous level of constraints on the configuration.

The primary objective of air-bearing tests is faithful representation of spacecraft dynamics. With the problem of a representative plant addressed, experimenters have used these simulators to evaluate control schemes ranging from rigid-body dynamics and control of a single spacecraft to jitter suppression in flexible systems. Some have considered problems of relaying laser light for communications or for transferring power; others have used air bearings for fluid-damping measurements, for missile-defense and formation flying demonstrations, and for testing the viability of agile spacecraft attitude control. Regardless of their scientific or engineering merits, air-bearing based simulators have proven to be valuable pedagogical tools and have, from time to time, played a marketing role during the proposal stages of commercial and government space programs.

In this chapter, we provide an overview of air-bearing spacecraft simulators. Natural divisions in testbed capabilities are used to organize the chapter. First, we present a survey of planar systems, those that give a payload freedom to translate and spin. These facilities are ideal for the understanding of tasks such as formation flying, rendezvous, and on-orbit construction. We then discuss several classes of rotational air bearings, which allow for the recreation of three-axis satellite attitude dynamics. We follow these sections with a discussion on perhaps the most interesting facilities: those that provide both translational and three-parameter rotational freedom. Within these three sections we outline the diverse capabilities air-bearing testbeds provide and the varied facilities which house them. We focus on the use of air bearings in the support of manned space flight in a separate section. Finally, we note that air-bearing performance can be enhanced through careful facility design. We discuss how such improvements have been achieved before offering some concluding thoughts and closing. We then provide an overview of GPS simulator testbeds used for analysis of formation flying problems.

3.1 Planar Motion

Planar motion — one rotational and two translational degrees-of-freedom — is of interest for simulations of rendezvous and docking. The other two axes of rotation and out-of-plane translation are arguably less important in the investigation of relative orbital dynamics, at least for the level of effort required. In almost all cases, the test body carries its own air supply and produces its own cushion of air, allowing it to hover on a polished surface. Although we have not found many specific historical references on these testbeds, such facilities were common enough by the mid-1970s to warrant a NASA Technical Memorandum on how to pour large floors that are sufficiently smooth and level for floating air-bearing vehicles.⁸⁰ We have also found documentation on the design of a payload support pad capable of floating 200 lb manned and unmanned test vehicles. This system was designed and manufactured by the Space Maneuvering Devices section of the Space Division of North American Rockwell Group in 1967 for NASA Marshall Space Flight Center.⁸¹

There are many contemporary planar air-bearing facilities being used to investigate topics in orbital rendezvous. These facilities typically float small, low-mass, generic test bodies, as they are more commonly used for controller validation than inertia-equivalent simulation of a flight payload. Researchers at Stanford University’s Aerospace Robotics Laboratory (ARL) have several air-bearing test facilities used to investigate many topics. One such subject of interest involves the challenges inherent in the use of robotics for on-orbit construction, servicing, assembly and repair. A crucial topic in the development

of robotic construction techniques is the level at which human operators should be involved. Currently, space robots such as the Space Station Remote Manipulator System are controlled by human teleoperation. This technique takes full advantage of the particular abilities that only a person can bring to a closed-loop control system. However, doing so leads to higher levels of cost and risk than would be present in an autonomous system. Experiments to define the useful envelope for human-assisted control are performed using a two-link manipulator arm operating on a passive, free-floating object. As shown in Figure 3.1, the arm and target body are able to travel freely on a 6 ft × 12 ft polished granite table.¹

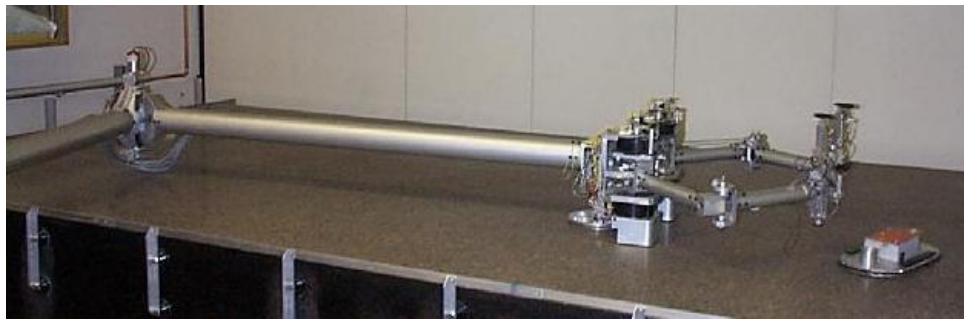


Figure 3.1: The Two-Link Manipulator Arm in Stanford University's Aerospace Robotics Laboratory¹

Another current area of interest in the field of on-orbit rendezvous is the problem of capturing a damaged satellite. Solving this problem is substantially more difficult than that of construction, as the target may be maneuvering autonomously and likely does not have effective grappling points. The Tokyo Institute of Technology is investigating this topic on a 10 ft × 16 ft plate glass planar air-bearing table with a pair of seven degree-of-freedom articulated arms; one arm randomly executes commands in simulation of a failing spacecraft, while the other attempts to capture it.⁸²

The University of Victoria has a planar air bearing that hosts a single robotic arm. It is being used to investigate the optimal joint trajectory of an articulated arm to minimize vibration excitation within the arm elements during a designated maneuver. Through this experimentation they have proven that joint trajectory optimization can significantly reduce the total strain energy incurred within structural elements during point-to-point motions.⁸³

The Naval Postgraduate School's Flexible Spacecraft Simulator includes a rigid central body and a two-link appendage, representative of a satellite with a flexible antenna. The main body can float on a set of air pads or remain fixed, and the arm is floated at each articulation point. This facility has primarily been used for the investigation of vibration

suppression within the arm.⁸⁴ It has recently been adapted for use in investigating formation flying.⁸⁵

Formation flying of two or more functional satellites presents its own set of optimization challenges. The Autonomous Extravehicular Robotic Camera (AERCam) is intended to fly freely about the Space Shuttle and International Space Station in order to provide video images of external features without requiring an EVA. AERCam Sprint was teleoperated within the payload bay during a 1997 Space Shuttle mission; AERCam II is intended to complete pre-assigned tasks autonomously during a future mission. Engineers have ground tested control algorithms for AERCam II on an air-bearing table equipped with six GPS pseudolites for real-time position and velocity sensing.⁸⁶

Similarly, a joint venture between three Japanese corporations has produced a 12 ft × 18 ft planar testbed, which is being used to test control laws for another EVA-replacement free-flying telerobot concept.⁸⁷ Stanford University is investigating the use of GPS measurements in formation flying algorithms on a 9 ft × 12 ft polished granite table top hosting three independent prototype spacecraft. These prototypes are modeled from their ORION microsatellite, also intended for launch on the Space Shuttle.⁸⁸

A useful testbed that has complete freedom in all six degrees is an unlikely achievement within the confines of an Earth-based laboratory. Therefore, students from the Massachusetts Institute of Technology took their Synchronized Position Hold, Engage, and Reorient Experimental Satellites (SPHERES) project on NASA's KC-135 "Vomit Comet" for short-term six degree-of-freedom experimentation in microgravity. Further, SPHERES has been manifested to fly on the International Space Station and Space Shuttle (ISS-12A.1 / STS-116), originally scheduled for May 2003 (no current launch date available). Initial experimental work, however, took place on a planar air-bearing table. Up to three SPHERES were floated on the 4 ft × 4 ft glass air-bearing table. Figure 3.2 shows a SPHERES unit mounted on a float interface for the planar testbed.⁸⁹

A tethered satellite system offers several design features: gravity gradient stability, vibration and electromagnetic isolation of subsystems, power production, and propulsion. Unfortunately, there has been only one successful tethered space system to date, TiPS, the Tether Physics and Survivability Satellite Experiment. Another effort from Stanford University's ARL, this time to understand some of the complications which lead to tether system failures, led to the development of a planar air-bearing testbed that simulates the microgravity field experienced by a 1.25 mi long tethered satellite. One end of the tether is fixed, while the natural dynamics of the free end are used to control the attitude of the payload.⁹⁰

Researchers at the University of Washington have investigated the usefulness of micro-



Figure 3.2: One of MIT's SPHERES During a Planar Test²

electromechanical system (MEMS) actuators for docking in the low-torque translational environment provided by a planar air bearing. Each ‘puck’ consists of a set of vertically stacked decks, floating by means of an on-board air system. Two cameras provide stereoscopic imagery for range finding. The effectiveness of such MEMS actuators scales: these experiments have proven their usefulness in moving a 1 lb puck with an actuator area of 0.3 in.², and scaling indicates that a patch of only 10 in. radius would be sufficient to position satellites weighing 90 lb when in orbit.⁹¹

3.2 Rotational Systems

The ideal spherical air-bearing testbed would allow its payload unconstrained angular motion in three axes. Actually providing this level of rotational freedom is difficult and in practice requires constraining payload volume. ‘Tabletop’ and ‘umbrella’ style platforms (Figure 3.3, parts (a) and (b), respectively) provide full freedom of spin in the yaw axis but pitch and roll motion are typically constrained to angles of less than $\pm 90^\circ$. The main structure of a tabletop system usually mounts directly onto the flat face of a hemispherical bearing, and components are mounted to this plate. Umbrella systems interface via an extension rod protruding from the top of a fully spherical bearing, and the primary structure typically extends outward and down, caging the bearing and pedestal like an umbrella held on a very short handle. Careful design of the pedestal and cradle can increase the motion-space of these configurations. Another possible style, again on a fully spherical bearing, offsets the mounting area away from the center of rotation by means of two opposing arms, ‘dumbbell’ style (Figure 3.4). This configuration greatly reduces structural interference within the rotation space of the payload and thereby provides unconstrained motion in both the roll and yaw axes. Note that the yaw axis for

each configuration is defined to be nominally parallel to the gravity vector. For dumbbell systems, the roll axis is defined by the mounting arms; roll and pitch are indistinguishable for tabletop and umbrella systems. The bearings illustrated in Figures 3.3 and 3.4 must of course each rest on top of a pedestal, not shown here for clarity. We continue the discussion of air-bearing test facilities keeping these geometries in mind.

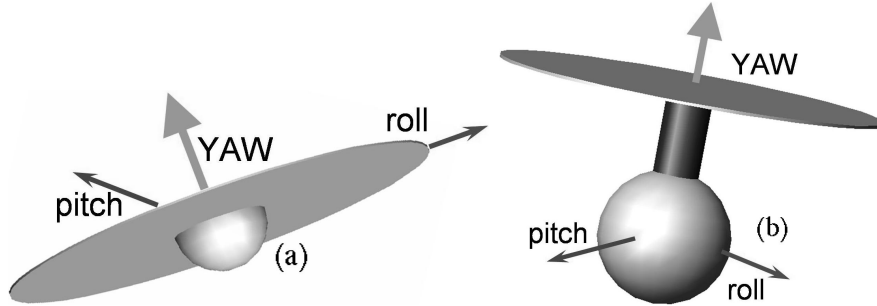


Figure 3.3: 'Tabletop' (a) and 'Umbrella' (b) styles: full freedom in yaw

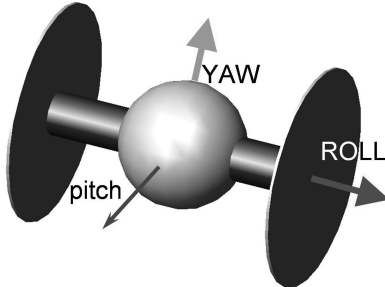


Figure 3.4: 'Dumbbell' style: full freedom in yaw and roll

3.2.1 Tabletops and Umbrellas: Freedom in Yaw

Open documentation is available for more than 10 spherical air bearings in use during the early 1960s. As is often the case with classic engineering, rigorous systems were successfully developed without the benefit of precedent or heritage. The earliest system on which we have complete information is shown in Figure 3.5: a three-axis spherical air bearing developed in 1959 at the Army Ballistic Missile Agency (this facility merged into NASA Marshall Space Flight Center in 1960). This umbrella style system provided a 900 lb payload full freedom in yaw and $\pm 120^\circ$ in pitch and roll.³ Such performance is impressive, even by modern standards. This air bearing was used in an experimental case study on the effects of bearing imperfections on disturbance torques;⁹² extensions of research on hydrostatic support structures had evolved into investigation of hydrodynamic air bearings by 1960.⁹³ Researchers at NASA Ames Research Center made use of

this testbed along with their own 4000 lb capacity tabletop testbed in the development of control laws for the NIMBUS second generation weather satellite (nadir pointing) and the proposed Orbiting Astronomical Observatory (inertially pointing).^{94,95,96}

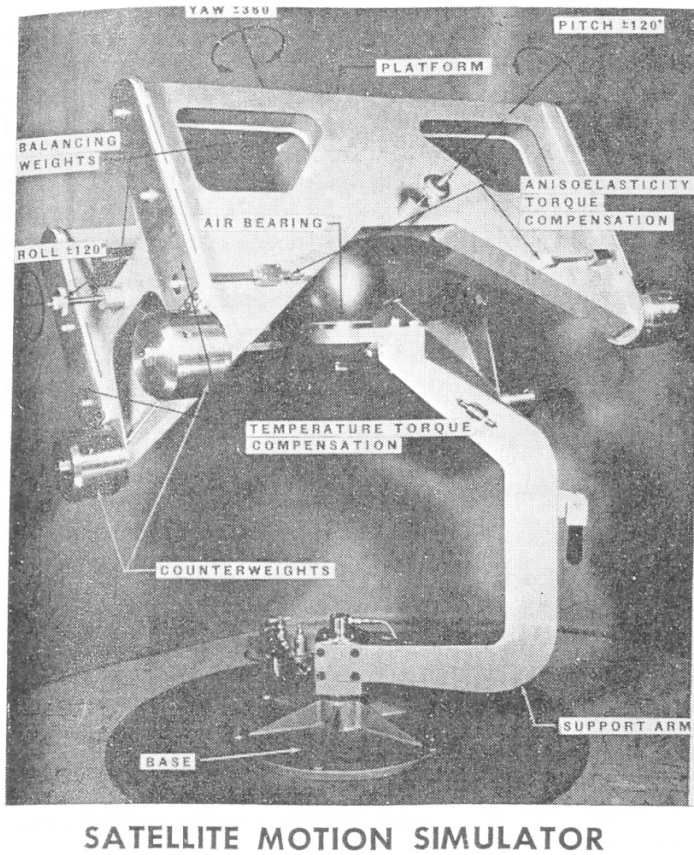


Figure 3.5: NASA Marshall Space Flight Center's Air Bearing, circa 1960³

NASA Goddard Space Flight Center developed an early umbrella configuration spherical air bearing designed for measuring energy dissipation. By 1976, poor (or nonexistent) modeling of dissipation effects had caused failures on several NASA spacecraft, including Explorer-1, Applications Technology Satellite-5, and TACSAT-1. Although the problem had been recognized by this time, it had not been well resolved: modeling the diverse processes that contribute to dissipation effects, including fluid slosh, mechanism movement, and structural bending, is prohibitively complex. Experimental identification of these processes had also proven challenging with previous facilities; measurement of internal dissipation is an area of experimentation where air bearings offer one of only a few possible solutions.⁹⁷

Four types of energy dissipation processes were quantified on this testbed: fuel slosh, passive dampers, reaction wheels, and active nutation dampers. In order to make the tests as realistic as possible, payload mass properties were tuned to those of the flight vehicle while actuator and sensor suite geometries were configured as per the flight vehicle. The testbed permitted nutation angles of 12° . Fuel-slosh tests were performed on six very different vehicle geometries with a range of fill ratios within each physical configuration. Engineering models of fluid-filled nutation dampers were installed on five flight-condition models to experimentally measure their effectiveness. Two reaction wheel designs were tested in simulation of nutation problems encountered during flight. Information gained from these tests led to further development and testing of two active nutation dampers.⁹⁷

The earliest spherical air bearing used at a university was evidently developed at Stanford University in 1975. This tabletop facility was used for center of mass identification in an otherwise fully known physical system. This research evolved from a preceding planar air bearing project.⁹⁸

These systems represent, at a minimum, the first generation of unclassified air-bearing test facilities. Concurrent literature makes reference to numerous other operational systems for which further documentation is not readily available.^{99,100} Early systems were more than likely government classified or company proprietary, and hence open documentation does not exist. During that time (and since) many other large- and small-scale air-bearing testbeds were built at the facilities of spacecraft prime contractors including Lockheed Martin, Boeing, TRW, and Hughes. However, because of the proprietary and, often, classified nature of those programs, open documentation describing these testbeds is generally unavailable.

Considering only the systems for which open documentation is available, however, the initial technological understanding demonstrated in these designs is impressive. Major efforts were made to keep the payload's center of mass coincident with the bearing's center of rotation to minimize gravity effects. Primary mounting decks were designed to maximize the useful rotation space of the systems, but were kept sufficiently rigid so as to avoid platform flexure with changes in attitude — the anisoelastic effect. Optical and other non-contact sensors were developed specifically for these facilities. This level of attentiveness to design details led to the development of unique, highly capable air-bearing test facilities at McDonnell Douglas Astronautics Company–West, the Jet Propulsion Laboratory, NASA Langley Research Center, United Aircraft Corporation, Grumman Aircraft Engineering Corporation, the General Electric Company, and TRW Systems by the early 1970s.^{101,99,102} Each of these systems was custom designed and built. Much of the design and manufacturing information on these early systems has been lost, and the machine shops that fabricated them closed. Modern commercial air

bearings do not typically provide the same air gap stability as these original systems; a group at NASA Marshall Space Flight Center has recently been recreating the historical designs and manufacturing processes from available documentation in an effort to regain this lost precision.¹⁰³

Early use of air-bearing systems was largely limited to government and industry laboratories. Now, state-of-the-art systems are common in university settings. The Naval Postgraduate School's Three Axis Attitude Dynamics and Control Simulator, shown in Figure 3.6 during an optical relay simulation (with Dr. Marcello Romano in the background), is currently used in the Optical Relay Spacecraft Laboratory of Naval Postgraduate School's Spacecraft Research and Design Center. First developed in 1995, this tabletop platform carries a suite of actuators and sensors including three reaction wheels, cold-gas thrusters, rate gyros, a magnetometer, and an optical attitude sensor.¹⁰⁴ The air bearing, a Guidance Dynamics Corporation system, provides a 450 lb payload full freedom in yaw and $\pm 45^\circ$ of tilt in pitch and roll.¹⁰⁵ One objective of the simulator is to demonstrate the dynamics and control of a twin-mirror bifocal relay satellite that receives and re-targets laser beams. The school's superintendent, Rear Admiral David R. Ellison, describes the project as the “epitome of the joint, interdisciplinary research efforts that will drive our nation’s future military capabilities, and which none of us could do alone.”⁴ The Naval Postgraduate School has begun development of another spherical air-bearing testbed in support of the bifocal relay mirror spacecraft program; the new facility is intended to verify flight hardware in the loop.¹⁰⁶



Figure 3.6: Naval Postgraduate School's Three Axis Attitude Dynamics and Control Simulator⁴

Students at Utah State University designed and constructed a custom air-bearing test facility in 1997; initial system requirements were sized for the intent of testing the attitude determination and control system of the Space Dynamics Laboratory's Skipper spacecraft.¹⁰⁷ The tabletop system provides $\pm 45^\circ$ of deviation from the horizon. Through the use of this testbed, "a significant number of integration problems [between spacecraft subsystems] were identified and resolved easily."¹⁰⁸

The Tele-Education in Aerospace and Mechatronics (TEAM) laboratory is an international project that makes use of modern multimedia and telecommunications technologies in order to host a virtual laboratory among the seven member universities: three in Canada, the Université de Sherbrooke, the University of Victoria, the University of Toronto, and four in Europe, the University FH Ravensburg-Weingarten, the Università di Bologna, the Aalborg University, and the University of Siegen. One of the lab facilities located at the Université de Sherbrooke is TEAMSAT. TEAMSAT is unique among air-bearing spacecraft simulators in that it is representative of the European Space Agency's PROBA spacecraft; all simulator hardware is mounted within the spacecraft's structural bus. Flexible mock solar panels have been added to the design in order to allow investigation of non-rigid body effects.¹⁰⁹

The School of Aerospace Engineering at Georgia Tech has also recognized the value of air-bearing research; they now have two tabletop style air bearings. Georgia Tech's first-generation system was developed to minimum operational capabilities in 2001. This system is primarily being used for undergraduate and graduate education. It was designed and manufactured by Specialty Components, Incorporated, and provides pitch and roll angles of $\pm 30^\circ$ for a 300 lb payload.^{110,111} Georgia Tech's second-generation system is designed with advanced investigations of nonlinear control in mind; it is equipped with a suite of eight cold gas thrusters and four variable speed control moment gyros, and has the same performance characteristics as their first-generation testbed.¹¹²

We have presented some of the diverse settings that air-bearing test facilities can be found in. Now we explore some of the many goals which are achieved through their use. Certainly experimental facilities are found to be most useful in the investigation of phenomena for which we do not have effective process models. The equations of motion (and their solutions) for the problem of a rigid spin-stabilized projectile are documented: solutions can be described by a slow precession mode with a fast nutation.¹¹³ In contrast, analytical models of projectiles with liquid-filled cavities or free-floating internal debris do not lend themselves to simple, closed-form solutions. Thus the accuracy of a testbed for the investigation of real-life projectiles may be verified analytically for simple rigid models and then extended upon for the investigation of more complex problems. Boeing Satellite Systems (previously Hughes Space and Communications) has for decades been

at the forefront of experimental research in fluid/structure interaction. Since the late 1980s, this research has included experimental testing using a small spherical air bearing that supports a dual-spin spacecraft configuration. This rig has successfully predicted damping time constants for several commercial and government spacecraft. Similarly, the Department of Mathematics and Ballistics of the British Royal Military College of Science developed a custom tabletop facility for the experimental study of low-mass (less than 2 lb), liquid-filled projectiles in the early 1980s. By exchanging test sections, they can investigate various model geometries and slosh materials with coning angles of 10° .¹¹⁴

Complex structural dynamics are also difficult to model accurately without some sample of experimental data for comparison. Two of the largest spherical air-bearing facilities, the Air Force Research Laboratory's Advanced Space Structure Technology Research Experiments (ASTREX) and the Naval Research Laboratory's Reconfigurable Spacecraft Host for Attitude and Pointing Experiments (RESHAPE), provide facilities for the investigation of control/structure interaction. Both facilities were developed in the early 1990s.

ASTREX can support massive loads, up to 15,000 lb. Shown in Figure 3.7, the core of this umbrella testbed is an 18.9 in. diameter spherical air bearing that provides full freedom in one axis and $\pm 20^\circ$ of freedom in the other two axes. The initial payload structure was modeled from a three-mirror space-based laser beam expander, a fairly generic yet realistic payload body for engineering questions of current interest.¹¹⁵ The ASTREX facility has been used to research topics ranging from robust nonlinear control and model reduction techniques to the design and implementation of coupled attitude control/energy storage schemes and lightweight composite structures with embedded sensors.⁵

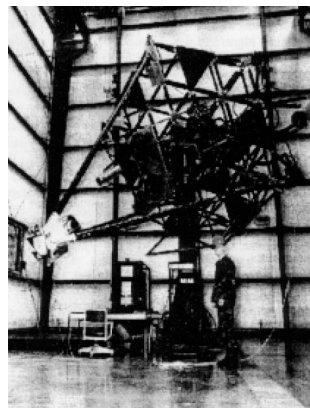


Figure 3.7: Air Force Research Laboratory's ASTREX Testbed⁵

RESHAPE provides $\pm 30^\circ$ of motion about the horizontal axes for a 2500 lb payload. More modest than ASTREX, this tabletop facility has nonetheless been used successfully in the

experimental verification of nonlinear controls of rigid bodies with flexible appendages.¹¹⁶ RESHAPE has been used to verify the effectiveness of smart structures and was used for early experimental work in GPS attitude determination techniques.¹¹⁷

Honeywell's Momentum Control System and Line of Sight (MCS/LOS) Testbed, shown in Figure 3.8, resembles an optical or radar satellite with a large dish at the nadir end. This 1000 lb testbed is the first phase in a project that will culminate with a 3000 lb system steered by six 225 ft-lb-sec control moment gyros (CMGs). The core of this testbed is an umbrella style spherical air bearing from Guidance Dynamics Corporation offering unconstrained motion about the vertical and $\pm 30^\circ$ of motion about the horizontal axes. The testbed structure is built of modular truss elements, any of which can be replaced with structural dampers (D-StrutsTM). The structure can be reconfigured to represent a number of spacecraft architectures, including those with booms and reflector dishes. Its array of six small CMGs (0.25 ft-lb-sec momentum and 1 ft-lb torque) can also be reconfigured to match any array geometry of interest. An array of three flight-quality reaction wheels has also been designed as a modular, drop-in replacement for the six small CMGs if reaction-wheel dynamics are of interest.

The CMG array is mounted on a hybrid active/pассив vibration isolation and steering system (VISS). The combination is known as a Momentum Control System (MCS). The VISS attenuates CMG-induced disturbances and can be used to augment the attitude control by steering the entire CMG array and introducing passive damping in the structure, generally adding phase to the attitude control. Mirrors mounted on the testbed are used to reflect laser light from a pneumatically isolated table onto three CCD cameras mounted on the same table. The resulting focal-plane data (six pieces of information) are resolved into sub-microradian jitter measurements at a sample rate of up to 30 Hz and, optionally, can be blended and used for attitude feedback as a virtual star tracker via Markley's FOAM algorithm. The rate sensor is an AG30 ring-laser gyro with less than $1^\circ/\text{rt-hr}$ angle random walk.

Phase two of the project will include Honeywell's Miniature Inertial Measurement Unit, which provides less than $0.01^\circ/\text{rt-hr}$ random walk. Both phases of the project will incorporate the same adaptive, closed-loop mass-balance system: three prismatic actuators with 10–50 lb weights used to eliminate mass-center offset from the air bearing rotational center to well within $0.1 \mu\text{m}$. Ultimately both the current, smaller testbed, and the larger one are expected to be operational within the same lab, using two air bearings simultaneously. The facility will offer not only MCS and line-of-sight research capabilities but also a testbed for intersatellite communication and relative-attitude steering for formation flying.

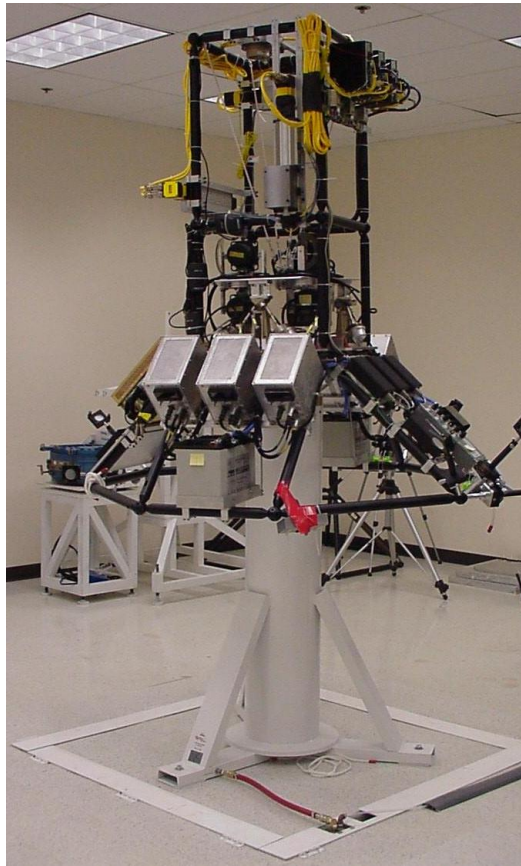


Figure 3.8: Honeywell Space Systems's Momentum Control System and Line of Sight Testbed⁶

The next generation of agile, precisely pointed space systems will demand novel approaches to attitude dynamics and control. The paradigm of ever stiffer, ever more massive designs is likely to give way to active, passive, or hybrid active/passive structural control of payloads with soft, well-damped bus-to-payload interfaces. Agility, often achieved through the use of CMGs, can also benefit from the highly damped, readily predictable dynamics characteristic of this new paradigm. The MCS/LOS testbed is designed to assist in research, demonstration, and validation of hardware and software architectures for such spacecraft. It is meant to be available not just to Honeywell, but also to Honeywell's customers, industry partners, and sponsoring government organizations.⁶

The problem of high-speed interception and rendezvous is also difficult to model without experimental validation. Guidance Dynamics Corporation designed and manufactured two tabletop test facilities to address this need. For Boeing North American Space Systems Division, Guidance Dynamics Corporation developed an air-bearing platform with $\pm 5^\circ$ of deviation from the horizontal for a 1000 lb payload. The platform includes

1000 cubic inches of regulated cold gas to feed sixteen 25 lb high response thrusters. The system also includes an arcminute-adjustable initialization and release system. In support of the Air Force Brilliant Pebbles Interceptor program Guidance Dynamics Corporation provided a system that supports a 100 lb payload through $\pm 15^\circ$ slews to Hughes Missile Systems Company. This testbed provides roll accelerations of over $5000^\circ/\text{s}^2$. To keep roll moments of inertia low, the flight guidance electronics were placed off-board and data are provided via a fiber-optic link.¹¹⁸

International use of air-bearing platforms is documented in the same time frame as work in the United States. Topics of interest are also comparable, including experimental validation of attitude control systems,¹¹⁹ and the stability characteristics¹²⁰ and controllability¹²¹ of spinning spacecraft. More recent work has involved attitude control by means of an actuated mass center¹²² and hardware in the loop testing of modern spacecraft.¹²³

3.2.2 Dumbbells: Freedom in Yaw and Roll

Perhaps the most drastic change in air-bearing test facilities since their earliest use is the flexibility to allow a payload unconstrained rotation in more than one axis. Although the facilities described above are undeniably useful tools for experimentation in nonlinear rotational dynamics, there are many flight conditions which cannot be adequately simulated with only one complete degree-of-freedom.

The University of Michigan's Triaxial Air Bearing Testbed, developed in the late 1990s, is based on an 11 in. diameter spherical air bearing produced by Space Electronics, Incorporated. As shown in Figure 3.9, a stiff shaft passes through the center of the sphere and supports a pair of mounting plates; the shaft is hollow, allowing the wiring harness to pass through the center of the bearing and reach hardware on either plate without interfering with the motion of the payload. The dumbbell configuration provides $\pm 45^\circ$ of tilt in one axis, with the other two axes entirely free of motion constraints. The triaxial testbed sensor suite includes a three-axis magnetometer, accelerometer, and rate gyro. Actuators for this 360 lb payload include six custom reaction wheels and four fans used as thrusters. Recent results include new approaches to parameter identification, adaptive control, and nonlinear attitude control.^{124, 125, 7}

The Air Force Institute of Technology's SIMSAT is based on a similar air-bearing system from Space Electronics, Incorporated; it can support a 375 lb payload and provides $\pm 30^\circ$ of freedom about the pitch axis. Developed in 1999, initial work with SIMSAT has involved basic attitude control and the functional multimedia interface; current work is



Figure 3.9: University of Michigan’s Triaxial Air Bearing Testbed⁷

investigating attitude determination requirements to recognize and locate parasite masses added to the system.¹²⁶

The bulk of the research effort detailed in this dissertation has led to a unique facility at Virginia Tech comprised of two spherical air-bearing platforms, the Distributed Spacecraft Attitude Control System Simulator. Both air bearings are Space Electronics, Incorporated, models: the smaller is a tabletop bearing supporting a 300 lb payload that can tilt $\pm 5^\circ$ from the horizontal; the larger system is the same model of air bearing being used for SIMSAT. Each air bearing is equipped with three-axis accelerometers and rate gyros for attitude determination. Attitude control options include three-axis momentum/reaction wheels, compressed air thrusters, and CMGs. The payload’s center of gravity can be maintained at the bearing’s center of rotation via a triad of linear actuators; alternatively, attitude control schemes by center of gravity placement can be investigated. The uniqueness of Virginia Tech’s system stems not from particular individual capabilities of either platform, but rather the ability to implement distributed control laws between the two. Coupled with a third, stationary system, it provides an experimental facility for formation flying attitude control simulation. Planar air bearings give the opportunity to test control schemes involving the relative motion of two bodies, but the required coordination in pointing is typically lost. This testbed allows algorithms for relative attitude control to be implemented.⁷⁹ More details on this system are provided in Chapter 4.

The UCLA / Cal Tech Model Spacecraft testbed uses a unique ‘Dyson Sphere’ design,[†]

[†]Terminology inspired by Freeman Dyson, “Search for Artificial Stellar Sources of Infrared Radiation,” *Science*, 1959, <http://www.sns.ias.edu/~dyson/>.

providing even more freedom than a dumbbell configuration. As shown in Figure 3.10, in contrast to all of the systems previously discussed, this testbed uses hollow spherical bearings with all hardware mounted internally. These small systems provide $\pm 180^\circ$ of freedom in all three axes. Despite this great advantage in attitude freedom, current tests involve only single axis rotations. Two of the payloads are floated simultaneously, and spin is controlled by an internal wheel. The ‘leader’ payload is given a predefined series of velocity commands, and the ‘follower’ spacecraft tracks and matches that profile. Future plans include formations with more than one follower spacecraft.⁸

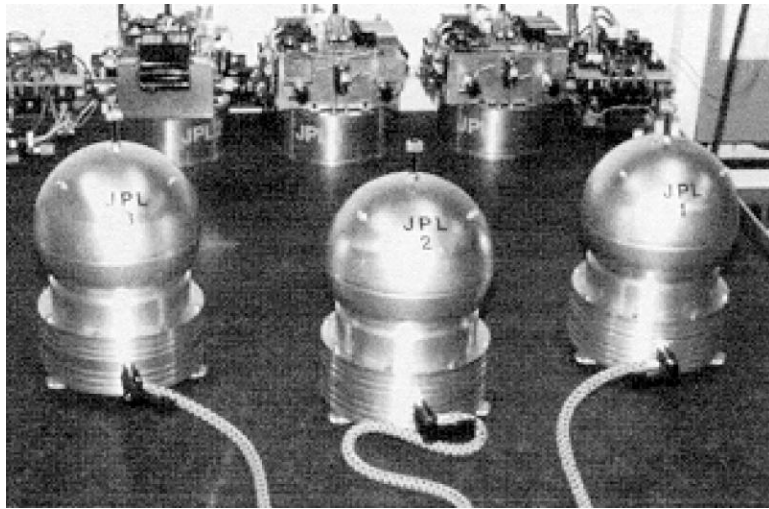


Figure 3.10: The UCLA / Cal Tech Model Spacecraft Spheres⁸

3.3 Combination Systems

The most elaborate air-bearing systems combine planar and rotational motion into simulators that provide up to six completely unconstrained degrees-of-freedom. Marshall Space Flight Center’s Flight Robotics Laboratory, described by the NASA Federal Laboratory Review in 1994 as “a facility that provides a quality, capability, capacity, product, technology, condition, or process recognized by the world aerospace community as among the best in the world” has a 44 ft \times 86 ft precision floor. The Air Bearing Spacecraft Simulator used on the planar floor provides a 400 lb payload six degree-of-freedom motion via a floating spherical air bearing coupled with a cylindrical lift. To further enhance simulations, the Flight Robotics Laboratory also provides facilities for two-way radio communication and a GPS satellite simulator. The Contact Dynamics Simulation Laboratory provides the finer resolution experimental facility needed to test docking mechanisms. These simulation capabilities can be linked into the Avionics System Testbed,

which produces real time simulations of the full mission timeline in the Vehicle Simulation Laboratory, the Engine Simulation Laboratory, and the Actuator Test Laboratory.¹²⁷

Lawrence Livermore National Laboratory has an ongoing effort to foster the development of autonomous, agile microsatellites (defined as satellites with a mass of 20–220 lb). Spacecraft of interest to Lawrence Livermore National Laboratory include those with the ability to perform precision maneuvers autonomously, including rendezvous, inspection, proximity operations, formation flying, docking, and servicing. Payloads up to 70 lb are provided full freedom in yaw, $\pm 15^\circ$ in pitch and $\pm 30^\circ$ in roll on a Dynamic Air Bearing test vehicle. The vehicle can then either be floated on a 5 ft \times 25 ft glass top Dynamic Air Table (first tested in the late 1990s), or can be mounted on one of two perpendicular 50 ft Dynamic Air Rails (a new development in this test facility). The planar testbed host is shown in Figure 3.11. The large-scale, outdoor, linear rail system shown in Figure 3.12 yields five relative — four individual — degrees-of-freedom for a pair of payloads.¹²⁸



Figure 3.11: Lawrence Livermore National Laboratory's Dynamic Air Table host⁹

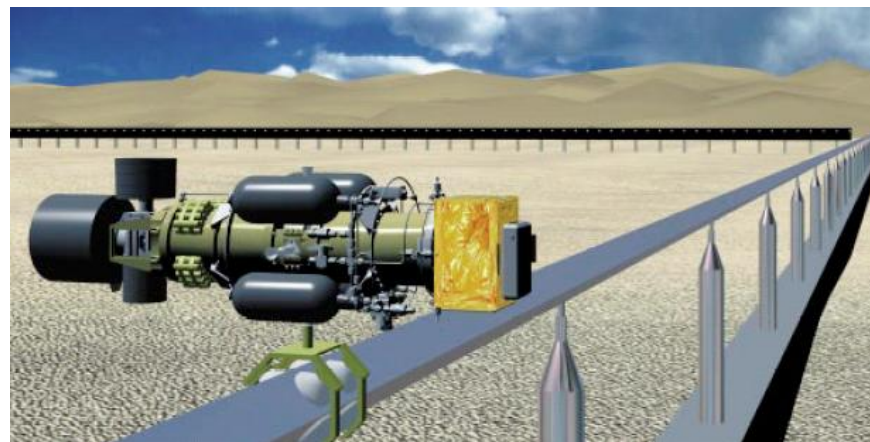


Figure 3.12: Lawrence Livermore National Laboratory's Dynamic Air Rail Concept⁹

We have previously discussed the experimental investigation of fuel slosh on three degree-of-freedom testbeds. These systems enforce a somewhat unrealistic constraint: the center of rotation of the test body is constrained to rotate about the center of curvature of the bearing — a fixed point in an Earth-fixed, rotating reference frame. Generally, the center of mass of the flight payload will be moving with respect to a body-fixed coordinate system due to internal mass motion and propellant usage. Oral Roberts University has developed a four degree-of-freedom air-bearing test facility for the investigation of coning stability characteristics of non-rigid, spinning spacecraft in the presence of thrust. They have solved the center of mass constraint problem by mounting a custom tabletop air bearing on a turntable. The turntable traverses the air bearing about an 128 in. diameter circular path at a speed of 1 Hz, providing a centripetal acceleration of 6.5 g's. Thus the 200 lb payload experiences a simulated thrust composed of the centrifugal and gravitational forces. Modern rocket motors rely on small, active thrusters to control coning motions; this testbed is being used to develop a passive mass-spring-damper control device to eliminate these motions in a less expensive way.¹¹³

A new air bearing facility for validation of formation flying algorithms has been developed for the Terrestrial Planet Finder (TPF) mission, the Formation Control Testbed at the NASA Jet Propulsion Laboratory. This facility will be used to demonstrate mission scenarios including aspects of formation acquisition, collision avoidance, and observation-on-the-fly maneuvers. The Formation Control Testbed allows up to five air-bearing vehicles to maneuver simultaneously. Each vehicle is a tabletop-style air bearing with three planar float pads, providing five degrees of freedom. A small amount of freedom in the sixth direction is available via a vertical articulated stage. The vehicles are equipped with flight-representative hardware, including thrusters, reaction wheels, and relative motion sensors.¹²⁹

3.4 Manned Space Flight

The US manned space flight program has benefitted from the use of air-bearing training facilities from the beginnings of the program. Starting in late 1959, each Mercury astronaut was scheduled for 12 hours of “Essential” level training on the Air-Lubricated Free-Attitude trainer, ALFA. Designed and developed by the NASA Manned Spacecraft Center, the trainer translated across the floor and had full freedom in roll and $\pm 35^\circ$ in pitch and yaw.¹⁰ Figure 3.13 shows the trainer. The astronaut would lie in the central open area, above the spherical bearing. The base pads (as in the lower right corner) provided the air cushion for planar motion.

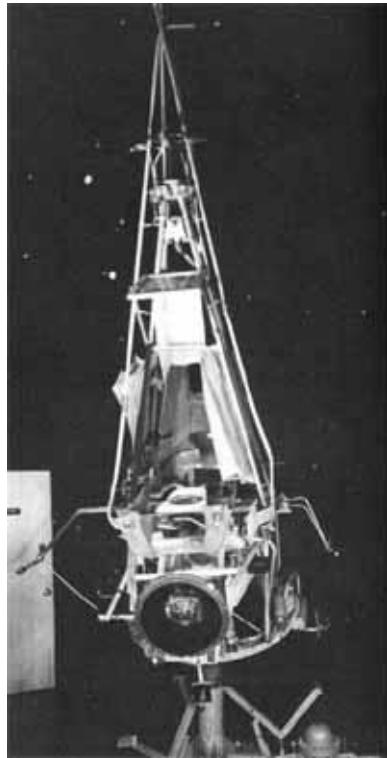


Figure 3.13: The ALFA Mercury Astronaut Trainer¹⁰

NASA Ames Research Center also had an early rotational motion training platform,⁹⁹ and the Boeing Company shortly followed suit in their development of a Lunar Orbiter Attitude Control Simulator.¹⁰⁰

The manned space program continues to make use of planar air-bearing research. In 1998, a NASA Technical Publication detailed the use of Marshall Space Flight Center's Precision Air Bearing Floor in experimental evaluation of skill in EVA mass handling. Astronauts were assigned various EVA-related challenges in order to evaluate their adaptability and skill in handling mass in a low-force environment. Although the planar motion testbed does not provide the same level of freedom as the EVA simulation water tank, it provides an easily instrumentable, low-drag facility.¹³⁰

3.5 Facility Enhancements

There are many advantages of air-bearing facilities over other mechanical options in providing an unconstrained motion-space. However, the low-torque setting provided by the bearing is reasonably only as useful as the facility in which it is housed: eliminating

gravity torque effects from the simulation provides little benefit if other environmental torques affect the motion. Devising ways to mitigate these other disturbance torques is nearly as well developed as the air-bearing facilities themselves. Depending upon required precision, it is perhaps in this area that the effectiveness of a facility can be measured.

If papers can be defined generationally, the grandfather of this work is a conference paper presented by G. Allen Smith at the Role of Simulation in Space Technology conference held at Virginia Tech in 1964.⁹⁹ Smith presented a description of several systems, along with an overview of the torques which act on the rotor of an air bearing. Smith defined four classes of disturbance torques and listed particular sources for each group, as shown in Table 3.1.

Table 3.1: Torques Acting on Air-Bearing Systems

I. Torques Arising from Platform	III. Torques from Environment
– Static Unbalance	– Air Damping
– Dynamic Unbalance	– Air Currents
– Anisoelasticity	– Magnetic Fields
– Material Instability (stress, temperature, humidity, evaporation)	– Vibration
– Gravity Gradient	– Radiation Pressure
–	– Equipment Motion (solenoids, relays)
II. Torques from Bearing	IV. Torques from Test System
– Aerodynamic Turbine Effect	– Electrical Wire to Base
– Exhaust Air Impingement	– Mass Shift in Bearings and Loose Fits
–	– Battery Discharge
–	– Reaction Jet Supply Discharge
–	– Replacement of Components

Torques from the groups I and IV can be mitigated through testbed design: well designed structures outfitted with well chosen components. Group II effects received more attention in the early development of air-bearing systems than they do now; although internal bearing effects may be important in the design and operation of industrial gas bearings, they impart a negligible effect upon the classes of systems we are considering. The third class of disturbance torques, those from the laboratory environment, are the most challenging to resolve.

Several facilities have developed large scale means to mitigate environmental torques. Thermal and air currents often cause the grossest effects and are simplest to eliminate:

several NASA facilities are installed within vacuum chambers.^{96,97} The facility designed for the Boeing Company's Lunar Orbiter Attitude Control Simulator could not make use of this solution, as it was piloted. Instead, the room design included full air circulation and thermal control. Further, the system was mounted on a 90,000 lb concrete slab supported by seven air springs; thus the system was effectively isolated from seismic effects.¹⁰⁰ Marshall Space Flight Center installed one of their systems within a set of Helmholtz coils in order to cancel the effect of the terrestrial magnetic field on the payload.⁹⁹

3.6 Summary of Air-Bearing Spacecraft Simulators

Sputnik launched in 1957. Explorer-1 launched in 1958. The earliest air-bearing spacecraft simulator is documented in 1960. Truly these systems have played an integral role in improving space technology since the beginnings of space exploration.

Planar air bearings provide an ideal testbed for simulating two-vehicle dynamics. Control techniques for relative orbital maneuvers — formation flying, rendezvous, docking, space construction, tethered systems — can be fully developed and tested prior to launch. Spherical air bearings offer the freedom to experiment with attitude control techniques: pointing, tracking, performing system identification, and compensating for unmodeled dynamics. Facilities that combine these techniques can nearly replicate the actual low-force, low-torque flight environment. Such systems have played a vital role in the development of both manned and unmanned spacecraft.

In Figures 3.14 and 3.15, we attempt to summarize the spherical air-bearing facilities discussed in this historical survey. Two measures of testbed effectiveness, payload weight and angular freedom, are plotted against testbed development date. As all of the systems provide full freedom in yaw ($\pm 180^\circ$), this value is not indicative of performance; the larger of the pitch and roll angles is plotted. We distinguish four classes of air-bearing systems in these plots. First we group by development setting: systems from government and industry laboratories versus those in university settings. We further subdivide each of these into domestic and international systems. Shaded symbols indicate government and industry facilities, and hollow symbols indicate university testbeds. Squares represent domestic systems, circles international. Note that the sampling of data in Figures 3.14 and 3.15 may appear inconsistent; the disparities are due to incomplete data recorded in the literature.

The payload weight distribution plot shown in Figure 3.14 demonstrates several trends. As might be expected, government and industry facilities were developed several years

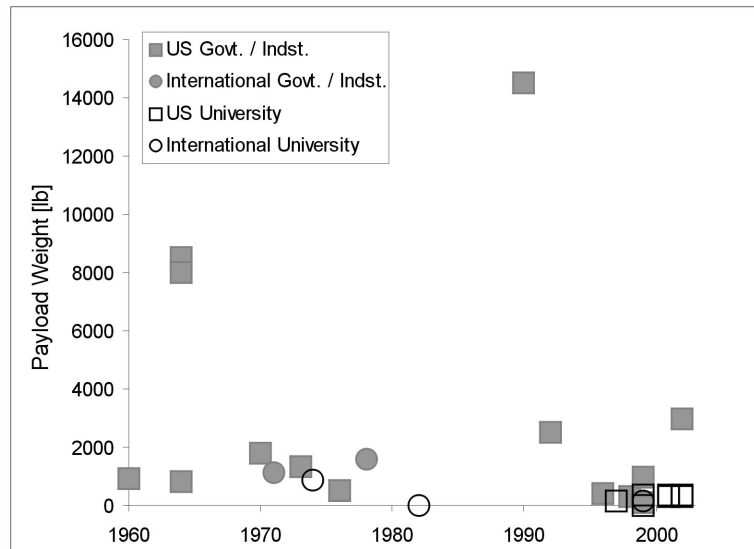


Figure 3.14: An Overview of Air-Bearing Testbed Capabilities: Payload Weight [lb]

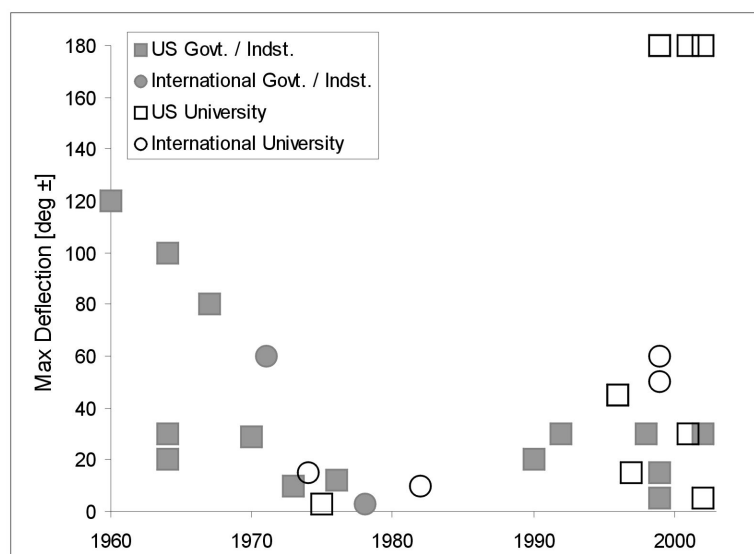


Figure 3.15: An Overview of Air-Bearing Testbed Capabilities: Tilt [deg ±]

prior to the first university facilities. This trend is likely due to the classified nature of the research and technology validation studies being performed. Also, because university facilities are typically smaller and less-equipped than government and industry labs, the payloads are necessarily smaller. Figure 3.15 demonstrates some additional trends. Early government and industry facilities were designed to provide heavy payloads a large motion-space to operate in, and each laboratory developed its own testbed. After an overall decline in testbed capabilities in the mid-1970s through the 1980s, there are now a few highly capable government and industry facilities that are shared by the community. Modern university facilities provide greater angular freedom than those in government and industry, perhaps because university researchers are more interested in the development and validation of new control schemes rather than demonstrating real-world technologies.

The list of references listed here is not exhaustive, though we have included at least one reference for each system. Some systems, ASTREX for example, have been involved in many research projects that are not cited here. We would encourage anyone interested in this subject to only begin their investigations making use of our bibliography. The facilities we have discussed will advance in capability, and new ones will develop. With further research, perhaps additional historical systems can be rediscovered.

3.7 GPS Testbeds

Air bearing testbeds can only serve to demonstrate the relative attitude dynamics or small-scale relative motion among elements of a formation. A different type of simulation is required in order to bring orbital dynamics back into the loop. Because position and relative position knowledge is of such importance in formation flying, much of the component development for these missions revolves around new GPS and cross-linking technologies.

There are several testbeds that have been developed, including the Formation Flying Testbed (FFTB) at NASA Goddard Space Flight Center.^{131,132} The FFTB has been used for several technology demonstrations, including hardware-in-the-loop testing and demonstration of GPS for precise decentralized relative navigation.^{133,134} Relative navigation using GPS involves more than simply differencing the filtered position and velocity solutions between spacecraft. Although such a process is certainly possible, it provides a relative navigation solution with errors on the order of the absolute navigation solution; improvements beyond this resolution are possible for spacecraft flying in formation because, typically, each of the formation spacecraft receive signals from the same set of GPS satellites. Moreover, the GPS signals are all traversing nearly the same path through the ionosphere. As such, the errors in the raw GPS signal are very similar for each spacecraft in the formation. By processing the relative signal in this form it is possible to achieve much greater accuracy in the relative navigation solution.¹³³ Carpenter and Schiesser have investigated the problem of semi-major axis knowledge via GPS orbit determination; they conclude that errors in the semi-major axis estimate are largely due to poor velocity solutions, and would not benefit from inclusion of carrier-phase data alone.¹³⁵ Proper filtering that takes advantage of orbital dynamics is necessary for an ideal solution, however, several simple techniques are available to provide improved estimates beyond the initial GPS solution. An example of such an enhanced filter is presented by Moreau *et. al.*¹³⁶

Researchers at Stanford University developed a planar air-bearing test facility with six pseudolite GPS transmitters for demonstration of GPS in a spacecraft formation.⁸⁸ They have used this system to demonstrate advanced processing of the GPS signal, including the use of carrier-phase and differential carrier-phase GPS sensors.^{137,138}

Technology combining standard crosslink communications with sensors for measuring relative ranges and range rates is being actively developed in support of formation flying missions.¹³⁹ More recently, GPS receivers have been packaged with crosslink transceiver systems for easy integration.^{140,141,142,143,142}

Chapter 4

The Distributed Spacecraft Attitude Control System Simulator

As described in the previous chapters, formation flying is an exciting new area of research and development. However it is also a difficult endeavour, and launching a group of satellites into space is an expensive and risky undertaking. Ventures in formation flying are not undertaken lightly.

The Distributed Spacecraft Attitude Control System Simulator (DSACSS) is a laboratory testbed designed for the purpose of developing and testing formation flying algorithms in a low-risk, low-cost environment. In this chapter, we describe the design and development of the air-bearing hardware and software. We present the equations of motion that govern DSACSS experiments. We describe the problems of real-time attitude estimation, as well as estimation of the mass properties of the systems.

4.1 Design and Development

The design and construction of the DSACSS payloads was as much of an educational experience as the dynamics and control aspects of the project. In this section, we present an overview of the design process for the two air-bearing payloads. As described in Chapter 3, the system dubbed ‘Whorl-I’ is a tabletop air-bearing with $\pm 5^\circ$ of freedom in tilt; ‘Whorl-II’ is a dumbbell-style system with $\pm 30^\circ$ of freedom; these two platforms are the basis of the DSCASS testbed. We also discuss design and development of the DSACSS Operational (DSACSS-Ops) software.

4.1.1 Whorl-I Hardware

The initial design concept was formed by a few preexisting components. The hemispherical air bearing, of course, was the focus of the design process. Early work with this air bearing led to the fabrication of a 3 ft diameter circular aluminum plate with an elaborate bolt pattern for mounting components. A SM3420 SmartMotor equipped with a solid, 6in outer-diameter bronze flywheel provided means for single-axis control. The SmartMotor was controlled by a laptop computer. The sensor suite included a three-axis linear accelerometer and a two-axis tilt sensor, both of which were sampled by a TattleTale8 microcontroller board. The system was powered by a pair of wet lead acid batteries.

System problems in this initial design necessitated several design changes. The primary disadvantage of this design was the system weight: the aluminum plate was unnecessarily massive, as were the wet lead acid batteries. Further, the laptop computer was bulky and awkward. The sensors and actuators functioned, but interfaced with different command computers, making real-time operation impractical. Therefore, after developing some level of comfort with these components, we refined the design.

This effort, which led directly to the configuration design of the Whorl-I payload, was in part dictated by preexisting knowledge held by team members; many components were, as in the initial design, selected unilaterally. Although such procedures do not follow an approved systems-engineering technique for selecting components, every project must start somewhere! This *laissez-faire* attitude should not suggest that design analysis was approached lightly. Rather, we began with performance goals to minimize payload weight and maximize system effectiveness. Effectiveness, in this case, involved finding a balance between available funding and ultimate performance.

The first major design decision was to switch from a solid aluminum plate to an aluminum honeycomb deck. Commercial grade honeycomb is reasonable in price, readily obtainable, and easy to machine. The main issue that arises when working with honeycomb is that screws cannot be inserted directly into the material; an insert must be installed first. This requirement must be considered in the design process, as the inserts — and the epoxy used to hold them in place — add a substantial amount of mass to the structure. However, in this case the added mass is not comparable to the mass of a solid plate structure. A secondary issue when considering honeycomb is the potential for re-machinability. As the system is used for more diverse tasks and new requirements are identified we expect additional mounting requirements to arise, and installing new inserts is less trivial than drilling new holes in a plate. We elected not to pre-install a uniform hole pattern to aid in future functionality because so few components would be able to interface with the pattern without the use of a bracket; brackets add unnecessary mass.

The selection of honeycomb was a good design choice. Weighing under 11 lb, the finished structure (including inserts, epoxy and protective edging) is 77% lighter than the original aluminum plate. The non-conductive outer surface of the honeycomb has an unintended benefit; it prevents many inadvertent electrical shorts. We have not added any new inserts to the honeycomb since its initial manufacture. However, the reticence to do so is largely due to the need to remove all of the current components, including the wiring harness; it is not clear that a solid aluminum structure would have been remachined in the interim, either. We were initially concerned about the potential for internal damage to the honeycomb due to impact shocks but thus far we have observed no weakening of the structure. The current Whorl-I configuration, including a control moment gyro (CMG) unit developed later, is shown in Figure 4.1.

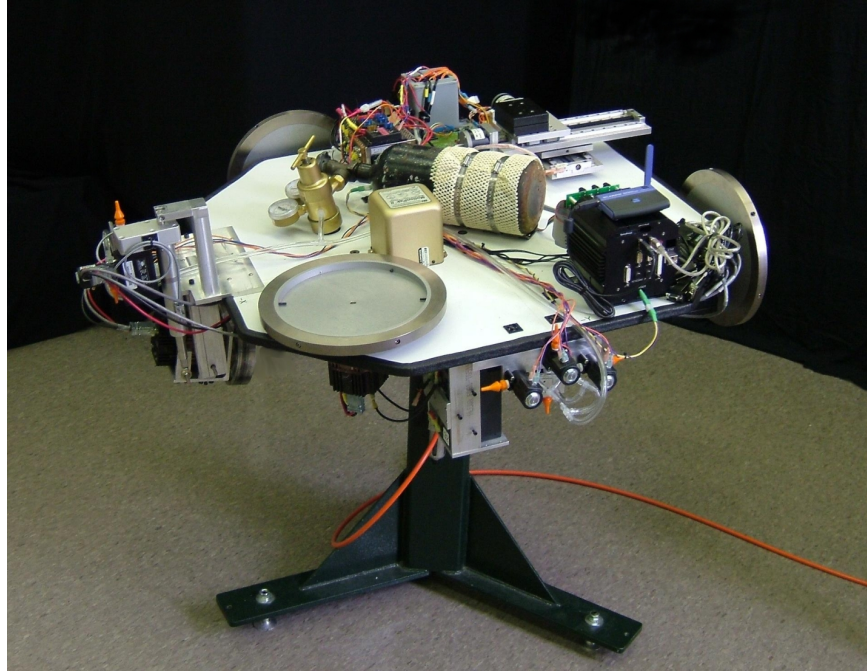


Figure 4.1: Whorl-I

We compared many performance metrics for several different battery chemistries. Sealed lead acid cells proved to be the most useful for this application, as they are widely available, robust, and reasonably compact. Using pairs of 6 VDC cells provided ease in configuration and a wide range of 12 VDC battery chargers to choose from. Several packs are visible hanging below the main structure in Figure 4.1. We initially designed a 48 VDC bus, but after damaging a SmartMotor through an over-voltage / back-EMF condition, stepped down to 24 VDC parallel bus. The lower bus voltage limits the maximum wheel speed, but provides a necessary safety margin and nearly twice the operational time as the original system. High voltage components are powered directly

from the bus; all other components receive power from a 24–12 V DC/DC converter. The converter system works well, as the low-voltage components are typically low power and often more sensitive to power conditioning. It is also a safer and more robust design than would be obtained by pulling different supply voltages off of a single power bus. Motor performance changes as the bus voltage drops, but this can be partly compensated for by including the current bus voltage in the low-level wheel speed controller. One important lesson in power system design that we did not learn early enough is to fuse the main bus and each individual component, and to choose wire gages appropriate for the fuse level. The current system has worked well overall, although we have damaged several batteries, probably due to improper charging.

We also recognized the inefficiency of the solid flywheel design at this point in the design process. For ease in manufacturing, we switched to a simple two-piece design with a steel rim and an aluminum hub. The steel / aluminum design is a good one for several reasons. First, it allows the flywheel rim to be much more massive than the hub, mitigating the need to machine a complex series of radial cuts in the hub to reduce mass. Also, aluminum has a lower rotational burst speed than steel, thus as the flywheel spins the interface between the two surfaces becomes tighter; if the opposite were true we would need a more complicated structural interface than radial bolts. These six bolts also serve as a simple means for balancing each flywheel in order to compensate for small variations in the machining process; washers can be individually added to adjust the mass in fine increments. This interface is apparent in the foreground of Figure 4.2.

The remainder of this design phase included additional component selection and configuration analysis. After damaging one SmartMotor beyond repair, we elected to upgrade to the SM3430 model for its improved performance and flatter continuous-torque profile. Based on experience from a previous project, we switched to a single sensor unit containing three-axis rate gyros and three-axis linear accelerometers, a BEI Systron Donner MotionPak II. More information on this component is provided in Section 4.4. As flight-grade thruster systems are prohibitively expensive, we designed a simple N₂ cold gas thruster system using solenoid valves and nozzles normally used for milling machine coolant systems. Portions of the thruster system can be seen in the foreground of Figure 4.1 and on the rear panel of Whorl-II in Figure 4.2.

Although a major focus of the configuration analysis was to co-locate the center-of-mass of the system with the center-of-rotation of the air bearing, we recognized that accurate static placement would be impossible. At a minimum, the gas tank for the thrusters will cause a change in center-of-mass during thruster maneuvers; although the tank is placed to cause a minimal mass center change in-plane, there is no way to prevent motion in all three directions. Further, a primary source of error in the configuration analysis is the

wiring harness; the harness is too complex to model effectively in a CAD program. As such, it is desirable to have the ability to easily adjust the mass center in all three axes. The battery brackets were designed with this in mind; they are slotted such that they can be moved to aid in coarsely balancing the system. We also chose to include three linear actuators to dynamically move mass in all directions. Each Servo Systems model LPS 8-20 actuator can traverse up to 30 lb across 8 in. This system has proven useful in fine manual balancing and will autonomously perform center-of-mass adjustment during experimental runs as necessary. Two of the Whorl-I linear actuators are visible in the background of Figure 4.1.

We selected components of a PC/104 computer stack after a semester elective course investigating real time systems. We determined that DSACSS does not have any hard real time critical operations, thus options for computer processors and operating systems were nearly unlimited. As shown in the foreground of Figure 4.1, the PC/104 form factor is a small, popular design for embedded computing applications. Each board performs a small set of functions, allowing for development of a fully customized computer. There are many PC/104 manufacturers and vendors, providing a wide selection of parts and competitive pricing. We initially selected a CPU board with a 32-bit 133MHz Tri-M MZ104+ ZFx86 processor with 64 MB of RAM running a lean, customized version of Slackware Linux. An upgrade of this system which will allow faster closed-loop performance is in progress. Several components are commanded through the serial communication interface on the CPU board, easily expandable through the USB bus. The MotionPak II is sampled by a 16-bit Diamond Systems DMM-32 A/D board. Along with the 32 analog channels, the DMM-32 also provides 24 programmable-direction and eight fixed-direction digital lines for logic switching. These digital lines are used to control the thruster solenoid valves. The stack is completed by a power conversion and conditioning board that provides a clean 5 VDC signal. The computers communicate via a local wireless area network.

Although the current Whorl-I design has proven to be viable, it became clear during the development process that more stringent analysis and peer review would be beneficial. This recognition led to a process of multiple, formal design reviews for all new hardware developments, including the design of the Whorl-II payload. We have been extremely successful with most of the components that were designed in this review-intensive environment.

4.1.2 Whorl-II Hardware

This Whorl-II hardware review will not include such elaborate detail as above, partly because the Whorl-II design was highly based on the Whorl-I design, leaving little to

accomplish beyond component placement (which was by no means an easy task). More to the point, I did not design the Whorl-II payload and thus have less commentary to include. These comments are largely based on my participation in the many design reviews leading up to the Whorl-II final design.

Whorl-II presented several new challenges because of the dumbbell system configuration. Components had to be positioned to impact neither the pedestal nor the surrounding cage. Geometric analysis of these constraints led to the development of the shaft extensions and honeycomb end panels as shown in Figure 4.2.



Figure 4.2: Whorl-II

We determined early in the review process that it would be undesirable to put the entire payload on one side of the bearing and balance with ballast on the other side. Instead, we run cables through the hollow center of the bearing as necessary. However, the cross-sectional area available for cabling is small, making it important to group components

intelligently. For example, all thruster components are grouped on one end panel to eliminate the need to route any plumbing through the bearing.

Balancing this payload is more difficult than with Whorl-I because all three axes must be neutrally aligned for proper operation. Moreover, it is not possible to simply place ballast as needed to account for changes in configuration. Instead, an elegant three-axis ballast system was designed. Three-axis linear actuators are also included; in this configuration use of the thrusters changes the mass center dramatically.

4.1.3 DSACSS Software

Our intent in the software development process was to develop modular, easy-to-use, easy-to-maintain code. We achieved this intent through the application of object-oriented software design concepts. In object-oriented programming, classes of software are sufficiently abstracted so as to be useful without requiring knowledge of the internal code. As such, a user can create an instance of a ‘rate gyro’ without regard to the specific rate gyro hardware in use, just the knowledge that it will return rates in a particular set of units. Similarly, the developer of the driver software for a new rate gyro component can construct his code wholly differently than any other developer; only the interface must match.

The DSACSS-Ops software tools are custom-designed with particular DSACSS hardware in mind. However, the abstraction obtained by use of object-oriented programming allows it to be easily extensible. As such, a research group using a similar payload outfitted with different hardware components would only have to modify the lowest level of the code; all higher-level usability interfaces would remain unchanged. The DSACSS-Ops code includes several key features:

1. Configuration parsing: Rather than recompiling the code in order to accommodate a new hardware configuration or controller gain setting, all options are defined in a configuration file that is read in at run time.
2. Algorithms: Includes observers and controllers. Adding a new control law is as simple as writing the equation in C++ syntax. We have written a family of Kalman filters, ready to customize for the dynamics of a particular system.
3. Logical devices: The algorithm interface with the hardware. This code is generic for a type of hardware (*e.g.* ‘rate gyro’) rather than a particular component.
4. Physical devices: The driver interface with the hardware. This code is customized

for the particular components used on the DSACSS (*e.g.* ‘Systron Donner Motion-Pak II rate gyro’).

In all, the object-oriented approach to the DSACSS code has gone well. We have contributed this software to the open source community, and hope that it will be beneficial to other students or system developers.* The primary operational complaint with the code structure is that object-oriented code runs slower than a comparable monolithic main file. However, it has proven to be reasonably readable and simple for new students to augment. Also, an inline documentation program, Doxygen, has proven invaluable in developing and maintaining software documentation.[†] We have had some problems with developers writing very low-level code that is difficult to read and poorly commented. In retrospect, it would have been useful to define a variable naming scheme; such policies are difficult to implement after the fact. The lab would benefit greatly if a dedicated student were to critique and improve the current software while implementing techniques to mandate the quality of new code.

4.2 Experimental Equations of Motion

In this section, we derive the equations of motion for the DSACSS air bearings. We begin with an outline of some of the available attitude representations. The attitude kinematics of a vehicle can be considered distinctly from its dynamics, so after describing these variants of the kinematic equations we then proceed on to the dynamics equations. We consider both a rigid body with only external torques and a gyrostat system with both external and internal torques.

4.2.1 Kinematic Equations

There are many ways to represent the kinematics of a rotating body. A thorough discussion of the many variables and their relative merits is beyond the scope of this text; we refer the reader to one of the many excellent mechanics texts available.^{144, 145, 12, 146, 147}

The set of rotations is defined by the group $SO(3)$, which is the set of all 3×3 orthonormal matrices with determinants of $+1$.¹⁴⁸ That is, $SO(3)$ is a three-dimensional manifold described by the set of proper rotations. A rotation matrix, \mathbf{R} , provides a valid description of the $SO(3)$ group, but is a nine-term parameterization. It is reasonable to

*Available for download at <http://dsacss.sourceforge.net/>.

[†] <http://www.doxygen.org/>

expect that a three-term parameterization of this three-dimensional space is possible, as is the case with Cartesian coordinates. We can parameterize the rotation matrix using only three-terms by making use of Euler angles, $\boldsymbol{\theta}$; just as with an aircraft, we can define roll, pitch, and yaw angles for a spacecraft. For example, a 3-1-3 rotation sequence of Euler angles is the classic choice to define the attitude of a spacecraft with respect to its local orbital frame. However, the Euler angle parameterization is not ideal. Specifically, any three-term attitude parameterization has at least one numerical singularity; for Euler angles, the singularities occur when the second rotation reaches some critical angle. The value of those angles depends upon the rotation sequence in question. Fundamentally, the problem with all three-term parameterizations is that the $SO(3)$ manifold is curvy. Unlike the rectilinear manifold of Cartesian space (which is fully spanned by any three-term set), the order of operations in $SO(3)$ is critical. This behavior provides some interesting dynamic properties — such as combining small changes in pitch and roll angles to achieve a change in yaw, or the ability to parallel park a conventional automobile — but requires a more complex mapping than is needed in a linear space.

The unit quaternion, $\bar{\mathbf{q}}$, often called the Euler parameter, is the lowest-order singularity-free attitude representation. This lack of singularities makes the unit quaternion extremely popular for use in analysis of unconstrained rotations. Moreover, use of the unit quaternion allows us to avoid the trigonometric manipulations required by Euler angle representations. However, the four terms of the unit quaternion doubly span the $SO(3)$ set: the negative of a unit quaternion defines the same rotation as the original set: $\bar{\mathbf{q}} = -\bar{\mathbf{q}}$. It is convenient to define two special quaternion operators, similar to the skew operator, \times , for ease in notation:¹⁴⁹

$$\left[\begin{array}{c} \mathbf{q} \\ q_4 \end{array} \right] \otimes \triangleq \left[\begin{array}{c|c} \mathbf{q}^\times + q_4 \mathbf{1} & \mathbf{q} \\ \hline -\mathbf{q}^\top & q_4 \end{array} \right] \quad (4.1)$$

$$\left[\begin{array}{c} \mathbf{q} \\ q_4 \end{array} \right] \circledast \triangleq \left[\begin{array}{c|c} -\mathbf{q}^\times + q_4 \mathbf{1} & \mathbf{q} \\ \hline -\mathbf{q}^\top & q_4 \end{array} \right] \quad (4.2)$$

where

$$\bar{\mathbf{q}}_3 = \bar{\mathbf{q}}_1 \otimes \bar{\mathbf{q}}_2 = \bar{\mathbf{q}}_2 \circledast \bar{\mathbf{q}}_1 \quad (4.3)$$

Note that four-term column vectors such as unit quaternions are denoted by an overbar.

Another useful attitude representation is the Modified Rodrigues Parameter (MRP), $\boldsymbol{\sigma}$. The MRPs are potentially more robust than other three-term attitude representations, as the sole singularity occurs at a rotation of 2π . This singularity can be avoided through use of a shadow set of MRPs phased from the original set by π .¹² For small rotations we can neglect the singularity entirely.

Each of the attitude representations follows a similar form in the kinematics. The kinematics in terms of a rotation matrix are

$$\dot{\mathbf{R}} = -\boldsymbol{\omega}^{\times}\mathbf{R} \quad (4.4)$$

where $\boldsymbol{\omega}$ is the angular velocity of any general coordinate system under analysis.

The Euler angle kinematics require the use of a 3×3 transformation matrix $\mathbf{S}(\boldsymbol{\theta})$ which must be uniquely derived for each of the 12 possible rotation sequences. We leave this matrix in its symbolic form,

$$\dot{\boldsymbol{\theta}} = \mathbf{S}(\boldsymbol{\theta})^{-1}\boldsymbol{\omega} \quad (4.5)$$

Using the quaternion operators defined above, we can write

$$\dot{\bar{\mathbf{q}}} = \bar{\mathbf{q}} \otimes \bar{\boldsymbol{\omega}} = \bar{\boldsymbol{\omega}} \otimes \bar{\mathbf{q}} \quad (4.6)$$

where the four-term angular velocity is $\bar{\boldsymbol{\omega}} \triangleq [\boldsymbol{\omega}^T \ 0]^T$.

The MRP kinematics are governed by

$$\dot{\boldsymbol{\sigma}} = \frac{1}{4} \left[(1 - \boldsymbol{\sigma}^T \boldsymbol{\sigma}) \mathbf{1} + 2\boldsymbol{\sigma}^{\times} + 2\boldsymbol{\sigma}\boldsymbol{\sigma}^T \right] \boldsymbol{\omega} \quad (4.7)$$

4.2.2 Rigid Body and Gyrostat Dynamics

Each DSACSS air bearing has two sets of three-axis control actuators: momentum wheels and cold gas thrusters. These two actuator suites are fundamentally different; thrusters produce external torques, whereas momentum wheels produce internal torques. The dynamics of a rigid body perturbed only by external torques are simpler to describe, so we begin our derivation there. We then proceed to the derivation of the gyrostat equations — those that govern a body with both internal and external torques. As with the kinematics, these equations are well documented in textbooks and so are stated here without proof.^{144, 145, 12, 146, 147}

The equations of motion for a spherical air bearing (with external torques only) are analogous to those in the classical problem of the spinning top, shown in Figure 4.3. In the case of a spinning top the pivot point of the top remains fixed, and this point is not coincident with the top's center-of-mass. There are two reasonable ways to approach this problem: define the origin of a body-fixed reference frame at either the center-of-mass or the center-of-rotation of the top. The center-of-mass representation is attractive because the first moment terms sum to zero, however, it requires knowledge of the normal

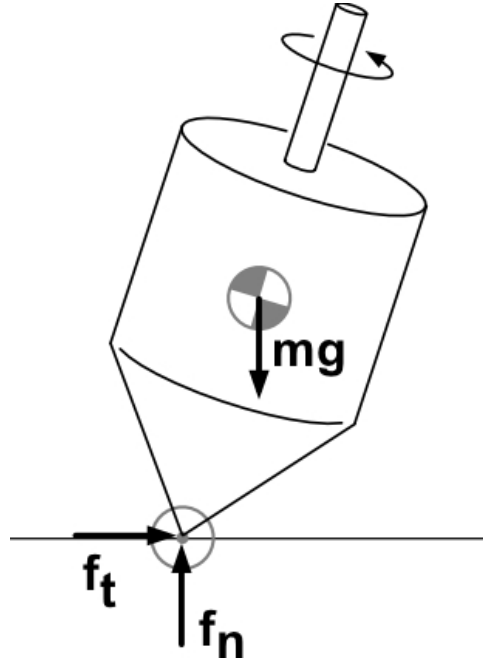


Figure 4.3: The Spinning Top

forces acting at the center-of-rotation. The center-of-rotation formulation requires the first moment terms to be retained but eliminates the external forces.¹⁴⁴ By consideration of this problem we recognize that formulating the equations about the center-of-mass will not ultimately be of use in our application; we have no way of knowing the forces acting inside the air bearing. We instead write the equations of motion about the center-of-rotation of the body, thereby eliminating all translational motion (and, importantly, bearing force) terms from the equations. Therefore, we state that the dynamics of a rigid body with external torques rotating about an inertially fixed point are governed by

$$\dot{\omega}^{bi} = \mathbf{I}_b^{-1} (-\boldsymbol{\omega}^{bi} \times \mathbf{I}_b \boldsymbol{\omega}^{bi} + \mathbf{g}_{ext}) \quad (4.8)$$

where the external torques can include control torques from the thrusters, a gravity torque from the offset of the mass center from the center-of-rotation, and other external disturbance torques such as drag. The superscript $\{\cdot\}^{bi}$ indicates a quantity of the body frame with respect to the inertial frame. Additionally, all terms are expressed in the body frame.

In the case of a gyrostat, it is convenient to make use of the definitions of total and axial angular momentum:

$$\mathbf{h}^{bi} = \mathbf{I}_b \boldsymbol{\omega}^{bi} + \mathbf{A} \mathbf{I}_s \boldsymbol{\omega}_s \quad (4.9)$$

$$\mathbf{h}_a = \mathbf{I}_s (\mathbf{A}^T \boldsymbol{\omega}^{bi} + \boldsymbol{\omega}_s) \quad (4.10)$$

where $\boldsymbol{\omega}_s$ is the length- n column matrix of wheel speeds with respect to the body, \mathbf{I}_s is a diagonal matrix containing the spin-axis moments of inertia of the wheels, and \mathbf{A} is a $3 \times n$ matrix that defines the alignment of each wheel in the body frame.

We can recapture the body angular velocity through

$$\boldsymbol{\omega}^{bi} = \mathbf{J}^{-1} (\mathbf{h}^{bi} - \mathbf{A}\mathbf{h}_a) \quad (4.11)$$

where we have defined an inertia-like matrix

$$\mathbf{J} = \mathbf{I}_b - \mathbf{A}\mathbf{I}_s\mathbf{A}^\top \quad (4.12)$$

Thus, the dynamics of a gyrostat are

$$\dot{\mathbf{h}}^{bi} = \mathbf{h}^{bi} \times \mathbf{J}^{-1} (\mathbf{h}^{bi} - \mathbf{A}\mathbf{h}_a) + \mathbf{g}_{ext} \quad (4.13)$$

$$\dot{\mathbf{h}}_a = \mathbf{g}_a \quad (4.14)$$

4.3 Perturbations

It is important to understand the dominant perturbations acting on the system. Perturbations potentially worthy of consideration for the DSACSS system include air currents (atmospheric drag), internal bearing drag, and the rotation of the Earth. We recognize, however, that modeling atmospheric drag of each Whorl is prohibitively complex. If the lab atmosphere were steady-state (particularly if the air mass was nearly stationary) we could develop a cross-sectional area model of each air-bearing payload and calculate a first-order drag model accordingly. However, the air currents change in time due to the building climate control system (which is out of our control). Given that we cannot include an accurate model of these torques in the system dynamics, any torques of lower magnitude can also be neglected. In this section, we derive the perturbations on the system due to the rotation of the Earth. We also analyze the atmospheric and bearing drag perturbations and compare the magnitudes of these three torques.

4.3.1 Rotating Earth Perturbation, Newtonian Derivation

We have already recognized the efficacy of writing the dynamic equations of each air bearing about its center-of-rotation. Now we consider an inertially fixed coordinate system located at the center of the Earth, \mathcal{F}_i . We define an intermediate reference frame at point l , the center of rotation of the air bearing and the origin of an Earth-fixed, local

reference frame. In this case, the linear velocity of \mathcal{F}_l is due solely to the rotation of the Earth.

The Earth-Centered Inertial (ECI) frame \mathcal{F}_i is defined in the conventional astronomical manner: $\hat{\mathbf{i}}$ and $\hat{\mathbf{j}}$ lay in the equatorial plane with $\hat{\mathbf{i}}$ in the direction of the vernal equinox, $\hat{\mathbf{v}}$, and $\hat{\mathbf{k}}$ points towards the geographic north pole.

The Earth-Fixed Local (EFL) frame \mathcal{F}_l is also defined in the conventional manner, this time from convenient local South-East-Zenith (SEZ) geometries. The $\hat{\mathbf{i}}$ vector is tangent to the meridian circle and points South. Similarly, $\hat{\mathbf{j}}$ is tangent to the parallel, pointing East. The $\hat{\mathbf{k}}$ vector is in the direction of the radial vector, $\vec{\rho}$, pointing from the center of the Earth to the point l on the surface and provides the local definition of ‘up’ (zenith).

We assume that the acceleration of the Earth about the Sun is negligible; such an assumption is a valid approximation for a laboratory reasonably far from the poles.¹⁴⁴ Blacksburg is located at a latitude of 37.21° North. We take the Earth to be a sphere of uniform density and assume that Earth’s axis of rotation is fixed in space. Thus, we represent the center of the Earth as a fixed point with the Earth spinning at a constant angular rate $\vec{\Omega}$ about true (geographic) North. Considering an Earth-fixed laboratory located in Blacksburg,

$$\vec{v}_{\text{Blacksburg}} = \vec{\Omega} \times \vec{r}_{\text{Blacksburg}} \quad (4.15)$$

It is useful to express the angular rate of the Earth in \mathcal{F}_l

$$\boldsymbol{\Omega}_l = -(\Omega \cos \lambda) \hat{\mathbf{i}} + (\Omega \sin \lambda) \hat{\mathbf{k}} \quad (4.16)$$

where λ is the latitude of point l , so that we can obtain the velocity equation

$$\mathbf{v}^{li} = \boldsymbol{\Omega}_l \times \boldsymbol{\rho}_l \quad (4.17)$$

We begin our dynamic analysis of the rotating Earth perturbation with the definitions of rigid body motion,

$$\dot{\mathbf{h}}^{bi} = -\boldsymbol{\omega}^{bi} \times \mathbf{h}^{bi} - \mathbf{v}^{li} \times \mathbf{p}^{bi} + \mathbf{g}_{\text{ext}} \quad (4.18)$$

where \mathbf{p}^{bi} is the linear momentum of the body with respect to inertial space, as follows

$$\mathbf{p}^{bi} = m\mathbf{v}^{li} - \mathbf{c}_b \times \boldsymbol{\omega}^{bi} \quad (4.19)$$

$$\mathbf{h}^{bi} = \mathbf{c}_b \times \mathbf{v}^{li} + \mathbf{I}_b \boldsymbol{\omega}^{bi} \quad (4.20)$$

and \mathbf{c}_b is the mass moment of inertia of the body.

We begin by rotating the velocity term into the body-fixed frame:

$$\dot{\mathbf{h}}^{bi} = -\boldsymbol{\omega}^{bi \times} \left(\mathbf{c}_b \times \mathbf{R}^{bl} (\boldsymbol{\Omega}_l \times \boldsymbol{\rho}_l) + \mathbf{I}_b \boldsymbol{\omega}^{bi} \right) + \mathbf{R}^{bl} (\boldsymbol{\Omega}_l \times \boldsymbol{\rho}_l)^{\times} (\mathbf{c}_b \times \boldsymbol{\omega}^{bi}) + \mathbf{g}_{ext} \quad (4.21)$$

Note that the total angular velocity of the body can be rewritten as

$$\boldsymbol{\omega}^{bi} = \mathbf{R}^{bl} \boldsymbol{\Omega}_l + \boldsymbol{\omega}^{bl} \quad (4.22)$$

Fully expanding, this equation becomes

$$\begin{aligned} \dot{\mathbf{h}}^{bi} = & -\boldsymbol{\omega}^{bl \times} \mathbf{I}_b \boldsymbol{\omega}^{bl} + \mathbf{g}_{ext} \\ & - (\mathbf{R}^{bl} \boldsymbol{\Omega}_l)^{\times} \mathbf{I}_b \boldsymbol{\omega}^{bl} + (\mathbf{c}_b \times \mathbf{R}^{bl} \boldsymbol{\Omega}_l \times \boldsymbol{\rho}_l)^{\times} \boldsymbol{\omega}^{bl} + (\mathbf{I}_b \mathbf{R}^{bl} \boldsymbol{\Omega}_l)^{\times} \boldsymbol{\omega}^{bl} + (\mathbf{R}^{bl} \boldsymbol{\Omega}_l \times \boldsymbol{\rho}_l)^{\times} \mathbf{c}_b \times \boldsymbol{\omega}^{bl} \\ & + (\mathbf{R}^{bl} \boldsymbol{\Omega}_l \times \boldsymbol{\rho}_l)^{\times} \mathbf{c}_b \times (\mathbf{R}^{bl} \boldsymbol{\Omega}_l) - (\mathbf{R}^{bl} \boldsymbol{\Omega}_l)^{\times} \mathbf{c}_b \times (\mathbf{R}^{bl} \boldsymbol{\Omega}_l \times \boldsymbol{\rho}_l) - (\mathbf{R}^{bl} \boldsymbol{\Omega}_l)^{\times} \mathbf{I}_b \mathbf{R}^{bl} \boldsymbol{\Omega}_l \end{aligned} \quad (4.23)$$

It is convenient to replace the angular momentum quantities with angular velocities. To do so, we must first take the time derivative of Equation 4.20 to obtain a second expression of $\dot{\mathbf{h}}^{bi}$:

$$\dot{\mathbf{h}}^{bi} = -\mathbf{c}_b \times \boldsymbol{\omega}^{bl \times} \mathbf{R}^{bl} \boldsymbol{\Omega}_l \times \boldsymbol{\rho}_l - \mathbf{I}_b \boldsymbol{\omega}^{bl \times} \mathbf{R}^{bl} \boldsymbol{\Omega}_l + \mathbf{I}_b \dot{\boldsymbol{\omega}}^{bl} \quad (4.24)$$

Substituting into Equation 4.23 and grouping like terms yields the following equations of motion

$$\begin{aligned} \mathbf{g}_{ext} = & \mathbf{I}_b \dot{\boldsymbol{\omega}}^{bl} + \boldsymbol{\omega}^{bl \times} \mathbf{I}_b \boldsymbol{\omega}^{bl} \\ & + \left[\mathbf{c}_b \times (\mathbf{R}^{bl} \boldsymbol{\Omega}_l \times \boldsymbol{\rho}_l)^{\times} + \mathbf{I}_b (\mathbf{R}^{bl} \boldsymbol{\Omega}_l)^{\times} + (\mathbf{R}^{bl} \boldsymbol{\Omega}_l)^{\times} \mathbf{I}_b \right. \\ & \left. - (\mathbf{c}_b \times \mathbf{R}^{bl} \boldsymbol{\Omega}_l \times \boldsymbol{\rho}_l)^{\times} - (\mathbf{I}_b \mathbf{R}^{bl} \boldsymbol{\Omega}_l)^{\times} - (\mathbf{R}^{bl} \boldsymbol{\Omega}_l \times \boldsymbol{\rho}_l)^{\times} \mathbf{c}_b \times \right] \boldsymbol{\omega}^{bl} \\ & - (\mathbf{R}^{bl} \boldsymbol{\Omega}_l \times \boldsymbol{\rho}_l)^{\times} \mathbf{c}_b \times (\mathbf{R}^{bl} \boldsymbol{\Omega}_l) + (\mathbf{R}^{bl} \boldsymbol{\Omega}_l)^{\times} \mathbf{c}_b \times (\mathbf{R}^{bl} \boldsymbol{\Omega}_l \times \boldsymbol{\rho}_l) + (\mathbf{R}^{bl} \boldsymbol{\Omega}_l)^{\times} \mathbf{I}_b \mathbf{R}^{bl} \boldsymbol{\Omega}_l \end{aligned} \quad (4.25)$$

where the expressions in the first line of this equation define the dynamics of the body with respect to the non-inertial reference frame \mathcal{F}_l . The terms in the last line are due to the motion of \mathcal{F}_l , and the bracketed term arises from the cross-coupling of the two motions.

4.3.2 Rotating Earth Perturbation, Lagrangian Derivation

A preferred method for verifying a derivation is to arrive at the same result using a different technique. In the case of dynamic equations, it is reasonable to suggest attempting a Lagrangian derivation to produce matching final equations. However, Lagrangian dynamics are not commonly used in attitude dynamics problems — for good reason! The curviness of the $SO(3)$ manifold causes the time derivatives to be quite complicated. While the derivation begins cleanly, the ultimate solution is bogged down in a great deal of algebra, not shown here.

We do not want to make any assumptions about the classes of forces acting on the system. Therefore, we start with the most basic form of Lagrange's equations:

$$\frac{d}{dt} \left(\frac{\partial \mathcal{L}}{\partial \dot{q}_j} \right) - \frac{\partial \mathcal{L}}{\partial q_j} = Q_{q_j} \quad (4.26)$$

where the Lagrangian is exactly the kinetic energy, $\mathcal{L} = T$. We choose our generalized coordinates to be any valid rotation sequence of Euler angles, $q_j = \theta_j$. Therefore, we recognize that our generalized forces, Q_θ , are something like torques.

The total kinetic energy of a rigid body is defined by

$$T = T_{\text{translation}} + T_{\text{rotation}} \quad (4.27)$$

$$= \frac{1}{2} m \mathbf{v}^{li\top} \mathbf{v}^{li} + \frac{1}{2} \boldsymbol{\omega}^{bi\top} \mathbf{I}_b \boldsymbol{\omega}^{bi} \quad (4.28)$$

$$= \boldsymbol{\omega}^{bi\top} \mathbf{c}_b^\times \mathbf{v}^{li} + \frac{1}{2} \boldsymbol{\omega}^{bi\top} \mathbf{I}_b \boldsymbol{\omega}^{bi} \quad (4.29)$$

$$= (\mathbf{R}^{bl} \boldsymbol{\Omega}_l + \boldsymbol{\omega}^{bl})^\top \mathbf{c}_b^\times \mathbf{R}^{bl} \boldsymbol{\Omega}_l^\times \boldsymbol{\rho}_l + \frac{1}{2} (\mathbf{R}^{bl} \boldsymbol{\Omega}_l + \boldsymbol{\omega}^{bl})^\top \mathbf{I}_b (\mathbf{R}^{bl} \boldsymbol{\Omega}_l + \boldsymbol{\omega}^{bl}) \quad (4.30)$$

We can take the partial derivatives with respect to $\boldsymbol{\theta}$ and $\dot{\boldsymbol{\theta}}$, the Euler angles and Euler angle rates of the body with respect to the lab. Note that the latter derivative is simplified by use of the chain rule:

$$\frac{\partial \mathcal{L}}{\partial \dot{\boldsymbol{\theta}}} = \frac{\partial \mathcal{L}}{\partial \boldsymbol{\omega}^{bl}} \frac{\partial \boldsymbol{\omega}^{bl}}{\partial \dot{\boldsymbol{\theta}}} \quad (4.31)$$

$$= \left(\mathbf{c}_b^\times \mathbf{R}^{bl} \boldsymbol{\Omega}_l^\times \boldsymbol{\rho}_l + \mathbf{I}_b (\mathbf{R}^{bl} \boldsymbol{\Omega}_l + \boldsymbol{\omega}^{bl}) \right) \mathbf{S}(\boldsymbol{\theta}) \quad (4.32)$$

Mundane algebraic manipulations are not included here. However, showing that the two derivations are equivalent requires two additional identities. First,

$$Q_\theta = \mathbf{S}(\boldsymbol{\theta})^\top \mathbf{g}_{\text{ext}} \quad (4.33)$$

This identity serves to transform the torques in the Newtonian formulation into the generalized torques of the Lagrangian equation. The derivation of this identity follows the derivation of the Euler angle kinematics, as in Equation 4.5, where the $\mathbf{S}(\boldsymbol{\theta})$ matrix transforms the Euler angle rates into the angular velocities.

Secondly, for any vector \mathbf{x} that is independent of the attitude,

$$\frac{\partial (\mathbf{R}\mathbf{x})}{\partial \boldsymbol{\theta}} = (\mathbf{R}\mathbf{x})^{\times} \mathbf{S}(\boldsymbol{\theta}) \quad (4.34)$$

where the matrices \mathbf{R} and $\mathbf{S}(\boldsymbol{\theta})$ refer to the same rotation. This expression can be derived starting from a well-known identity:

$$\frac{d\mathbf{R}}{dt} = -\boldsymbol{\omega}^{\times} \mathbf{R} \quad (4.35)$$

$$\frac{d(\mathbf{R}\mathbf{x})}{dt} = -\boldsymbol{\omega}^{\times} \mathbf{R}\mathbf{x} \quad (4.36)$$

$$\frac{d(\mathbf{R}\mathbf{x})}{dt} = -(\mathbf{S}(\boldsymbol{\theta})\dot{\boldsymbol{\theta}})^{\times} \mathbf{R}\mathbf{x} \quad (4.37)$$

$$\frac{\partial(\mathbf{R}\mathbf{x})}{\partial \boldsymbol{\theta}} \frac{d\boldsymbol{\theta}}{dt} = (\mathbf{R}\mathbf{x})^{\times} \mathbf{S}(\boldsymbol{\theta})\dot{\boldsymbol{\theta}} \quad (4.38)$$

From this point all that need be done is to cancel the time derivative terms to regain Equation 4.34. Note that this derivation is not a new proof, although we had derived it independently before finding it in the literature.¹⁵⁰

4.3.3 Drag Perturbations

Having derived the effect of Earth's rotation on the motion of the air-bearing payloads, it is necessary to evaluate the relative magnitude of this perturbation with respect to the other unmodeled forces acting on the system. As described in Chapter 3, the most advanced testbeds are housed in such a way to mitigate as many perturbations as practical, including seismic effects and atmospheric drag. Further, the highest precision bearings are ground precisely to effectively eliminate internal bearing forces. The DSACSS facility includes none of these advances and thus we must be aware of these perturbations in order to ensure robustness against them.

From observation of the uncontrolled air-bearing payloads it is apparent that local air currents cause the dominant perturbation on the system. However, because the air currents are neither under our control nor steady state it is impractical to predict the effects of this phenomenon. A comparison of the magnitudes of this drag torque against the rotating Earth torque resolves the question of whether to model the rotation of the Earth.

The minimum drag case will occur when the air mass in the laboratory is stationary. We can create a simple cross-sectional area model to analyze this case by manipulating three-view projections of the CAD model; we consider the Whorl-I configuration. The flat-spin motion is the minimum-drag motion for the system; we consider a fast flat-spin of 5 rad/s with large out-of-plane angular excursions ($\pm\pi/3$). We recall from basic aerodynamics that the drag force is governed by $D = \frac{1}{2}\rho V^2 A C_D$. Errors in the simple cross-sectional area model are of the same order as those from an assumed drag coefficient of $C_D = 1$ for a low-speed bluff body. More important is an accurate velocity model; we assume a uniform linear velocity proportional to the angular velocity, and adjust the cross-sectional area terms to reflect the minimal contribution of the central components. Errors from these simple assumptions are mitigated by investigating a range of angular velocities.

The internal bearing dissipation should be negligible when the bearing is working properly; we include a simple, constant friction model of the this perturbation for comparison.⁹²

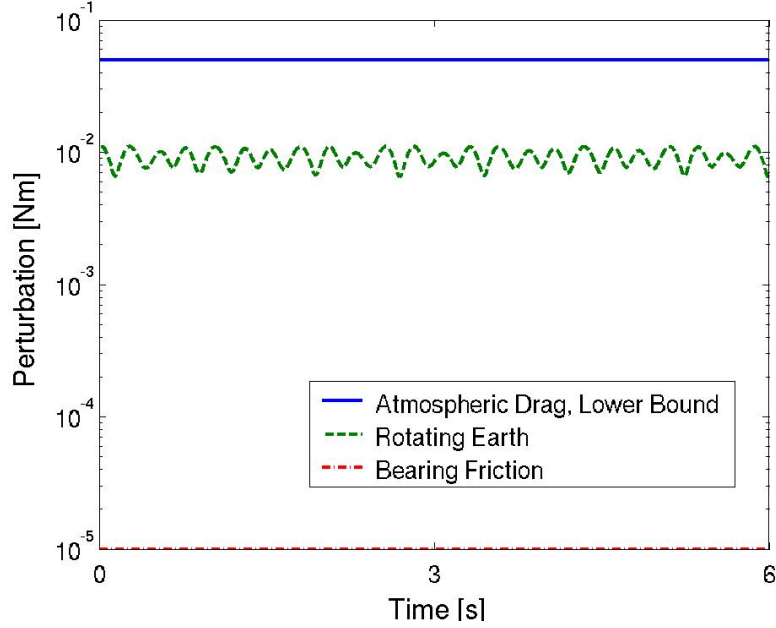


Figure 4.4: Magnitude of Perturbation Torques

Figure 4.4 shows the results of this analysis. The uncertainty in the atmospheric drag torque is high; it will increase with consideration of dynamic air currents. However, it is clear that even in the stationary air mass model the atmospheric drag torque dominates the other perturbations. Therefore, we need not include the model of the Earth's rotation in the operational equations of motion. Having determined that the rotating Earth

perturbation can be neglected, we limit the scope of the equations of motion to just one angular velocity, the motion of the body with respect to the lab. As such, we can simplify notation by dropping the superscript $\{\cdot\}^{bi}$ when describing this term.

4.4 Whorl Sensor Equations

The nominal sensor suite for the Whorl payloads includes three-axis rate gyros and three-axis linear accelerometers. Note that this sensor data is insufficient for complete attitude determination — a minimum of two vector measurements are required for complete attitude determination. With low-noise sensors the incomplete measurement would not be a noteworthy problem because the rates could be integrated smoothly, but the rate gyros are noisy in the velocity range applicable for DSACSS maneuvers.

The rate gyros measure the angular velocity of the system directly.

$$\mathbf{y}_{rg} = \boldsymbol{\omega} \quad (4.39)$$

The accelerometers measure

$$\mathbf{y}_{accel} = \dot{\boldsymbol{\omega}}^x \mathbf{r}_y + \boldsymbol{\omega}^x \boldsymbol{\omega}^x \mathbf{r}_y - g \mathbf{R}^{bi} \hat{\mathbf{k}} \quad (4.40)$$

where \mathbf{r}_y is the position of the sensor with respect to the center-of-rotation of the air bearing and g is the magnitude of gravity, assumed to be 9.81 m/s².

Note that any constant offsets due to perturbations acting on the system are calibrated out of the sensor measurements. Periodic variations are masked by the random noise spectrum added to the system.

The MotionPak II provides data through either a digital or an analog interface. The digital signal is pre-processed by an internal algorithm and updated at a rate of 32 Hz.¹⁵¹ It is unclear what signal manipulations are performed on the digitized data; we assume that, minimally, it has been de-biased due to temperature variations. Regardless, the digital signal is both slow and noisy. Working with the raw analog data, although more computationally and processor intensive, provides dramatically better results. At this time we are not compensating for temperature variation; we recommend further investigation in this area.

The family of Kalman filters expect Gaussian sensor noise. Thus, it is reasonable to investigate if the MotionPak II sensors produce signals with a Gaussian distribution. Further, an understanding of the sensor characteristics provides a good starting point for filter

tuning. We seek to identify the mean and standard deviation of the stationary signals and verify that the signals closely match this Gaussian distribution. Further, we desire to verify the output response of the sensor with respect to the published specifications.

Characterizing three-axis accelerometer response requires data sampled in six orthogonal sensor orientations. The configuration for this procedure is shown in Figure 4.5. The sensor is positioned on a platform with adjustable-height feet and aligned using a circular bubble level for reference. Bubble level readings are not consistent across the outer casing of the MotionPak II; errors of up to 1.0° are attributable to this uncertainty. Most alignments are verifiable to well within 0.5° . To obtain non-zero rate data, the MotionPak II is rotated a known distance about a single axis; the data can then be integrated to obtain and verify the angular position in time. This setup is shown in Figure 4.6.

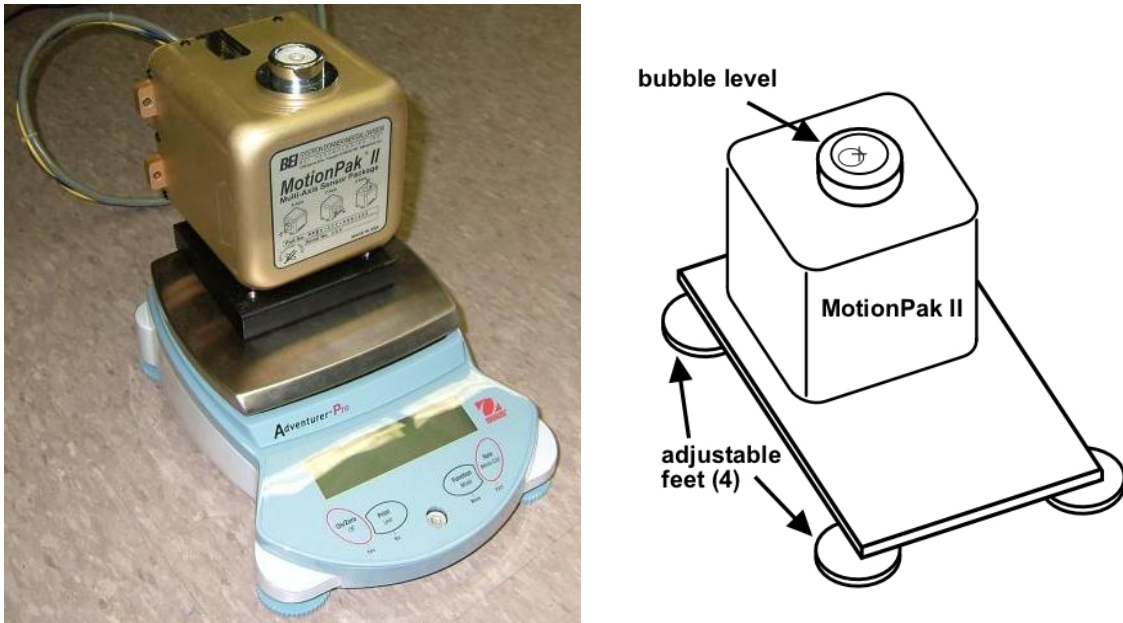


Figure 4.5: MotionPak II Test Setup for Accelerometer Calibration

The mean, μ , and standard deviation, σ , of the signals are easily calculable. The zero-mean values are used to determine the offset for each sensor; the misalignments described previously produce small variations in the zero-mean signal values. The non-zero means are used to calculate the response slope of the accelerometers; these values agree with the published specifications to within 2%. A sample of these data is shown in Figure 4.7. The integrated rate gyro data can be compared to the known boundary conditions in order to calculate the response slope, as in Figure 4.8. Again, experimental data agree with the published specifications to within 5%.

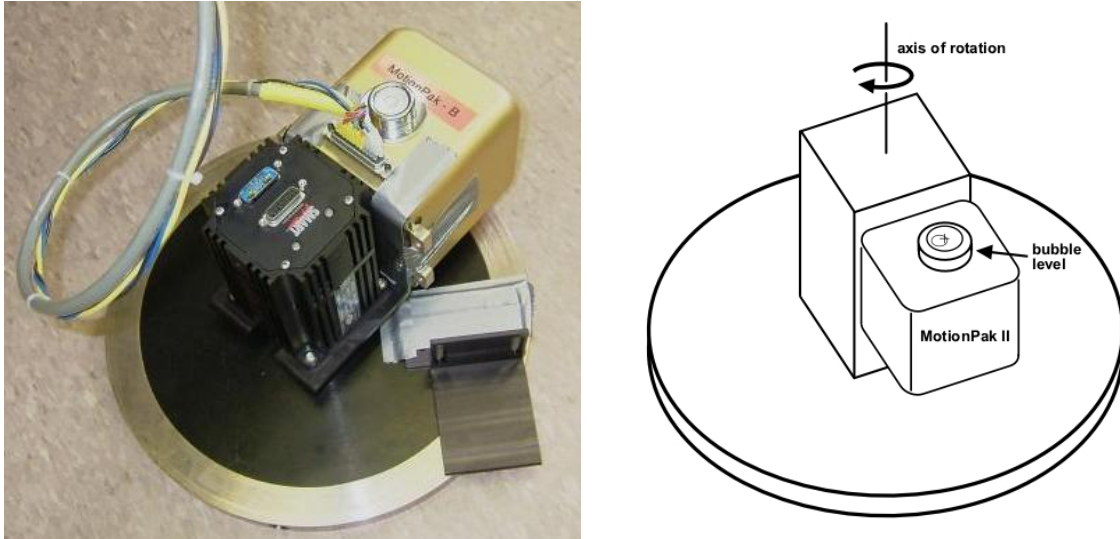


Figure 4.6: MotionPak II Test Setup for Rate Gyro Calibration

We use the chi-squared goodness-of-fit test to verify the applicability of the ideal Gaussian distribution to the experimental data. We sort the raw data into a histogram with k class intervals nominally using the optimal bin width of $k = 0.4\sigma$.¹⁵² However, class intervals need not be of equal width; bins with fewer than five counts are merged with the adjacent class closer to the mean. A data histogram and ideal normal distribution are shown in Figure 4.9. The top of each histogram bar represents the observed frequency in that interval, \mathcal{O}_i . The value of the normal distribution at the center of each class interval defines the expected frequency, \mathcal{E}_i . The test statistic is¹⁵³

$$\chi_0^2 = \sum_{i=1}^k \frac{(\mathcal{O}_i - \mathcal{E}_i)^2}{\mathcal{E}_i} \quad (4.41)$$

If the data follows the expected distribution then χ_0^2 has, approximately, a chi-square distribution with $\nu = k - p - 1$ degrees of freedom. The factor p compensates for the reduced degree(s) of freedom caused by using experimental statistics to define the expected distribution. For this analysis, $p = 2$, as we have calculated the mean and standard deviation of the Gaussian distribution via inspection of the data set.

Therefore, we wish to verify that $\chi_0^2 < \chi_{\alpha,k-2-1}^2$, where α defines the $100(1 - \alpha)\%$ confidence region.¹⁵³ The value of $\chi_{\alpha,\nu}^2$ is given by

$$\chi_{\alpha,\nu}^2 = \frac{e^{-0.5x} x^{0.5\nu-1}}{2^{0.5\nu} \Gamma(0.5\nu)} \quad \text{for } x \geq 0 \quad (4.42)$$

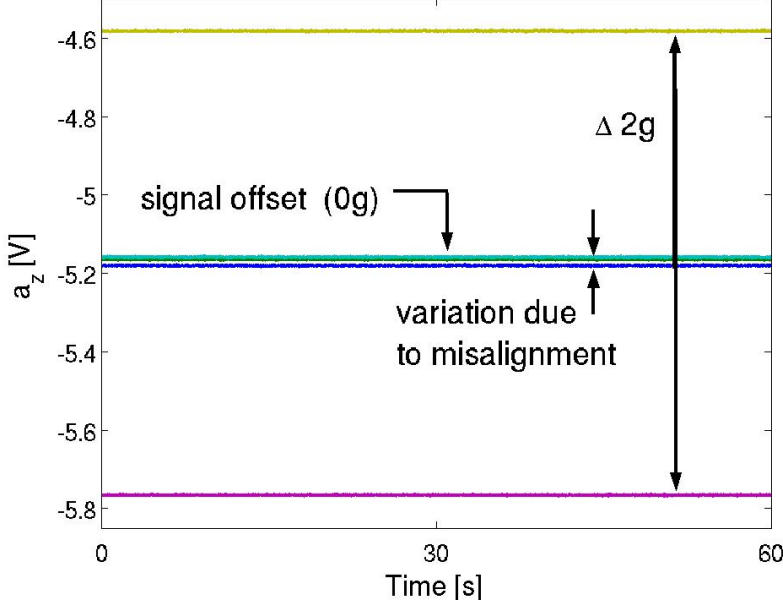


Figure 4.7: MotionPak II Acceleration Calibration Data

where

$$\Gamma(a) = \int_0^\infty t^{a-1} e^{-t} dt \quad (4.43)$$

However, the value of $\chi^2_{\alpha,\nu}$ is most often obtained by using a lookup table of common (α, ν) pairs.

The data set shown in Figure 4.9 is divided into 19 classes. We choose a typical confidence region, $\alpha = 0.01$, yielding the specific test condition $\chi^2_0 < \chi^2_{0.01,16} = 32.0$.¹⁵³ The calculated chi-square value for this data set is $\chi^2_0 = 31.0$, which passes the goodness-of-fit test. Therefore we can conclude that the data is well-represented by the ideal Gaussian distribution. We can demonstrate this performance on each of the raw signals.

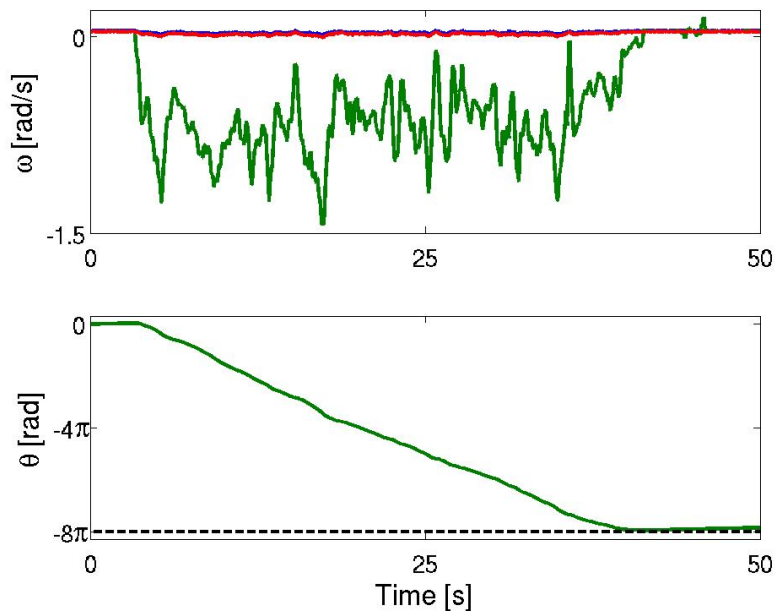


Figure 4.8: MotionPak II Rate Gyro Calibration Data

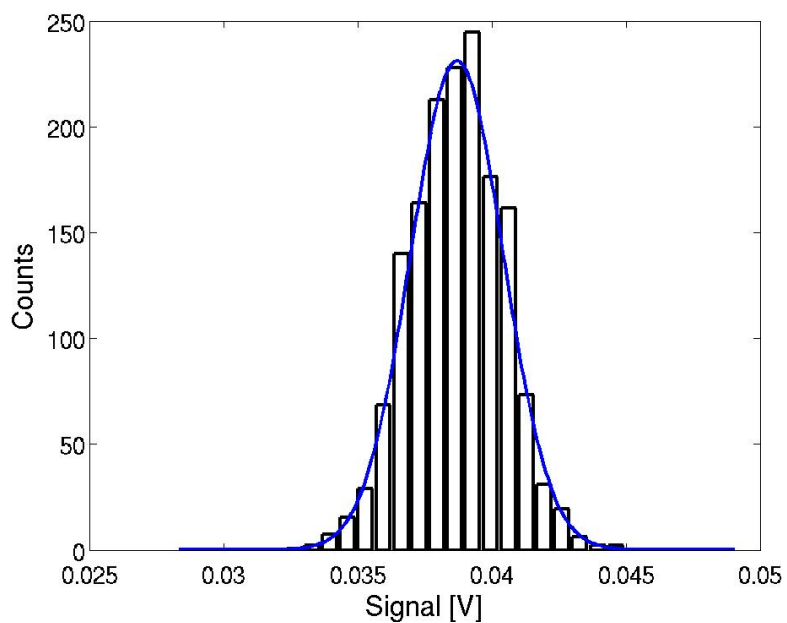


Figure 4.9: Histogram of MotionPak II Data and Ideal Gaussian Distribution

4.5 Extended Kalman Filter

A major step toward getting DSACSS operational is a working sequential, real-time state estimation technique. The standard algorithm in the aerospace industry for such a problem is the Extended Kalman Filter (EKF). The DSACSS air bearings follow either the gyrostat or rigid body equations of motion, depending upon the control suite in use. The development of Kalman filters for this application is well documented. The answer, however, is not as straightforward as one might be led to believe by the simplicity of the algorithm presented below. In this section, we outline the EKF algorithm and analyze the different options for the attitude estimation problem. We demonstrate the effectiveness of the final algorithm through comparison of simulated and experimental data.

4.5.1 Extended Kalman Filter Equations

The family of Kalman filters can be developed in both continuous- and discrete-time forms. We make use of a hybrid set of equations that are continuous in the process and discrete in the measurement. We do not present a thorough derivation and instead refer the reader to one of the several excellent estimation texts available.^{154, 155, 156}

The time-update step for the continuous / discrete EKF is

$$\dot{\hat{\mathbf{x}}}(t) = \mathbf{f}(\hat{\mathbf{x}}(t), \mathbf{u}(t), \boldsymbol{\Pi}, t) \quad (4.44)$$

$$\dot{\mathbf{P}}(t) = \mathbf{F}(t)\mathbf{P}(t) + \mathbf{P}(t)\mathbf{F}(t)^T + \mathbf{Q}(t) \quad (4.45)$$

$$\tilde{\mathbf{y}}_k = \mathbf{h}(\mathbf{x}_k) \quad (4.46)$$

where the first-order Jacobian approximation to the derivative of the process equation is

$$\mathbf{F}(t) \triangleq \left. \frac{\partial \mathbf{f}}{\partial \mathbf{x}} \right|_{\mathbf{x}(t)=\hat{\mathbf{x}}(t)} \quad (4.47)$$

The model is initialized with the expected value and uncertainty of the initial state estimate

$$\hat{\mathbf{x}}(t_0) = \hat{\mathbf{x}}_0 \quad (4.48)$$

$$\mathbf{P}_0 = E\left\{ (\mathbf{x}(t_0) - \hat{\mathbf{x}}_0)(\mathbf{x}(t_0) - \hat{\mathbf{x}}_0)^T \right\} \quad (4.49)$$

The first order approximation to the ideal (linear) Kalman gain matrix is calculated by

$$\mathbf{K}_k = \mathbf{P}_k^{-}\mathbf{H}_k^{-T} \left[\mathbf{H}_k^{-}\mathbf{P}_k^{-}\mathbf{H}_k^{-T} + \mathbf{R}_k \right]^{-1} \quad (4.50)$$

where

$$\mathbf{H}_k^- \triangleq \left. \frac{\partial \mathbf{h}}{\partial \mathbf{x}} \right|_{\mathbf{x}_k = \hat{\mathbf{x}}_k^-} \quad (4.51)$$

The Kalman gain is used in the measurement-update step for both the state vector and the covariance matrix

$$\hat{\mathbf{x}}_k^+ = \hat{\mathbf{x}}_k^- + \mathbf{K}_k \left[\tilde{\mathbf{y}}_k - \mathbf{h}(\hat{\mathbf{x}}_k^-) \right] \quad (4.52)$$

$$\mathbf{P}_k^+ = \left[\mathbf{1} - \mathbf{K}_k \mathbf{H}_k^- \right] \mathbf{P}_k^- \quad (4.53)$$

4.5.2 Quaternion / Angular Velocity Filter

It is intuitive to design a filter with a state vector containing the quaternion and angular velocity vector of the body-fixed coordinate system with respect to inertial space. The rigid body dynamics for this system are described by the vector field

$$\mathbf{f} = \begin{bmatrix} \bar{\boldsymbol{\omega}} \otimes \bar{\mathbf{q}} \\ \mathbf{I}_b^{-1} \left(-\boldsymbol{\omega}^\times \mathbf{I}_b \boldsymbol{\omega} - mg \mathbf{r}_g^\times \mathbf{R}^{bi} \hat{\mathbf{k}} + \mathbf{g}_{\text{ext}} \right) \end{bmatrix} \quad (4.54)$$

The Jacobian matrix for these dynamics is naturally divided into four quadrants:

$$\mathbf{F} = \left[\begin{array}{c|c} \bar{\boldsymbol{\omega}} \otimes & \bar{\mathbf{q}} \otimes \\ \mathbf{I}_b^{-1} \left(-mg \mathbf{r}_g^\times \frac{\partial \mathbf{R}^{bi}}{\partial \bar{\mathbf{q}}} \hat{\mathbf{k}} \right) & \mathbf{I}_b^{-1} \left(-\boldsymbol{\omega}^\times \mathbf{I}_b + (\mathbf{I}_b \boldsymbol{\omega})^\times \right) \end{array} \right] \quad (4.55)$$

We can define three-term vectors to aid in expressing the derivatives of the rotation matrix with respect to the quaternions, $\mathbf{q}_{\pm l, \pm m, \pm n} \triangleq [\pm q_l, \pm q_m, \pm q_n]^\top$, such that

$$\frac{\partial \mathbf{R}^{bi}}{\partial \bar{\mathbf{q}}} \hat{\mathbf{i}} = 2 [q_1 \mathbf{1} + \mathbf{q}_{4,-3,2}^\times \mid \mathbf{q}_{4,-3,2}] \quad (4.56)$$

$$\frac{\partial \mathbf{R}^{bi}}{\partial \bar{\mathbf{q}}} \hat{\mathbf{j}} = 2 [q_2 \mathbf{1} + \mathbf{q}_{3,4,-1}^\times \mid \mathbf{q}_{3,4,-1}] \quad (4.57)$$

$$\frac{\partial \mathbf{R}^{bi}}{\partial \bar{\mathbf{q}}} \hat{\mathbf{k}} = 2 [q_3 \mathbf{1} + \mathbf{q}_{-2,1,4}^\times \mid \mathbf{q}_{-2,1,4}] \quad (4.58)$$

Now that we have developed the state filter equations we progress to the measurement equations. One crucial difference between the ‘industry standard’ and the DSACSS is that the air bearings are not equipped with a complete sensor suite. Rather, the Motion-Pak II sensor provides measurements of the angular velocities and linear accelerations

only. Recall that full-state feedback in the attitude sense is achieved by angular velocity measurements (which we have) and at least two vector measurements (which we do not have). Note that the accelerometer vector has much more nonlinear dynamics than a simple inertial vector, making it more complex to integrate into a first-order filter. For the purpose of theoretical development, we also include a suite of three orthogonal vector measurements.

$$\mathbf{h} = \begin{bmatrix} \omega \\ \dot{\omega}^x \mathbf{r}_y + \omega^x \omega^x \mathbf{r}_y - g \mathbf{R}^{bi} \hat{\mathbf{k}} \\ \mathbf{R}^{bi} \hat{\mathbf{i}} \\ \mathbf{R}^{bi} \hat{\mathbf{j}} \\ \mathbf{R}^{bi} \hat{\mathbf{k}} \end{bmatrix} \quad (4.59)$$

The sensor Jacobian can be subdivided in a similar manner to the state Jacobian,

$$\mathbf{H} = \left[\begin{array}{c|c} \mathbf{0} & \mathbf{1} \\ (\mathbf{r}_y^x \mathbf{I}_b^{-1} m g \mathbf{r}_g^x - g \mathbf{1}) \frac{\partial \mathbf{R}^{bi} \hat{\mathbf{k}}}{\partial \bar{\mathbf{q}}} & -\mathbf{r}_y^x \mathbf{I}_b^{-1} (-\omega^x \mathbf{I}_b + (\mathbf{I}_b \omega)^x) - (\omega^x \mathbf{r}_y)^x - \omega^x \mathbf{r}_y^x \\ \frac{\partial \mathbf{R}^{bi} \hat{\mathbf{i}}}{\partial \bar{\mathbf{q}}} & \mathbf{0} \\ \frac{\partial \mathbf{R}^{bi} \hat{\mathbf{j}}}{\partial \bar{\mathbf{q}}} & \mathbf{0} \\ \frac{\partial \mathbf{R}^{bi} \hat{\mathbf{k}}}{\partial \bar{\mathbf{q}}} & \mathbf{0} \end{array} \right] \quad (4.60)$$

The first problem with this filter stems from the requirement that the quaternion be of unit length. This constraint causes several issues. First, the quaternion update in this filter is additive, making it unclear as to when to enforce the constraint. That is, if the quaternion is normalized during integration it will not be of unit length after the measurement update. Normalizing at several points in the filter is not satisfactory analytically. Secondly, note that the derivatives shown above assume that the quaternions are independent — which is incorrect. Finally, the interdependency of the quaternions causes the covariance matrix to be singular.^{157, 158, 159, 160, 161, 162, 163}

4.5.3 Attitude Error / Angular Velocity Filter

There are several possible solutions that can be used to account for the normalization problem. Clearly, one option is to change to a different set of variables; as the primary benefit of the quaternion formulation is the lack of singularities in the kinematics equations, if the attitude is known to be constrained, a singularity-free Euler angle rotation sequence could be used. A more general solution is to use the filter to update a three-component attitude error term. This error rotation can be defined in terms of a variety

of attitude representations — the vector part of the quaternion, the Gibbs vector, the Modified Rodrigues Parameter — and the representations are identical to second order.

Thus they are all equivalent within the context of an EKF.¹⁶⁴ We choose to use a modified form of the Gibbs vector, $\mathbf{a} \triangleq 2\mathbf{q}/q_4$, where the factor of 2 is included so, for small rotations, $\sqrt{\mathbf{a}^\top \mathbf{a}} \approx \phi$, where the rotation angle ϕ is as defined in an Euler axis / angle pair.¹⁶⁴ This multiplicative ‘quaternion error’ is defined as

$$\bar{\mathbf{q}} = \delta\bar{\mathbf{q}}(\mathbf{a}) \otimes \bar{\mathbf{q}}_{\text{ref}} \quad (4.61)$$

with kinematics of

$$\dot{\bar{\mathbf{q}}}_{\text{ref}} = \bar{\boldsymbol{\omega}}_{\text{ref}} \otimes \bar{\mathbf{q}}_{\text{ref}} \quad (4.62)$$

$$\dot{\mathbf{a}} = \left(\mathbf{1} + \frac{1}{4}\mathbf{a}\mathbf{a}^\top \right) (\boldsymbol{\omega} - \boldsymbol{\omega}_{\text{ref}}) - \frac{1}{2}(\boldsymbol{\omega} + \boldsymbol{\omega}_{\text{ref}})^\times \mathbf{a} \quad (4.63)$$

The state dynamics for this filter are

$$\mathbf{f} = \begin{bmatrix} \left(\mathbf{1} + \frac{1}{4}\mathbf{a}\mathbf{a}^\top \right) (\boldsymbol{\omega} - \boldsymbol{\omega}_{\text{ref}}) - \frac{1}{2}(\boldsymbol{\omega} + \boldsymbol{\omega}_{\text{ref}})^\times \mathbf{a} \\ \mathbf{I}_b^{-1} \left(-\boldsymbol{\omega}^\times \mathbf{I}_b \boldsymbol{\omega} - mg \mathbf{r}_g^\times \mathbf{R}^{bb_{\text{ref}}}(\mathbf{a}) \mathbf{R}^{b_{\text{ref}}i}(\bar{\mathbf{q}}_{\text{ref}}) \hat{\mathbf{k}} + \mathbf{g}_{\text{ext}} \right) \end{bmatrix} \quad (4.64)$$

with

$$\mathbf{F} = \left[\begin{array}{c|c} \frac{1}{4}\mathbf{a}(\boldsymbol{\omega} - \boldsymbol{\omega}_{\text{ref}})^\top + \frac{1}{4}\mathbf{1}(\boldsymbol{\omega} - \boldsymbol{\omega}_{\text{ref}})^\top \mathbf{a} - \frac{1}{2}(\boldsymbol{\omega} + \boldsymbol{\omega}_{\text{ref}})^\times & \mathbf{1} + \frac{1}{4}\mathbf{a}\mathbf{a}^\top + \frac{1}{2}\mathbf{a}^\times \\ -mg\mathbf{I}^{-1}\mathbf{r}_g^\times (\hat{\mathbf{r}}_{\text{ref}3}^\times - \hat{\mathbf{r}}_{\text{ref}3}\mathbf{a}^\top + \frac{1}{2}\mathbf{a}^\top \hat{\mathbf{r}}_{\text{ref}3}\mathbf{1} + \frac{1}{2}\mathbf{a}\hat{\mathbf{r}}_{\text{ref}3}^\top) & \mathbf{I}^{-1}(-\boldsymbol{\omega}^\times \mathbf{I} + (\mathbf{I}\boldsymbol{\omega})^\times) \end{array} \right] \quad (4.65)$$

where $\hat{\mathbf{r}}_{\text{ref}3}$ is the third column of $\mathbf{R}^{b_{\text{ref}}i}(\bar{\mathbf{q}}_{\text{ref}})$ and we have made use of a second-order approximation

$$\mathbf{R}^{bb_{\text{ref}}}(\mathbf{a}) = \frac{1}{1 + \frac{1}{4}\mathbf{a}^\top \mathbf{a}} \left(\mathbf{1} - \mathbf{a}^\times - \frac{1}{2} \left(\frac{1}{2}\mathbf{a}^\top \mathbf{a}\mathbf{1} - \mathbf{a}\mathbf{a}^\top \right) \right) \quad (4.66)$$

$$\approx \mathbf{1} - \mathbf{a}^\times - \frac{1}{2}(\mathbf{a}^\top \mathbf{a}\mathbf{1} - \mathbf{a}\mathbf{a}^\top) \quad (4.67)$$

The sensor function is as in the previous subsection. However, the sensor Jacobian must be restated in terms of the new state vector:

$$\mathbf{H} = \begin{bmatrix} 0 \\ (\mathbf{r}_y^\times \mathbf{I}_b^{-1} m g \mathbf{r}_g^\times - g \mathbf{1}) (\hat{\mathbf{r}}_{\text{ref}3}^\times - \hat{\mathbf{r}}_{\text{ref}3} \mathbf{a}^\top + \frac{1}{2} \mathbf{a}^\top \hat{\mathbf{r}}_{\text{ref}3} \mathbf{1} + \frac{1}{2} \mathbf{a} \hat{\mathbf{r}}_{\text{ref}3}^\top) \\ \hat{\mathbf{r}}_{\text{ref}1}^\times - \hat{\mathbf{r}}_{\text{ref}1} \mathbf{a}^\top + \frac{1}{2} \mathbf{a}^\top \hat{\mathbf{r}}_{\text{ref}1} \mathbf{1} + \frac{1}{2} \mathbf{a} \hat{\mathbf{r}}_{\text{ref}1}^\top \\ \hat{\mathbf{r}}_{\text{ref}2}^\times - \hat{\mathbf{r}}_{\text{ref}2} \mathbf{a}^\top + \frac{1}{2} \mathbf{a}^\top \hat{\mathbf{r}}_{\text{ref}2} \mathbf{1} + \frac{1}{2} \mathbf{a} \hat{\mathbf{r}}_{\text{ref}2}^\top \\ \hat{\mathbf{r}}_{\text{ref}3}^\times - \hat{\mathbf{r}}_{\text{ref}3} \mathbf{a}^\top + \frac{1}{2} \mathbf{a}^\top \hat{\mathbf{r}}_{\text{ref}3} \mathbf{1} + \frac{1}{2} \mathbf{a} \hat{\mathbf{r}}_{\text{ref}3}^\top \\ 1 \\ -\mathbf{r}_y^\times \mathbf{I}_b^{-1} (-\boldsymbol{\omega}^\times \mathbf{I}_b + (\mathbf{I}_b \boldsymbol{\omega})^\times) - (\boldsymbol{\omega}^\times \mathbf{r}_y)^\times - \boldsymbol{\omega}^\times \mathbf{r}_y^\times \\ 0 \\ 0 \\ 0 \\ 0 \end{bmatrix} \quad (4.68)$$

This filter works well if each of the terms in the dynamics equation is well-known. That is, we must have a good model for the mass properties of the system. We must also have a thorough understanding of the control suite performance, and confidence that all unmodeled disturbance torques are small. Moreover, we must derive a new filter using the gyrostat equations if momentum wheel control is to be used. The Jacobian matrix approximations for both the dynamic equations and the accelerometer measurements are already lengthy; these terms will only become more complex if the gyrostat dynamics are included.

4.5.4 Attitude Error / Rate Gyro Bias Filter

An alternative representation for the angular velocity is to use the rate gyro bias as the state rather than the angular velocity.^{165, 157, 164}

In such a filter, the rate gyro measurements are used in the state equations rather than in the measurement equations. The advantage of such a filter is that it requires no knowledge of the parameters in the dynamics equations, nor the applied torques (internal or external), allowing a sensor system to be developed for multiple platforms simultaneously. Thus we now have the following state equations

$$\mathbf{f} = \begin{bmatrix} -\boldsymbol{\omega}_{\text{ref}}^\times \mathbf{a} + (\mathbf{1} + \frac{1}{4} \mathbf{a} \mathbf{a}^\top + \frac{1}{2} \mathbf{a}^\times) (\mathbf{b}_{\text{ref}} - \mathbf{b} - \boldsymbol{\eta}_1) \\ \boldsymbol{\eta}_2 \end{bmatrix} \quad (4.69)$$

where \mathbf{b} is the rate gyro bias and \mathbf{b}_{ref} is the reference bias associated with $\boldsymbol{\omega}_{\text{ref}}$. Note that now it is clear where noise enters into the equations, making the choice of the \mathbf{G} matrix

trivial. These terms are, of course, neglected in the propagation phase of the filter. Also recall that the attitude error must be reset to zero at the beginning of each propagation step. Because the bias is a random process it must also be reset to zero at each step.

The state Jacobian matrix now simplifies to

$$\mathbf{F} = \begin{bmatrix} -\boldsymbol{\omega}_{\text{ref}}^{\times} + \frac{1}{4}\mathbf{a}^T(\mathbf{b}_{\text{ref}} - \mathbf{b})\mathbf{1} + \frac{1}{4}\mathbf{a}(\mathbf{b}_{\text{ref}} - \mathbf{b})^T - \frac{1}{2}(\mathbf{b}_{\text{ref}} - \mathbf{b})^{\times} \\ \mathbf{0} \\ \dots \\ -(\mathbf{1} + \frac{1}{4}\mathbf{a}\mathbf{a}^T + \frac{1}{2}\mathbf{a}^{\times}) \\ \mathbf{0} \end{bmatrix} \quad (4.70)$$

The only measurements available are from the accelerometer and the false vector sensors we include for development purposes, thus

$$\mathbf{h} = \begin{bmatrix} \frac{\Delta\mathbf{b}}{\Delta t}^{\times} \mathbf{r}_y + (\mathbf{y}_{\text{rg}} - \mathbf{b})^{\times}(\mathbf{y}_{\text{rg}} - \mathbf{b})^{\times} \mathbf{r}_y - g\mathbf{R}^{bi}\hat{\mathbf{k}} \\ \mathbf{R}^{bi}\hat{\mathbf{i}} \\ \mathbf{R}^{bi}\hat{\mathbf{j}} \\ \mathbf{R}^{bi}\hat{\mathbf{k}} \end{bmatrix} \quad (4.71)$$

with sensor Jacobian matrix

$$\mathbf{H} = \begin{bmatrix} -g(\hat{\mathbf{r}}_{\text{ref}3}^{\times} - \hat{\mathbf{r}}_{\text{ref}3}\mathbf{a}^T + \frac{1}{2}\mathbf{a}^T\hat{\mathbf{r}}_{\text{ref}3}\mathbf{1} + \frac{1}{2}\mathbf{a}\hat{\mathbf{r}}_{\text{ref}3}^T) \\ \hat{\mathbf{r}}_{\text{ref}1}^{\times} - \hat{\mathbf{r}}_{\text{ref}1}\mathbf{a}^T + \frac{1}{2}\mathbf{a}^T\hat{\mathbf{r}}_{\text{ref}1}\mathbf{1} + \frac{1}{2}\mathbf{a}\hat{\mathbf{r}}_{\text{ref}1}^T \\ \hat{\mathbf{r}}_{\text{ref}2}^{\times} - \hat{\mathbf{r}}_{\text{ref}2}\mathbf{a}^T + \frac{1}{2}\mathbf{a}^T\hat{\mathbf{r}}_{\text{ref}2}\mathbf{1} + \frac{1}{2}\mathbf{a}\hat{\mathbf{r}}_{\text{ref}2}^T \\ \hat{\mathbf{r}}_{\text{ref}3}^{\times} - \hat{\mathbf{r}}_{\text{ref}3}\mathbf{a}^T + \frac{1}{2}\mathbf{a}^T\hat{\mathbf{r}}_{\text{ref}3}\mathbf{1} + \frac{1}{2}\mathbf{a}\hat{\mathbf{r}}_{\text{ref}3}^T \\ -((\mathbf{y}_{\text{rg}} - \mathbf{b})^{\times} \mathbf{r}_s)^{\times} - (\mathbf{y}_{\text{rg}} - \mathbf{b})^{\times} \mathbf{r}_s^{\times} \\ \mathbf{0} \\ \mathbf{0} \\ \mathbf{0} \end{bmatrix} \quad (4.72)$$

One could eliminate the terms which depend upon the position of the sensor, \mathbf{r}_y . This simplification would make the sensor model platform independent, as the state model already is. Although this causes only a small change in the sensor model, such an assumption makes the sensor Jacobian matrix become singular; this approximation effectively linearizes the sensor dynamics and causes a substantial degradation in filter performance. If we assume that the accelerometer is located in the geometric center of the MotionPak II structure, this vector is easily determined from a CAD model and must be called as a variable within the EKF algorithm.

Several simulations are used to test filter performance, considering both air bearings' mass properties and attitude freedoms. Because the bias filter does not assume any dynamics,

filter performance does not change with the application of control torques. Therefore, we can test the filter in a simple, uncontrolled simulation with periodic dynamics and see which errors grow in time.

We demonstrate the performance of the filter for a nominal Whorl-I maneuver in Figures 4.10 – 4.14. The bulk motion is a flat spin about the z -axis with an initial rate of $\frac{\pi}{4}$ rad/s. The asymmetry of the body causes small out-of-plane deflections. The filtered estimates of the states are shown in Figure 4.10.

The error of the estimates with respect to the simulated truth model are shown in Figure 4.11. Also shown are the maximum covariance estimates for the attitude and rate. The covariance estimates bound the errors in a reasonable way; thus we can conclude that the filter is well-tuned. For consistency, we maintain this set of tuning parameters for all results.

We consider a two-term attitude parameterization in order to demonstrate the importance of the second vector measurement. With only one vector measurement (from the linear accelerometer) the filter may still be able to estimate out-of-plane motions accurately. However, the clocking angle about the nadir vector will be poorly determined. We introduce a pair of angles, (ψ, θ) , where θ is the maximum out-of-plane deflection and ψ defines the orientation of that angle in the local $x - y$ inertial plane. These definitions are shown in Figure 4.12. The estimates of these angles are shown in Figure 4.13. Note that the clocking angle ψ in fact grows continuously in time; we bound the plot range for convenience.

Both the truth value of the two-angle attitude parameterization and the estimated values from the filter are shown in Figure 4.13. However, the estimates are of sufficient quality that the filtered points are not clearly distinguishable from the exact solution. The errors in the two-angle attitude estimates are shown in Figure 4.14. The amplitude of the scatter in the errors is based on the quality of the sensor suite. Note that the accelerometer appears to provide better data than the true vector sensor; this performance is more likely attributable to the small out-of-plane deviations rather than some benefit from including additional nonlinearities in the filter dynamics.

Figures 4.14 and 4.15 demonstrate the importance of the second vector measurement. The filter results presented in Figure 4.15a are based on a vector sensor that is an order of magnitude noisier than the sensors in the previous filter (Figure 4.14). Reasonably, the noisier sensor causes the filter to produce lesser quality estimates. However, the error is again random; there is no persistent drift. The filter results presented in Figure 4.15b are calculated without the benefit of a second vector measurement; the estimate of the clocking angle diverges from the truth.

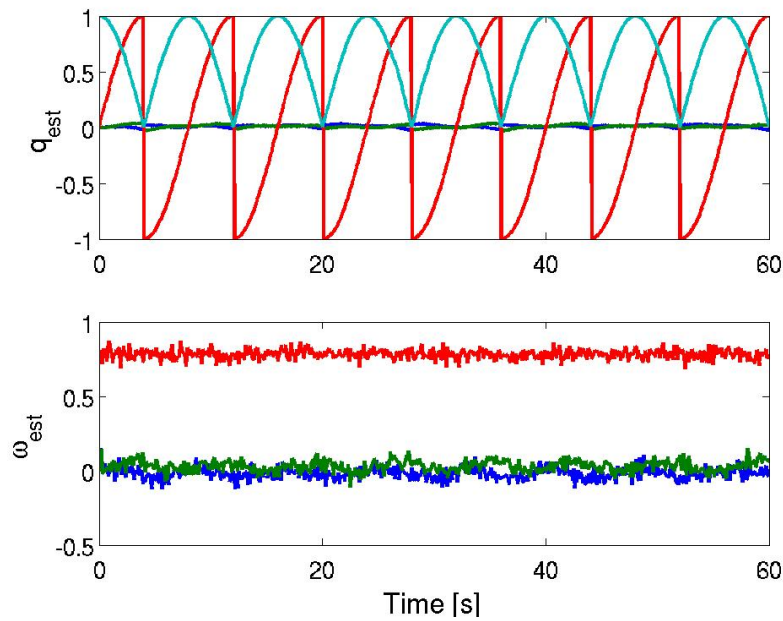


Figure 4.10: Estimated Attitude and Angular Velocity, $\hat{\mathbf{x}}^{bi}$, for Nominal Whorl-I Maneuver

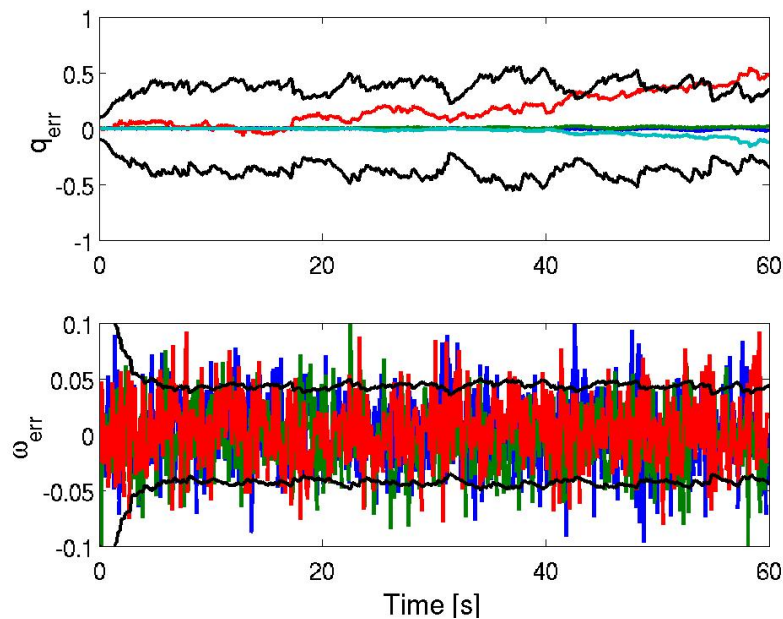


Figure 4.11: Filter Error and Covariance Envelope, $\hat{\mathbf{x}}^{bb}$, for Nominal Whorl-I Maneuver

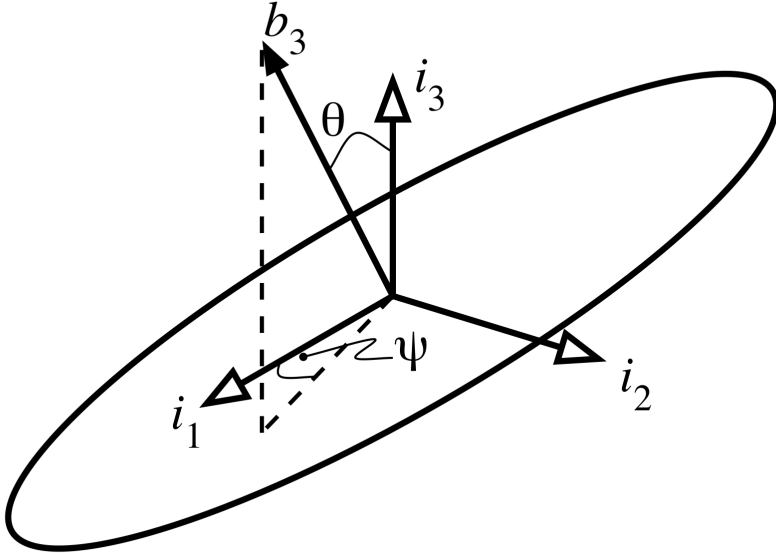


Figure 4.12: Definition of Two-Angle Parameterization

The rate at which the clocking angle estimate drifts is a function of the flat spin rate. Recall that the results presented to this point are based on an initial spin rate of $\frac{\pi}{4}$ rad/s. Figure 4.16 presents the effect of spin rate on the divergence of this estimate. Figure 4.16a shows the filter results for a π rad/s maneuver; Figure 4.16b for a 2π rad/s maneuver. As might be expected, the faster the spin, the faster the estimate diverges.

It is also interesting to consider motions with large out-of-plane deflections that could be performed by Whorl-II. The simulation shown in Figure 4.17 in fact goes beyond the performance bounds of the Whorl-II air bearing but is useful in demonstrating filter behavior. Figure 4.17a presents the truth model and estimates of the solution for a π rad/s flat spin with out-of-plane deflections up to 60° . The error plot in Figure 4.17b shows less periodicity in the spin angle than seen in the Whorl-I maneuvers, but again demonstrates the filter's ability to accurately estimate the out-of-plane angle even for large displacements.

Thus we can conclude that the limitations of the current sensor suite prevent accurate large slew maneuvers. However, it is worthwhile to explore the performance of the filter when estimating maneuvers consisting of largely out-of-plane motions. Figure 4.18 shows the results of out-of-plane motions achievable by Whorl-I (a) and Whorl-II (b). The out-of-plane angle is estimated well in both simulations. The clocking angle in the

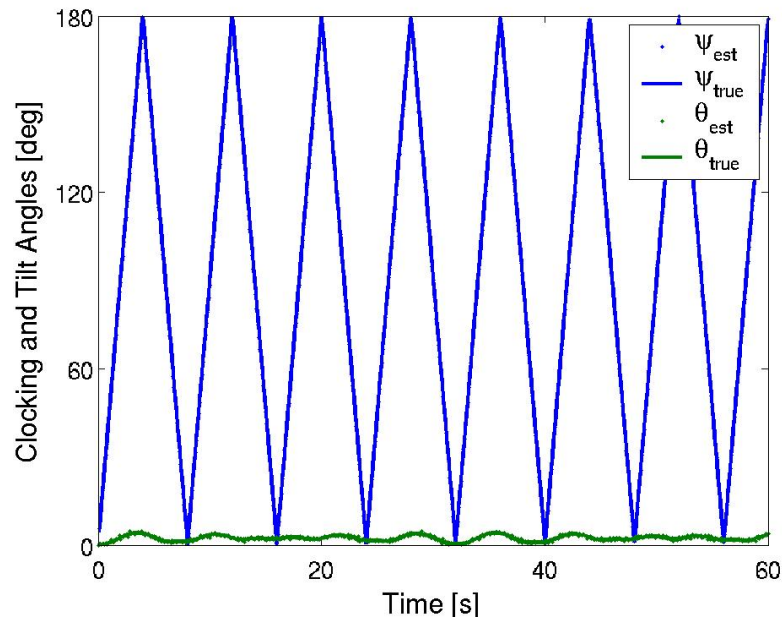


Figure 4.13: True and Estimated Two-Angle Attitude for Nominal Whorl-I Maneuver

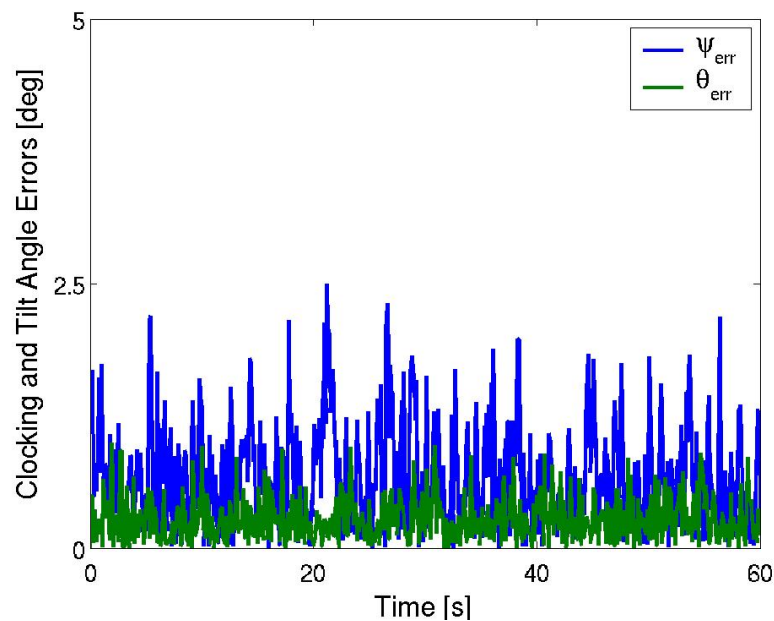


Figure 4.14: Two-Angle Attitude Error for Nominal Whorl-I Maneuver

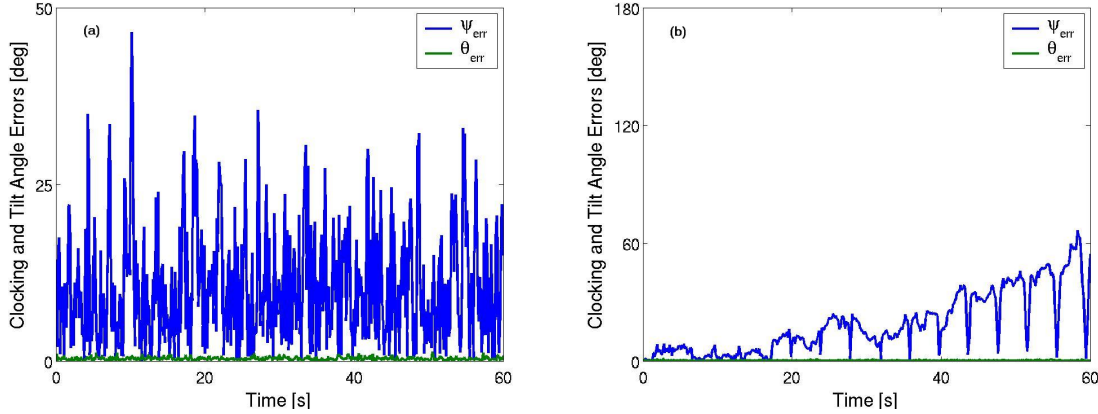


Figure 4.15: Two-Angle Attitude Error for Nominal Whorl-I Maneuver. (a) Low-Quality Vector Sensor; (b) No Vector Sensor

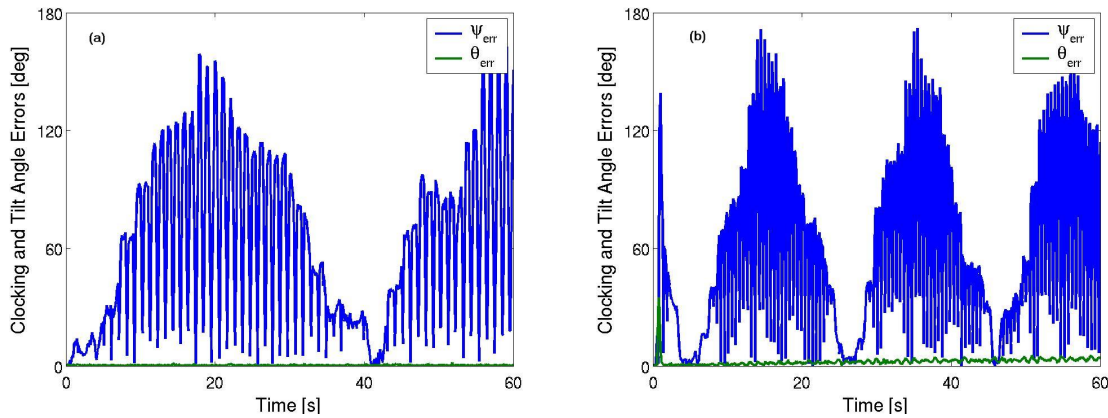


Figure 4.16: Effect of Spin Rate on Two-Angle Attitude Error, No Vector Sensor. (a) π rad/s Flat Spin; (b) 2π rad/s Flat Spin

Whorl-I simulation quickly drifts, reaching an error of 90° in less than 60 s of simulation time. Interestingly, the larger out-of-plane deviations in the Whorl-II simulation prevent the clocking angles from diverging; the component of gravity measured in the ψ direction during the large excursions provides a reset to the estimate. This phenomenon is analogous to magnetometer-only attitude determination, wherein the slowly-varying magnetic field vector can be used to incrementally estimate the complete attitude.

4.5.5 Experimental Filter Performance

Qualifying the experimental performance of an estimation scheme is challenging because the truth model is unknown. We can prevent the Whorl-I air bearing from moving, thereby providing a simple signal for the filter to analyze as well as a reasonably known truth model. The results from this testing are shown in Figure 4.19. The full-state estimate is shown in part (a), and the two-angle attitude parameterization is shown in part (b). The out-of-plane deflection estimate appears reasonable, although we do not have independent verification of the value. The clocking angle errors exhibit some random chatter effects, but begin to drift after only 60 s.

Results from a more elaborate maneuver are shown in Figure 4.20. In this maneuver, the Whorl-I platform was articulated about the x -axis in a periodic manner. Initial motion was maintained at a 4 s period; after 30 s the motion changed to a 6 s period. The filter again appears to accurately capture the out-of-plane motions. However, the spin estimate quickly drifts. We expect this result based on results of the simulation shown in Figure 4.18a. Note that neither of these filters were calculated in real-time. The filters are extremely sensitive to sensor offset values; these corrections are easily applied during post-processing, but real-time filtering is not feasible at this point.

In this section we documented the development of an EKF for the DSACSS air bearings. We discussed the current limitations of the attitude determination hardware and have demonstrated the expected capabilities of the filter for both the current and future sensor suites. Although experimental performance at this point is not adequate, we demonstrated the effectiveness of these techniques through simulation and provided a simple framework through which the current software can be modified to include additional sensor information.

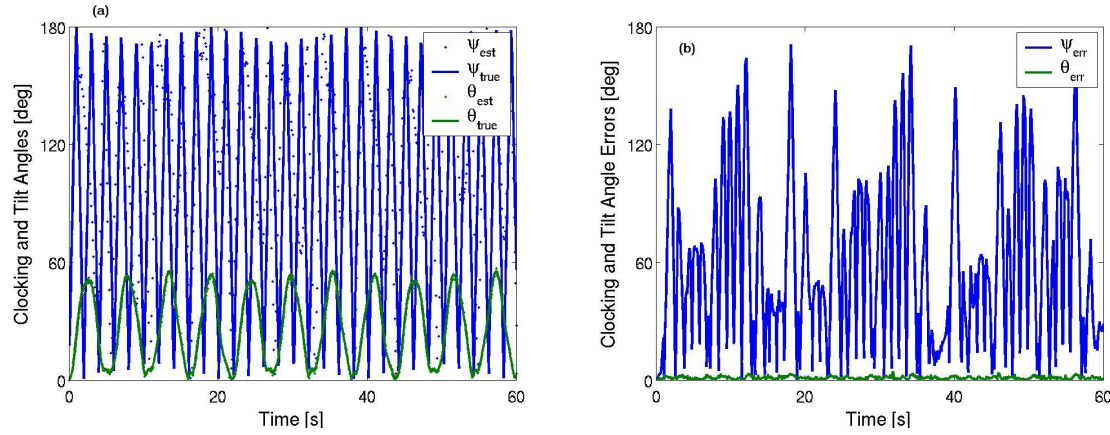


Figure 4.17: Effect of Out-of-Plane Motion on Two-Angle Attitude Error, No Vector Sensor.
(a) Angle Estimates; (b) Angle Errors

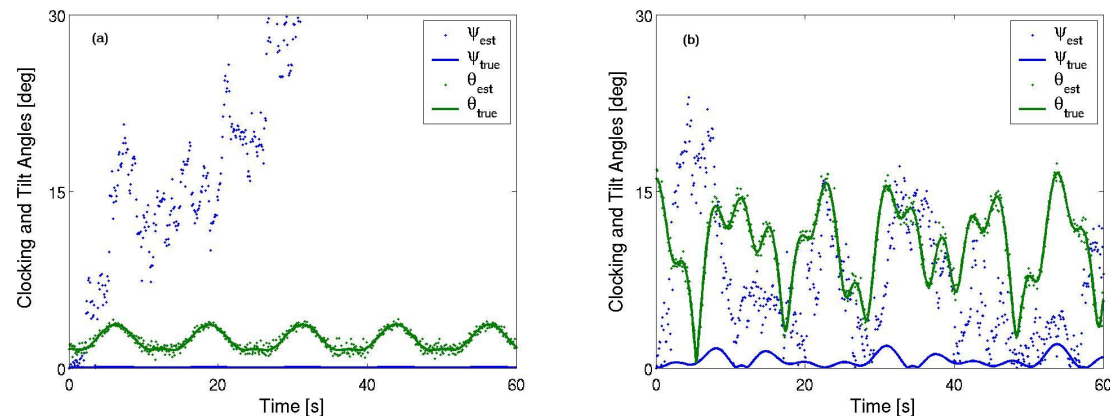


Figure 4.18: Two-Angle Attitude Estimation for Out-of-Plane Maneuver. (a) Whorl-I; (b) Whorl-II

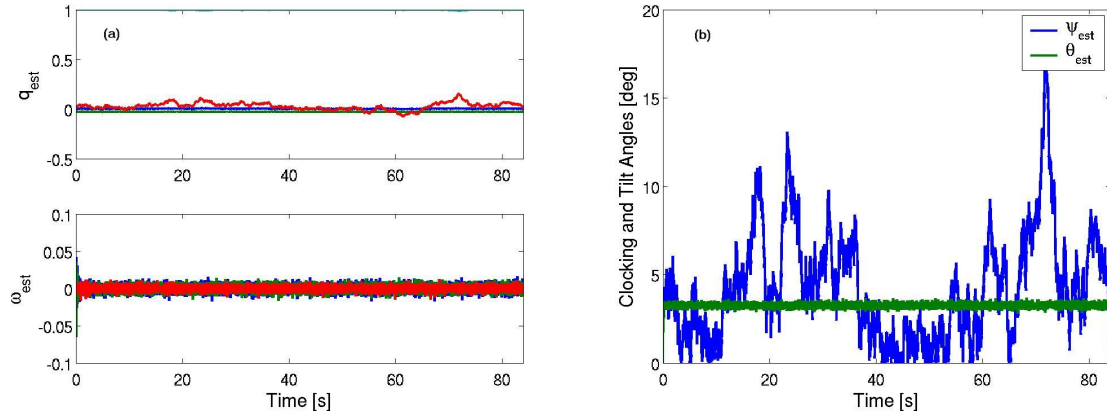


Figure 4.19: Experimental Performance, Non-moving Platform. (a) Full-State Estimates; (b) Two-Angle Estimates

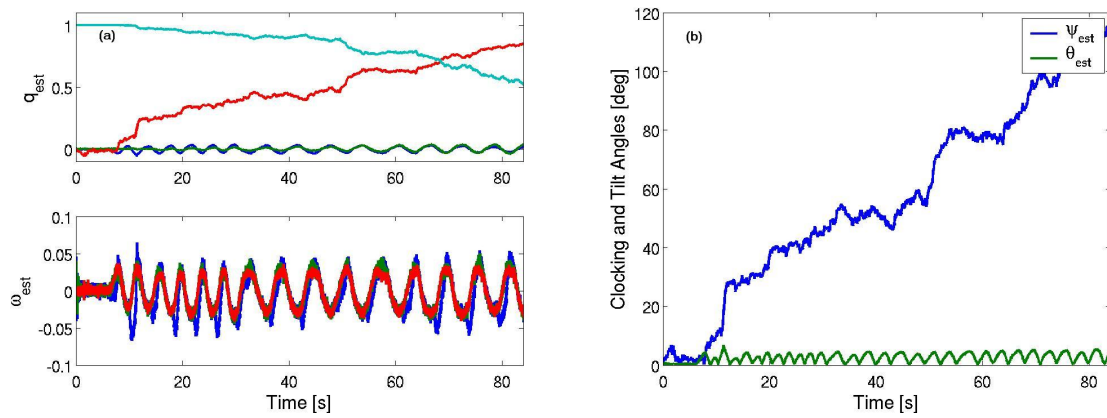


Figure 4.20: Experimental Performance, Small-Amplitude x -Rotation. (a) Full-State Estimates; (b) Two-Angle Estimates

4.6 Parameter Estimation

For many applications, high-precision knowledge of the mass properties of a system is not required. Alternatively, it may be more practical to accept the loss in performance from freezing the model of a system to a set of inaccurate parameters rather than taking the risk of adjusting these terms during a mission and causing potentially unpredictable changes. For such cases — both the low-cost and the high-risk — a simple batch estimation technique for parameter determination is ideal. When maximizing performance is crucial, the computational costs and potential risks associated with an on-line, adaptive estimation scheme become acceptable. In the case of DSACSS, we have the freedom to experiment with both techniques in a low-risk environment.

Most modern aerospace engineering design efforts begin within the framework of a computer-assisted drawing / design (CAD) program. Many CAD programs can be used to compute estimates of the model's mass properties. Such system models can be extremely high resolution: for example, many programs include libraries of fasteners and commonly used commercial parts that are easy to incorporate. However, commercial components are typically drawn as volume models with uniform density. Moreover, flexible items including thruster air harnessing and system wire harnessing can be prohibitively complex to model, yet significantly massive. Particularly in less formal engineering environments (such as those in university settings) production-time design changes may not be reflected in the CAD model. Therefore, the mass properties estimate from a CAD model can be considered a useful tool and an accurate starting place for analysis, but may require substantial improvement.

A reasonable first step for parameter estimation is to use the mass properties from a CAD model to design a maneuver. The subsequently obtained attitude and rate data can then be used as the inputs for a batch estimation technique such as least-squares estimation (LSE). Such schemes have been used successfully for the air-bearing spacecraft simulators at Georgia Tech¹¹⁰ and the Air Force Institute of Technology.^{166, 107, 167} Improvements in batch estimation effectiveness and efficiency are possible through careful choice of the input signal used to excite the system. These kinds of algorithms have been used for the Naval Postgraduate School's air-bearing system,¹⁶⁸ the University of Michigan's spherical air bearing,¹⁶⁹ as well as for simulated and flight-data analysis of several spacecraft.^{170, 171, 172, 173, 174, 175}

The literature on batch estimation techniques extends far beyond simple LSE. We could enhance the realism of the model by means of a recursive optimization technique in which constraint equations are enforced.^{176, 177} A recursive least squares algorithm could enforce Sylvester's inequalities and the triangle inequalities, preventing physically unrealizable

solutions. Alternatively, we could invoke a recursive algorithm that attempts to minimize the difference between the estimated parameters and the best-guess of the parameters as obtained from the CAD model.¹⁷² Modeling uncertainty through a Markov estimate rather than using LSE could also lead to improved convergence behavior.^{178,171} With improved attitude estimation, we could make use of a total least squares algorithm.¹⁷⁵

Adaptive, or sequential, techniques vary widely. Adjustments can be made within the observer or the controller algorithm; we consider only the adaptive observer problem here. There are two possible techniques for updating the parameters of a system within the observer step in a classical Kalman filter context: dual- and joint-filtering.¹⁷⁹ A joint filter estimates the states and parameters simultaneously within a single nonlinear Kalman filter (EKF or otherwise). A dual filter intertwines two filters, one for state estimation and a second for parameter estimation. We have investigated multiple techniques for sequential parameter estimation, with varying levels of success.^{179,180,181} We provide a basic motivation and approach to this problem but do not elaborate on the details.

In this section we document the development and application of batch system identification techniques for the DSACSS air bearings. We demonstrate the parameter dependencies within the equations of motion of the system. We document the initial estimate for the parameters obtained from a CAD model and derive several candidate LSE techniques that could be used to refine this estimate. The usefulness of each of these techniques is demonstrated through simulation. We identify possible sources of error in an effort to predict the accuracy of the experimental results. Current experimental results are not adequate due to deficiencies in the sensor suite, as explained in Section 4.5. We conclude with a brief discussion of sequential filtering techniques.

4.6.1 Equations of Motion

Accurate system identification of both the state vector of attitude quaternions and body angular velocities, along with the nine-term parameter vector (the six unique elements of the moment of inertia matrix along with the three components of the center-of-gravity vector)

$$\boldsymbol{\Pi} = \{I_{xx}, I_{xy}, I_{xz}, I_{yy}, I_{yz}, I_{zz}, mg\ r_{gx}, mg\ r_{gy}, mg\ r_{gz}\}^T \quad (4.73)$$

is crucial for successful control of the DSACSS.

In order to show that a linear least squares formulation is applicable to the problem we must first demonstrate that the system is linear with respect to the parameters. Note that the parameter vector does not enter into the kinematic equation. However, the

attitude of the system is coupled into the solution of the parameters due to the gravity gradient torque. Spacecraft attitude is typically not coupled in the analysis of a torque-free gyrostat rotating about its center of mass.

We begin with consideration of the simpler problem formulation of a rigid body. This restatement of the problem, although not applicable in the final solution, is a cleaner statement of the equations. We restore the cross-coupling gyrostat terms in the derivation later. The dynamic equations for both systems were presented previously.

By intelligently grouping like terms, the dynamics can be written in such a way that the system is clearly linear with respect to the parameters:

$$\mathbf{g}_{\text{ext}} = \mathbf{I}_b \dot{\boldsymbol{\omega}} + \boldsymbol{\omega}^{\times} \mathbf{I}_b \boldsymbol{\omega} + mg \mathbf{r}_g^{\times} \mathbf{R}^{bi} \hat{\mathbf{k}} \quad (4.74)$$

$$= [\dot{\boldsymbol{\omega}}] \{\mathbf{I}_b\} + [\boldsymbol{\omega}^2] \{\mathbf{I}_b\} + [\bar{\mathbf{q}}^2] \{mg \mathbf{r}_g\} \quad (4.75)$$

$$= \left[([\dot{\boldsymbol{\omega}}] + [\boldsymbol{\omega}^2]), [\bar{\mathbf{q}}^2] \right] \cdot \mathbf{\Pi} \quad (4.76)$$

$$\triangleq \boldsymbol{\Omega}' \cdot \mathbf{\Pi} \quad (4.77)$$

Equation 4.74 is a trivial rearrangement of Equation 4.8. In Equations 4.75 and 4.76 we manipulate terms in order to form matrices of the states multiplied by vectors of the parameters. Thus $[\dot{\boldsymbol{\omega}}]$ is a 3×6 matrix composed of elements that are functions of $\boldsymbol{\omega}$, $[\boldsymbol{\omega}^2]$ is a 3×6 matrix filled with quadratic functions of $\boldsymbol{\omega}$, and $[\bar{\mathbf{q}}^2]$ is a 3×3 matrix containing quadratic functions of the quaternions. The term $\{\mathbf{I}_b\}$ is a vector of the six unique elements in the inertia matrix, and $\{mg \mathbf{r}_g\}$ completes the parameter vector $\mathbf{\Pi}$ with the components of the center-of-gravity vector, as in Equation 4.73. It is clear from Equation 4.75 that the moments and products of inertia can be calculated given knowledge of the control torques, the angular velocities, and their derivatives. The mass and center of gravity are coupled and cannot be determined independently of one another; these terms are functions of the control torques and the attitude only.

4.6.2 *A Priori* Estimates

We obtain initial estimates of the parameters through mass properties analysis of a CAD model. This model is of sufficient detail to include many minor components but does not include the wiring harness. All commercial components are assumed to be uniform in density. Values obtained from the CAD model are shown in Table 4.1.

Table 4.1: Parameter Estimates From CAD Model

Parameter	Estimate
I_{xx}	$6.2 \text{ kg}\cdot\text{m}^2$
I_{xy}	$-0.9 \text{ kg}\cdot\text{m}^2$
I_{xz}	$-0.2 \text{ kg}\cdot\text{m}^2$
I_{yy}	$7.5 \text{ kg}\cdot\text{m}^2$
I_{yz}	$0.1 \text{ kg}\cdot\text{m}^2$
I_{zz}	$12.1 \text{ kg}\cdot\text{m}^2$
$mg\cdot r_{g_x}$	-0.02 Nm
$mg\cdot r_{g_y}$	-0.07 Nm
$mg\cdot r_{g_z}$	-2.0 Nm

4.6.3 Batch Least-Squares Parameter Estimation

One way to update the values obtained from a CAD model is through a least-squares estimation (LSE) algorithm. We investigate the basic requirements for effective use of an LSE method and develop several formulations for comparison. Fundamentally, LSE only implies use of some technique to find the best solution to an overdetermined problem in a least-squares sense. The development of the particular formulation of technique requires a working understanding of the physics of the system. In this subsection, we derive three different techniques for solving the parameter estimation problem within the context of LSE.

Torque Method

The progression from Equation 4.77 into the first least squares implementation requires only the definition of the pseudo-inverse. Using the definition of the matrix Ω' , we solve Equation 4.77 via

$$\hat{\Pi} = (\breve{\Omega}'^\top \breve{\Omega}')^{-1} \breve{\Omega}'^\top \breve{g}_{\text{ext}} \quad (4.78)$$

where the overbreve notation indicates that the torque vector and state matrix are augmented by multiple sets of data. That is, $\breve{\Omega}' = [\Omega'^\top|_{t_1}, \Omega'^\top|_{t_2}, \Omega'^\top|_{t_3}, \dots]^\top$ and so too with the torque vector. Note that the Ω' matrix must have more rows than columns for implementation of a regression technique, thus requiring the use of the pseudo-inverse equation as shown. This formulation is dubbed the torque method.¹⁷¹ Implementation

requires application of a control torque to provide a persistent excitation to the system. The applied control must sufficiently excite every parameter in order for the algorithm to converge.

Recall that the matrix Ω' contains functions of the states as well as the derivatives of the angular velocities. In an alternative formulation we integrate Equation 4.77, leaving functions of the states and their integrals. The integrated form of the torque method is simply

$$\int_{t_0}^t \Omega' \cdot \Pi \, d\tau = \int_{t_0}^t \mathbf{g}_{\text{ext}} \, d\tau \quad (4.79)$$

$$\Omega \cdot \Pi = \int_{t_0}^t \mathbf{g}_{\text{ext}} \, d\tau \quad (4.80)$$

where the new matrix of states, Ω , contains functions of the angular velocities, quaternions, and their integrals — but no derivative terms. Motivation for this step is provided below.

The torque method is the most intuitive LSE formulation to derive. More refined LSE schemes for spacecraft parameter estimation make use of some of the special characteristics of the attitude dynamics associated with an orbiting spacecraft: the conservation of energy and the conservation of angular momentum. Before progressing to these techniques, however, we must expand this derivation to the gyrostat equations.

Rewriting Equations 4.13 and 4.14 in terms of body and wheel angular velocities rather than angular momenta results in

$$\mathbf{I}_b \dot{\boldsymbol{\omega}} + \boldsymbol{\omega}^\times \mathbf{I}_b \boldsymbol{\omega} + mg \mathbf{r}_g^\times \mathbf{R}^{bi} \hat{\mathbf{k}} = \mathbf{A} \mathbf{I}_s \mathbf{A}^\top \dot{\boldsymbol{\omega}} - \boldsymbol{\omega}^\times \mathbf{A} \mathbf{I}_s \boldsymbol{\omega}_s - \mathbf{A} \mathbf{g}_a + \mathbf{g}_{\text{ext}} \quad (4.81)$$

where all of the terms on the right hand side are considered to be known. The left hand side is of the identical form to the rigid body equations, thus

$$\Omega' \cdot \Pi = \mathbf{A} \mathbf{I}_s \mathbf{A}^\top \dot{\boldsymbol{\omega}} - \boldsymbol{\omega}^\times \mathbf{A} \mathbf{I}_s \boldsymbol{\omega}_s - \mathbf{A} \mathbf{g}_a + \mathbf{g}_{\text{ext}} \quad (4.82)$$

Integrating both sides of the equation yields

$$\Omega \cdot \Pi = -\mathbf{A} \mathbf{I}_s \boldsymbol{\omega}_s - \int_{t_0}^t \boldsymbol{\omega}^\times \mathbf{A} \mathbf{I}_s \boldsymbol{\omega}_s \, d\tau + \int_{t_0}^t \mathbf{g}_{\text{ext}} \, d\tau \quad (4.83)$$

Momentum Integral

An extension of the torque method LSE implementation is the momentum integral. This method makes use of the ideally torque-free nature of the system such that for any pair

of data points in time, t_1 and t_2 , the total angular momenta differ only by the rotation of the body in that time, \mathbf{R}^{21} , yielding

$$(\boldsymbol{\Omega}' \cdot \boldsymbol{\Pi} - \mathbf{g}_{\text{ext}})_{t_2} = \mathbf{R}^{21} (\boldsymbol{\Omega}' \cdot \boldsymbol{\Pi} - \mathbf{g}_{\text{ext}})_{t_1} \quad (4.84)$$

$$\left(\boldsymbol{\Omega}'|_{t_2} - \mathbf{R}^{21} \boldsymbol{\Omega}'|_{t_1} \right) \cdot \boldsymbol{\Pi} = \mathbf{g}_{\text{ext}}|_{t_2} - \mathbf{R}^{21} \mathbf{g}_{\text{ext}}|_{t_1} \quad (4.85)$$

This formulation is a time-shifted difference of two torque method equations, and as such can be integrated in exactly the same way. The length of the time lag is determined by the magnitude of the shift: if t_2 and t_1 are subsequent data points, we term that a singly-shifted momentum integral technique. The momentum integral technique offers an advantage of additional smoothing of the data. Skipping one or more data points (doubly- or triply-shifting) can further smooth the data, but becomes unstable in the presence of unmodeled dissipation forces. Note that this technique halves the size of the data set, requiring a longer time span for data collection.

Energy Balance

The energy balance has been proposed as a more computationally efficient technique because it combines the three equations obtained at each time step into a single equation.^{170,171} This energy-like expression is obtained by dotting the angular velocity vector with the equations of motion of the system

$$\boldsymbol{\omega}^T (\mathbf{I}_b \dot{\boldsymbol{\omega}}_b + \boldsymbol{\omega}^\times \mathbf{I}_b \boldsymbol{\omega} + mg \mathbf{r}_g^\times \mathbf{R}^{bi} \hat{\mathbf{k}}) = \boldsymbol{\omega}^T (\mathbf{g}_{\text{ext}}) \quad (4.86)$$

This transformation eliminates the rigid body contribution to the motion, because

$$\boldsymbol{\omega}^T (\boldsymbol{\omega}^\times \mathbf{I}_b \boldsymbol{\omega}) = 0 \quad (4.87)$$

However, by only considering the motion in the direction of the angular velocity vector there is a risk of losing observability of one or more parameters.¹⁷¹

The integrated form of the energy balance equation is

$$\int_{t_0}^t \boldsymbol{\omega}^T (\mathbf{I}_b \dot{\boldsymbol{\omega}} + mg \mathbf{r}_g^\times \mathbf{R}^{bi} \hat{\mathbf{k}}) d\tau = \int_{t_0}^t \boldsymbol{\omega}^T (\mathbf{g}_{\text{ext}}) d\tau \quad (4.88)$$

Note that the first term is the derivative of rotational kinetic energy

$$\boldsymbol{\omega}^T \mathbf{I}_b \dot{\boldsymbol{\omega}} = \frac{1}{2} \boldsymbol{\omega}^T \mathbf{I}_b \dot{\boldsymbol{\omega}} + \frac{1}{2} \dot{\boldsymbol{\omega}}^T \mathbf{I}_b \boldsymbol{\omega} \quad (4.89)$$

$$= \dot{T}_{\text{rotation}} \quad (4.90)$$

and as such can be symbolically integrated to obtain

$$\boldsymbol{\omega}(t)^\top \mathbf{I}_b \boldsymbol{\omega}(t) - T_{\text{rotation}}(t_0) + \int_{t_0}^t \boldsymbol{\omega}^\top (mg \mathbf{r}_g \times \mathbf{R}^{bi} \hat{\mathbf{k}}) d\tau = \int_{t_0}^t \boldsymbol{\omega}^\top (\mathbf{g}_{\text{ext}}) d\tau \quad (4.91)$$

Unfortunately, there is no analog to the energy balance formulation for the gyrostat equations. Considering Equations 4.82 and 4.91 we can see a term involving the integration of $\dot{\boldsymbol{\omega}}$ and $\boldsymbol{\omega}_s$. It is not possible to evaluate this integral analytically. Numerical evaluation results in calculation of derivative terms, a step we are endeavoring to avoid. As such, we choose not to implement the energy balance technique.

4.6.4 Least-Squares Estimation Performance

In the previous subsection we developed three different LSE techniques. We have already discounted one of these techniques due to the requirement of calculating a numerical derivative. We justify this position below.

Several factors contribute to the convergence of the estimates. The control input must provide excitation of each parameter. Because we are relying on a simple numerical integration technique, step size plays a significant role in maintaining accurate numeric integration. Moreover, the dynamics of the system dictate the minimum step size for full observation as per the Nyquist criterion. Simulation time determines the size of the data set; however, longer simulation times lead to increased uncertainty levels due to inadequacies of the available sensor suite, discussed previously. Robustness to sensor noise is imperative. Note that noise can only impair the quality of an estimation: if a noise-free data set is degenerate in estimating one or more parameters, those parameters will not be accurately identified after the addition of random noise. Any apparent improvement is a numerical artifact only.

If any of the parameters are unobservable (or nearly so), $\check{\boldsymbol{\Omega}}^\top \check{\boldsymbol{\Omega}}$ will have a corresponding number of singular values that approach zero. A singular value of exactly zero indicates a parameter that is not affecting the motion: such terms can be dropped from the solution set without loss of information. However, very small singular values may indicate only that a significant parameter is not being sufficiently excited, thus potentially leading to inaccurate estimation of the entire vector of parameters.

Natural vs. Integrated Forms

Batch estimation techniques compensate for random noise. However, the original matrix of states, $\boldsymbol{\Omega}'$, includes the derivatives of the angular velocity. Such terms must be

computed numerically from the noisy rate gyro data; numerical derivatives, regardless of order, are highly unstable in the presence of noise. As such, performing LSE analysis by computing the natural form of the state matrix, as in Equations 4.82, 4.85, and 4.91 results in parameter estimates that are highly sensitive to the sensor noise. In contrast, the solution of the integrated form shown in Equation 4.83 requires that we compute numerical integrals rather than derivatives; numerical integration is robust to random noise.

We demonstrate this phenomenon in Figure 4.21. These plots present the performance of the natural (left plot) and integrated (right plot) forms of the torque method technique. We simulated a rigid body excited by a square wave thruster profile, firing about the z -axis only. The period of the square wave input, used as the ordinate axis for these plots, is representative of the excitation of the input. The amplitude of simulated white, zero-mean, constant amplitude sensor noise defines the abscissa. The colormap axis presents the median percent-error of the nine-term parameter estimate. The parameter estimation problem is inherently numerically ill-conditioned: these physical values can easily span three orders of magnitude. This range of values does not cause problems in the numeric solution of the LSE, but it can make the results of the percent-error calculation unclear — the same absolute error in two parameters can yield very different percent error results. As such, the median value of the nine-term percent error vector provides a more consistent representation of algorithm performance than either the maximum value or the mean.

It is clear from the plots in Figure 4.21 that the integrated form of the equations is a much more stable formulation of the problem. High-frequency excitations are not observable due to the step size of the simulation; this Nyquist frequency cutoff is indicated by the label ‘Ny’ on the ordinate axis. It is well-understood that these data will not produce valid estimates regardless of sensor quality. However, once the system is maneuvering in an observable way, we expect that noisy sensor data could still be used to observe large-amplitude maneuvers, whereas higher-quality data should be able to produce good estimates from smaller motions. We see this behavior from the integrated techniques only. The natural form of the equations produces estimates only as good as the sensor data, regardless of the input signal: that is, the convergence of the solution is driven by the quality of the numerical derivatives. Whereas the natural form only produces valid results with up to 1% sensor noise, the integrated form is shown to be robust to data with ten times that noise level. We continue considering only the integrated forms, and therefore only the torque method and momentum integral techniques.

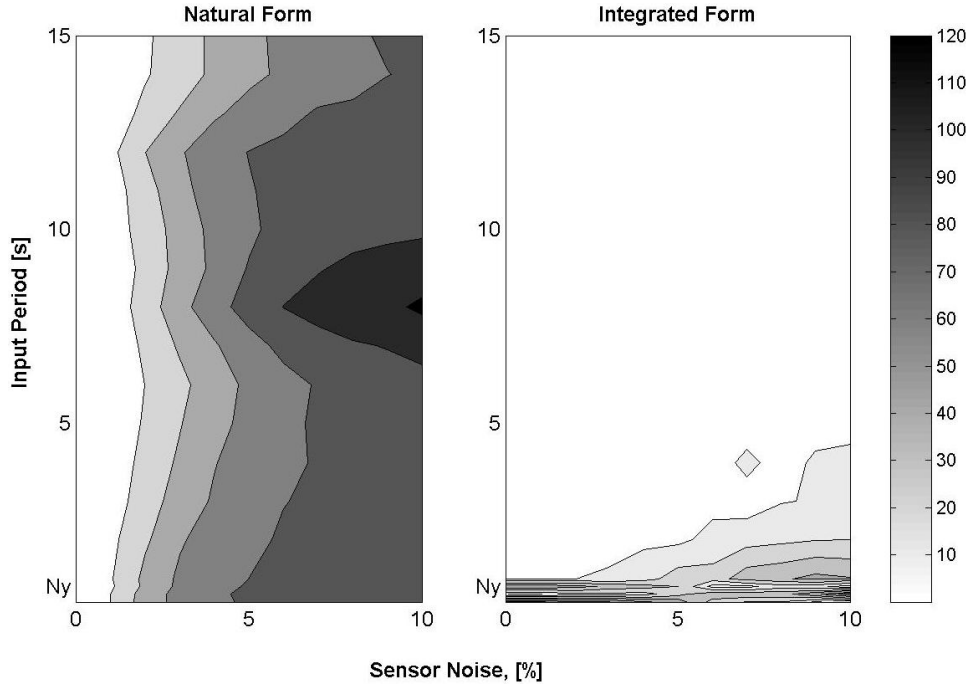


Figure 4.21: Torque Method LSE Performance in Natural and Integrated Forms [% Median Error]

Data Generation and Sample Performance

Here we present the full simulation of the Whorl-I gyrostat. We begin with the simulation of a rigid body controlled by thrusters. We choose a simple, bang-bang thrust profile about the x -axis. The open-loop controller applied ± 0.01 Nm external torques at a period of 10 s. This controller produces out-of-plane motions up to 5° , the limit of the Whorl-I air bearing. We run 100 s simulations with a step size of 0.1 s. The parameter estimates using data from the noise-free simulation are shown in Table 4.2.

The results shown in Table 4.2 demonstrate that the parameters are well excited and therefore easily identified to great accuracy. This performance is as expected for the zero-noise case. The two integrated techniques perform comparably; all error is due to the step-size of the first-order numerical integration technique. Note that a negative percent error indicates that the estimated parameter is smaller than the expected value.

In order to predict the realistic performance of the LSE algorithms, we add noise to the sensor data and process it through the EKF, as described in Section 4.5. We consider both the two-vector and accelerometer-only sensor configurations. We assume that the

Table 4.2: Parameter Estimates Obtained Using Perfect Data

Parameter	Torque Method		Momentum Integral	
	Estimate	% Error	Estimate	% Error
I_{xx}	6.15	0.77	6.15	0.73
I_{xy}	-0.89	-0.86	-0.89	-0.98
I_{xz}	-0.20	-0.48	-0.20	-1.02
I_{yy}	7.44	0.81	7.43	0.97
I_{yz}	0.10	0.47	0.10	0.74
I_{zz}	12.05	0.45	11.97	1.04
$mg \cdot r_{g_x}$	-0.02	-0.80	-0.02	-0.97
$mg \cdot r_{g_y}$	-0.07	-0.80	-0.07	-0.95
$mg \cdot r_{g_z}$	-1.98	-0.80	-1.98	-0.96

external torques are exactly known; we have investigated the effects of several sources of uncertainty on LSE performance previously.¹⁸⁰

The results using estimates from a filter with a second vector measurement are shown in Table 4.3. These results demonstrate that some parameters were more effectively excited than others, thereby allowing them to be better identified in the presence of noise. This effect can be mitigated by applying a more elaborate control law, or by combining several simple maneuvers into one augmented data set. Regardless, this simulation clearly demonstrates the effectiveness of the LSE techniques for experimental scenarios. The torque method performance is superior to the momentum integral technique; this trend holds for all simulations.

In contrast, the estimates obtained using simulations of the current sensor suite are unacceptable. These results are shown in Table 4.4. Batch estimation techniques are robust to random noise but not to persistent drifting of the state estimates. As such, attempting experimental parameter estimation is impractical at this time.

4.6.5 Sequential Parameter Estimation

The Extended Kalman Filter (EKF) is the most commonly used sequential filter for online estimation of spacecraft attitude dynamics. A first-order nonlinear filter, its optimality cannot (as in the case of the linear Kalman filter¹⁸²) be proven. However, the EKF is commonly successfully used to provide state estimates of continuous-time, non-

Table 4.3: Parameter Estimates Obtained Using Filtered Data, Two Vector Sensors

Parameter	Torque Method		Momentum Integral	
	Estimate	% Error	Estimate	% Error
I_{xx}	6.34	2.32	6.96	12.3
I_{xy}	-0.84	-7.00	-1.06	-18.2
I_{xz}	-0.00	-99.4	0.05	-123.
I_{yy}	7.72	2.99	8.49	13.2
I_{yz}	-0.20	295.	-0.02	119.
I_{zz}	0.14	98.9	0.09	99.3
$mg \cdot r_{g_x}$	-0.02	-3.90	-0.02	-11.6
$mg \cdot r_{g_y}$	-0.07	-3.52	-0.08	-11.7
$mg \cdot r_{g_z}$	-2.07	-3.58	-2.25	-12.5

linear dynamic systems from noisy, discrete-time measurements. Attempts to address the first-order approximation shortcomings of the EKF — which can lead to instability of the filter — are not new.^{183, 184, 185, 186, 187, 188} Coupled attitude and parameter estimation techniques benefit from these higher-order nonlinear filters because the problem is so tightly coupled. The current sensor suite will not support sequential parameter estimation, but such techniques are worth exploring for future application.

Recent proposed improvements to the EKF have branched out into two areas of research. The two branches offer improved performance against different sources of error.¹⁸⁹ One technique seeks to improve the convergence of the first-order filter by iterating at the measurement update step. These Iterated Extended Kalman Filters (IEKF) reduce the effective measurement noise. As such, they can be more tolerant to process noise and errors in initial conditions. Iterating in the measurement step also provides robustness against the first-order approximations of the derivatives.^{156, 189}

The second family of modified nonlinear filters improve performance by eliminating the Jacobian representation of the derivatives. These filters can yield drastically improved behavior beyond the convergence of the EKF for the same order of floating point operations (flops). A thorough review of these Linear Regression Kalman Filters (LRKF) is beyond the scope of this dissertation.^{190, 191, 192, 193, 194, 195, 196, 197, 198, 199, 200, 201, 202, 203} Some of these techniques have been further enhanced to capitalize on the improvements obtained through iteration in the IEKF and apply similar techniques to these higher-order filters. The Unscented Kalman Filter (UKF), a member of the LRKF family, has recently been documented for application to spacecraft attitude and orbital dynamics; such ap-

Table 4.4: Parameter Estimates Obtained Using Filtered Data, Accelerometer-Only Sensor Suite

Parameter	Torque Method		Momentum Integral	
	Estimate	% Error	Estimate	% Error
I_{xx}	0.03	99.5	0.01	99.9
I_{xy}	0.03	-103.	-0.06	-92.8
I_{xz}	-0.03	-87.4	-0.04	-80.4
I_{yy}	-0.02	100.	-0.04	100.
I_{yz}	0.01	89.0	-0.07	171.
I_{zz}	-0.00	100.	-0.13	101.
$mg \cdot r_{gx}$	0.00	-103.	0.00	-101.
$mg \cdot r_{gy}$	0.00	-103.	0.00	-105.
$mg \cdot r_{gz}$	0.07	-103.	0.04	-102.

plications are unusual in a literature dominated by theory papers and neural network applications.^{204, 205, 181}

There are two simple extensions that can be applied to any Kalman filter. These techniques — joint and dual filtering — use an analogous filter to estimate the parameters concurrently with the states. The joint method is the simpler to conceptualize: the parameter vector of interest is simply appended onto the true state vector. The time-update for the latter portion of the augmented state vector allows no changes beyond the effects of process noise (*i.e.*, the parameters should be constant) but the entire augmented covariance matrix is propagated as one.^{155, 154, 156, 206} The dual filtering technique intertwines a pair of distinct sequential filters, one estimating the true states and the other estimating the parameters.^{200, 207, 208, 206, 209, 210, 211, 212} The parameter estimation equations for each of the aforementioned filter types are similar to those for state estimation. We present the parameter estimation equations in the EKF context below and do not provide explicit derivations for the IEKF and UKF filters here. We have investigated this problem in previous works.^{179, 181}

Joint Filtering The joint filter is initialized with

$$\hat{\mathbf{x}}_{\text{aug}}(t_0) = [\hat{\mathbf{x}}_0^\top, \hat{\mathbf{P}}_0^\top]^\top \quad (4.92)$$

$$\mathbf{P}_{\text{aug}0} = E\left\{ (\mathbf{x}_{\text{aug}}(t_0) - \hat{\mathbf{x}}_{\text{aug}0})(\mathbf{x}_{\text{aug}}(t_0) - \hat{\mathbf{x}}_{\text{aug}0})^\top \right\} \quad (4.93)$$

with a time update step of

$$\dot{\hat{\mathbf{x}}}_{\text{aug}}(t) = \begin{bmatrix} \mathbf{f}(\hat{\mathbf{x}}(t), \mathbf{u}(t), \hat{\boldsymbol{\Pi}}, t) \\ \mathbf{0} \end{bmatrix} \quad (4.94)$$

The actual filtering equations are as in the standard Kalman filter.

Dual Filtering The Dual Filtering equations are analogous to the state filtering equations. The time-update equations are the trivial (constant) case, provided here in discrete time form

$$\hat{\boldsymbol{\Pi}}_k^- = \hat{\boldsymbol{\Pi}}_{k-1}^+ \quad (4.95)$$

$$\mathbf{P}_{\boldsymbol{\Pi}_k^-} = \mathbf{P}_{\boldsymbol{\Pi}_{k-1}^+} + \mathbf{Q}_{\boldsymbol{\Pi}_{k-1}} \quad (4.96)$$

There are several techniques for choosing the parameter process-noise matrix, $\mathbf{Q}_{\boldsymbol{\Pi}}$. We follow the ‘forgetting factor’ technique here,

$$\mathbf{Q}_{\boldsymbol{\Pi}_k} \triangleq (\lambda^{-1} - 1)\mathbf{P}_{\boldsymbol{\Pi}_k}^+ \quad (4.97)$$

$$\mathbf{P}_{\boldsymbol{\Pi}_k^-} = \mathbf{P}_{\boldsymbol{\Pi}_{k-1}^+} + (\lambda^{-1} - 1)\mathbf{P}_{\boldsymbol{\Pi}_k}^+ \quad (4.98)$$

$$= \lambda^{-1}\mathbf{P}_{\boldsymbol{\Pi}_{k-1}^+} \quad (4.99)$$

The memory constant $\lambda \in (0, 1]$; λ is typically in the range from $0.997 - 0.999$.²⁰⁸

The Kalman gain and associated measurement-update equations for the parameter EKF are

$$\mathbf{K}_{\boldsymbol{\Pi}_k} = \mathbf{P}_{\boldsymbol{\Pi}_k^-} \mathbf{E}_k^\top \left[\mathbf{E}_k \mathbf{P}_{\boldsymbol{\Pi}_k^-} \mathbf{E}_k^\top + \mathbf{R}_{\boldsymbol{\Pi}_k} \right]^{-1} \quad (4.100)$$

$$\hat{\boldsymbol{\Pi}}_k^+ = \hat{\boldsymbol{\Pi}}_k^- + \mathbf{K}_{\boldsymbol{\Pi}_k} \mathbf{e}_k \quad (4.101)$$

The innovations process of a dual filter can be conceptualized as the error in the equation of interest. To determine the parameters of an arbitrary system of equations, the error, \mathbf{e} , and its Jacobian matrix (with respect to the parameters, $\boldsymbol{\Pi}$), \mathbf{E} , are defined as

$$\mathbf{e}_k = \mathbf{d}_k - \mathbf{G}_k \quad (4.102)$$

$$\mathbf{E}_k = -\frac{\partial \mathbf{e}}{\partial \boldsymbol{\Pi}} \Big|_{\boldsymbol{\Pi}=\hat{\boldsymbol{\Pi}}_k^-} \quad (4.103)$$

To learn the parameters that dictate the state dynamics, $\mathbf{d}_k \rightarrow \dot{\hat{\mathbf{x}}}(t_k)$ and $\mathbf{G}_k \rightarrow \mathbf{f}(\hat{\mathbf{x}}_k, \hat{\boldsymbol{\Pi}}_k)$, yielding first-order approximate equations of

$$\mathbf{e}_k = \frac{\hat{\mathbf{x}}_k^+ - \hat{\mathbf{x}}_{k-1}^+}{t_k - t_{k-1}} - \mathbf{f}(\hat{\mathbf{x}}_k^+, \hat{\boldsymbol{\Pi}}_k^-) \quad (4.104)$$

$$\mathbf{E}_k = \frac{\partial \mathbf{f}(\hat{\mathbf{x}}_k^+, \hat{\boldsymbol{\Pi}}_k^-)}{\partial \boldsymbol{\Pi}} \Big|_{\boldsymbol{\Pi}=\hat{\boldsymbol{\Pi}}_k^-} \quad (4.105)$$

The measurement-update equations could be recast in terms of the IEKF framework by iterating to evaluate the error vector of Equation 4.104 and its Jacobian (Equation 4.105) with the updated parameters. Of course, both of these techniques can be restated in terms of the IEKF, UKF, or any other LRKF.

Chapter 5

Conclusions and Recommendations

This dissertation documents the design and development of a unique laboratory testbed, the Distributed Spacecraft Attitude Control System Simulator (DSACSS). The DSACSS is not yet fully operational, but a great deal of work has already gone into its development. When a few additional components are included the system will be fully functional. Ultimately, the DSACSS will prove to be a valuable testbed for spacecraft formation flying analysis and demonstration.

5.1 Summary

We motivate the development of the DSACSS by providing a brief review of the formation flying problem. Formation flying has proven to be an exciting area of research, the bulk of which focuses exclusively on the orbital dynamics aspect of the problem. We demonstrate a deficit in the literature: the need to address the entire dynamic system in a coupled attitude and orbital dynamics problem. The DSACSS will be a useful tool in experimental demonstration of this work.

We place the DSACSS in an experimental context through a survey of air-bearing space-craft simulators. These systems have been documented as important test facilities since 1960. This family of experimental facilities is highly diverse, ranging from miniature desktop models to massive 15,000 lb payloads. Some have just one complete degree-of-freedom, others are nearly unlimited in both translation and rotation. Systems may be manned. They may be used in a nominal laboratory environment or maintained within vacuum chambers and mounted on seismic dampening structures. Some air bearings are custom designed and built for government or industry use, while others are developed

by engineering students in university labs. Such a range of systems provides the ability to investigate a wide array of research topics. The DSACSS adds yet another new capability, by allowing investigation of multi-vehicle systems.

We also present an exciting new tool for experimental demonstration of formation flying: GPS simulators. Far from serving only as a *deus ex machina* plot device in a James Bond movie,* GPS simulators allow for closed-loop experimental demonstration of orbit control schemes. When coupled with the DSACSS true six degree-of-freedom experimental formation flying will be possible.

We provide a wide range of information on the DSACSS system in this dissertation, including a brief history of the design choices that led to the present hardware and software configuration. We derive and analyze the experimental equations of motion for the system and for the sensor suite. Using this knowledge, we derive and simulate the performance of nonlinear estimation schemes using the Extended Kalman Filter algorithm. We extend the estimation problem to also include the mass properties. We demonstrate the performance of these algorithms and their robustness to noise.

5.2 Recommendations

The most obvious recommendation from this work is to develop an additional attitude sensor. Effective attitude determination requires either another vector measurement or higher quality rate gyros. Better rate gyros are likely to be prohibitively expensive and would mask the problem rather than solving it. However, there is an interesting body of work which documents using suites of linear accelerometers for angular rate sensing; this would be an interesting future development for use on DSACSS.^{213,214} Possible spacecraft-like techniques for additional vector measurements include lab-based sun sensors, star (pattern) cameras, and magnetic field sensors. Several of these techniques are currently under investigation by students in the lab.

Another key recommendation involves the DSACSS-Ops software. Much of this code was rapidly developed with minimal team input. It would be beneficial — especially with the large personnel turnover currently taking place in the lab — to thoroughly review the software architecture. Certainly there are constructs which were implemented early in the coding process that are no longer useful. Further, it is likely that the current state of the software will suggest new methods. Although aerospace engineers are typically reticent to develop code, it is important to maintain the quality of the software so that

* *Tomorrow Never Dies*, R. Spottiswoode (director), Metro-Goldwyn-Mayer Studios, 1997.

it remains useful for many generations of students.

In a related note, it would be beneficial to develop software simulation stubs for all of the DSACSS hardware. Currently, the only way to run DSACSS-Ops code, even in the initial phases of testing, is to run it on the embedded computer system with all of the hardware in-the-loop. This operational requirement is troublesome for several reasons. For example, if a component is removed from the system, otherwise functional code will crash. More importantly, there is no opportunity for debugging software safely. Certainly it is possible to comment out or artificially limit commands to the hardware. However, it is not feasible to wholly debug algorithms in this limited operational state. A DSACSS software simulator[†] would allow developers to run with the hardware only when ready, and would allow for multiple students to test code simultaneously. Current plans for the software include implementing a communications strategy which runs all computationally-intensive algorithms on a modern desktop processor; fast PC/104 processor cards are much more expensive than comparable desktop processors. This infrastructure opens up the possibility for real-time linking with Matlab®. This would also ease in the debugging process, as most controller and observer algorithms are first developed in this environment.

In all, the first DSACSS team has developed an exciting new facility with much promise. It will be interesting to follow the system's progress and learn of new developments that have not presently even been conceived.

[†]DSACSSSS, perhaps?

Appendix A

Lessons in Management from the Space Systems Simulation Laboratory

This dissertation would be incomplete (and I would be remiss in the telling) were it not to include a section on the lab that hosts the DSACSS, the Space Systems Simulation Laboratory (SSSL). Although much of the Whorl-I hardware was in hand as early as 1999, the program did not really begin to come together until the right group of students began working together several years later. Prior to that time the students working in the SSSL all had very similar skill sets. We were finally able to bring together a sufficiently disparate team, with interests and knowledge ranging from low-level computer operation to mechanical analysis and design. Since then, the SSSL has been a host to a diverse group of graduate and undergraduate students. We recognize the long-term benefits of maintaining a broad team, from freshmen through doctoral students.

As the senior graduate student in the lab, it has been my responsibility and privilege to help direct the course of lab activities. Whether I have done well in these tasks I suppose will only be reflected in how much of what I have started is maintained after I am gone.* I certainly hope that the lab has benefitted from my efforts as much as I have from the work of the individuals in our lab group.

Running lab activities has also provided a unique component of my graduate work. In this section I provide a brief listing of some of the lessons I have learned as a leader and as a systems engineer. It is my hope that this section will prove beneficial to the next

*Among other things, I hope that the lab webpage will continue to be maintained at <http://www.aoe.vt.edu/research/groups/sssl>.

SSSL group leader.

I learned a great deal about leadership through my managerial roles in the HokieSat and ION-F programs. However, work in the lab has a very different dynamic. The SSSL team is a much smaller group of students; as such, I have been better able to interact with each team member. In turn, this has required me to learn the best way to motivate each individual. This is a much harder problem than when dealing primarily with subsystem team leaders, as such students are typically the most interested and motivated subset of the greater team: the elite tend to manage themselves. I do not wish suggest that SSSL members are not dedicated — quite the contrary! However, the team is largely comprised of unpaid students with many commitments. Some students spread themselves too thin unless kept in check. Others produce very little unless tightly managed or put in charge of a small team of their own. It has been a challenge to determine the best managerial strategy for each group member — which is not to say that I have done so successfully.

It is not important for the team leader to be friends with every person on the team. What is important is that each member of the group respect the lab and its goals. It is easier if each person also has a modicum of professional respect for the team leader, but even that is not required; it is possible to work with a student indirectly through other team members if need be. However, it is indicative of a problem if multiple team members are not friendly with an individual: this tends to signal that the student in question has lost sight of the goals of the lab and is focused on individual achievements. Sometimes it is possible to resolve these conflicts by discussing the problem with the student, and such efforts should be attempted. If such talks are not successful, it is difficult, but the best thing to do is to eliminate reliance on this student from progress in the critical path of the program. Students work best on what interests them, and their energies may still lead to something of use for the lab in the long term. However, such a person is no longer an effective member of the team and cannot be counted on to produce on demand.

Meetings should be ‘long enough,’ but as brief as possible. Importantly, meetings should only contain content that is relevant to most everyone in attendance; subsystem meetings are useful for those areas that only affect a few students’ work. The team leader should not be afraid to cut off a member who is overly expounding on a topic and redirect that conversation to another time. Meeting notes are important, even if it seems that no one reads them. Deadlines and targeted goals are very useful, and it is not impractical to assign a target date to every item on the list.

Design reviews are critical for several reasons. The Preliminary Design Review (PDR) forces a student to fully understand the purpose of the component under design. It allows the student freedom to be creative and brainstorm unique solutions to the problem. Even

if the ‘most obvious’ solution is selected as the best option after this review, the PDR has still forced the student to think fundamentally about the problem rather than diving directly into analysis. Further, PDR presentations are difficult to give. A student will typically come prepared with hand sketches and half-formed ideas rather than a flashy slide show littered with complex equations. It is much easier for the rest of the team to ask relevant hard questions at a PDR than at any of the other design reviews. This level of interaction is good, because it is important for the team to learn to think critically and for the presenter to learn how to receive professional criticisms.

The Conceptual Design Review (CoDR) allows the student to present what he believes to be the best design based on the results of the PDR. This review is the best time for input from the support staff from the electrical and machine shop (although their attendance at all design reviews should be encouraged!) and from those students who have experience in related tasks. This design review often includes a description of algorithms that can be difficult to convey quickly, thus the presenter should be encouraged to take as much time as needed to wholly describe the solution he has devised. If the CoDR goes well, the Critical Design Review (CDR) can often be performed quickly and informally, as a part of a normal meeting.

We have implemented a good design review policy for the design of major components. However, small parts typically skip through the review phase, sometimes causing a single piece to be remanufactured several times due to design flaws. Further, we have not instituted design reviews for software, nor for individual research projects. Software would be difficult to fit into the three-stage review process, but would benefit from peer critique. A team critique of individual research project goals and procedures would provide students with perspectives of how their work could be integrated into the lab activities. I believe that instating reviews of these processes would produce an overall improvement in lab effectiveness.

Documentation is critical in a student laboratory due to high personnel turnover. However, students typically dislike writing documentation and will neglect it if possible. Operational procedures for new hardware are necessary in order to prevent inadvertent damage to components due to misuse. Importantly, students must also be told to read and understand the documentation!

Software documentation is an ongoing process, eased by the use of a software self-documenting program, Doxygen.[†] By formatting comments in a Doxygen-specific way we are able to auto-generate a helpful web interface to the code documentation. We do not as yet have an automated technique for updating this site, but the process to upload

[†] <http://www.doxygen.org>

a new webpage is simple. Further, use of Concurrent Versions System (CVS) for software storage provides a robust tool for version control and documentation of changes.[‡] In order to be a part of the open-source software community (and to avoid maintaining a CVS repository on our own), we commit software changes to a repository hosted by SourceForge.net.[§] Each time a file is recommitted to the repository the author indicates what changes have been made; these notes are automatically logged at the bottom of the file and noted on the repository website. By use of a few key tools we have made software documentation as simple as possible. Thus far it has been quite successful.

[‡] <http://www.cvshome.org>

[§] <http://sourceforge.net>

References

- [1] H. C. Schubert and J. P. How, "Space Construction: An Experimental Testbed to Develop Enabling Technologies," in *Proceedings of the Conference on Telemanipulator and Telepresence Technologies IV*, no. 98-17930, (Pittsburgh, Pennsylvania), pp. 179–188, October 14–15, 1997.
- [2] D. Miller, A. Saenz-Otero, J. Wertz, A. Chen, G. Berkowski, C. Brodel, S. Carlson, D. Carpenter, S. Chen, S. Cheng, D. Feller, S. Jackson, B. Pitts, F. Perez, J. Szuminski, and S. Sell, "SPHERES: A Testbed For Long Duration Satellite Formation Flying In Micro-Gravity Conditions," in *Proceedings of the AAS/AIAA Space Flight Mechanics Meeting*, (Clearwater, Florida), pp. 167–179, January 23–26, 2000.
- [3] W. Haeussermann and H. Kennel, "A Satellite Motion Simulator," *Astronautics*, vol. 5, pp. 22–23, 90–91, December 1960.
- [4] J. Stanton, "Navy, Air Force to Develop Twin-Mirror Laser-Retargeting Satellite Technology," *National Defense Magazine*, August 2002.
- [5] D. T. Radzykewycz, J. L. Fausz, and W. R. James, "Energy Storage Technology Development at the Air Force Research Laboratory Space Vehicles Directorate," in *Proceedings of the Space Technology Conference and Exposition*, no. 99-4503, (Albuquerque, New Mexico), September 28–29, 1999.
- [6] M. A. Peck, L. Miller, A. R. Cavender, M. Gonzalez, and T. Hintz, "An Airbearing-Based Testbed for Momentum-Control Systems and Spacecraft Line of Sight," in *Proceedings of the 13th AAS/AIAA Space Flight Mechanics Winter Meeting*, no. AAS 03-127, (Ponce, Puerto Rico), February 9–13, 2003.
- [7] S. Cho and N. H. McClamroch, "Feedback Control of Triaxial Attitude Control Testbed Actuated by Two Proof Mass Devices," in *Proceedings of the 41st IEEE Conference on Decision and Control*, (Las Vegas, Nevada), pp. 498–503, December 2002.

- [8] P. K. C. Wang, J. Yee, and F. Y. Hadaegh, "Synchronized Rotation of Multiple Autonomous Spacecraft with Rule-Based Controls: Experimental Study," *Journal of Guidance, Control, and Dynamics*, vol. 24, no. 2, pp. 352–359, March–April 2001.
- [9] G. Wilt and A. Ledebuhr, "Down-to-Earth Testing of Microsatellites," *Science and Technology Review*, pp. 24–26, September 1998.
- [10] R. B. Voas, H. I. Johnson, and R. Zedekar, "Mercury Project Summary," Tech. Rep. NASA-SP-45.
- [11] R. L. DeFazio, S. Owens, and S. Good, "Follow That Satellites: EO-1 Maneuvers Into Close Formation with Landsat-7," in *Proceedings of the AAS/AIAA Astrodynamics Specialists Conference*, no. AAS 01-450, (Quebec City, Quebec, Canada), July 30–August 2, 2001.
- [12] H. Schaub and J. L. Junkins, *Analytical Mechanics of Space Systems*. Reston, Virginia: American Institute of Aeronautics and Astronautics, 2003.
- [13] M. S. de Queiroz, V. Kapila, and Q. Yan, "Adaptive Nonlinear Control of Multiple Spacecraft Formation Flying," *Journal of Guidance, Control, and Dynamics*, vol. 23, no. 3, pp. 385–390, May–June 2000.
- [14] G. W. Hill, "Researches in the Lunar Theory," *American Journal of Mathematics*, vol. 1, no. 1, pp. 5–26, 1878.
- [15] G. W. Hill, "Researches in the Lunar Theory," *American Journal of Mathematics*, vol. 1, no. 2, pp. 129–147, 1878.
- [16] G. W. Hill, "Researches in the Lunar Theory," *American Journal of Mathematics*, vol. 1, no. 3, pp. 245–260, 1878.
- [17] W. H. Clohessy and R. S. Wiltshire, "Terminal Guidance System for Satellite Rendezvous," *Journal of the Aerospace Sciences*, vol. 27, no. 9, pp. 653–658, 674, September 1960.
- [18] W. H. Clohessy and R. S. Wiltshire, "Terminal Guidance System for Satellite Rendezvous," in *Institute of the Aerospace Sciences Summer Meeting*, no. 59-93, (Los Angeles, California), June 1959.
- [19] H. S. Seifert, ed., *Space Technology*, ch. 26-5, Satellite Rendezvous, pp. 26/28–26/29. New York, New York: John Wiley and Sons, Inc., 1959.

- [20] L. W. Spradlin, “The Long-Time Satellite Rendezvous Trajectory,” *Aerospace Engineering*, vol. 19, pp. 32–37, June 1960.
- [21] J. M. Eggleston, “Optimum Time to Rendezvous,” *ARS Journal*, vol. 30, pp. 1089–1091, November 1960.
- [22] F. T. Geyling, “Satellite Perturbation from Extra-Terrestrial Gravitation and Radiation Pressure,” *Journal of the Franklin Institute*, vol. 269, no. 5, pp. 375–407, 1960.
- [23] C. Sabol, R. Burns, and C. A. McLaughlin, “Satellite Formation Flying Design and Evolution,” *Journal of Spacecraft and Rockets*, vol. 38, no. 2, pp. 270–278, March–April 2001.
- [24] R. H. Vassar and R. B. Sherwood, “Formationkeeping for a Pair of Satellites in a Circular Orbit,” *Journal of Guidance, Control, and Dynamics*, vol. 8, no. 2, pp. 235–242, March–April 1985.
- [25] R. A. Howard, T. A. Lovell, and K. R. Horneman, “Collision Avoidance During Rendezvous via Relative Motion Approximation,” in *AAS/AIAA Astrodynamics Specialists Conference*, no. AAS 03-650, (Big Sky, Montana), August 3–7, 2003.
- [26] V. Kapila, A. G. Sparks, J. M. Buffington, and Q. Yan, “Spacecraft Formation Flying: Dynamics and Control,” *Journal of Guidance, Control, and Dynamics*, vol. 23, no. 3, pp. 561–564, May–June 2000.
- [27] S. M. Veres, S. B. Gabriel, D. Q. Mayne, and E. Rogers, “Analysis of Formation Flying Control for a Pair of Nanosatellites,” *Journal of Guidance, Control, and Dynamics*, vol. 25, no. 5, pp. 971–974, September–October 2002.
- [28] H.-H. Yeh, E. Nelson, and A. Sparks, “Nonlinear Tracking Control for Satellite Formations,” *Journal of Guidance, Control, and Dynamics*, vol. 25, no. 2, pp. 376–386, March–April 2002.
- [29] S. A. Schweighart and R. J. Sedwick, “High-Fidelity Linearized J_2 Model for Satellite Formation Flight,” *Journal of Guidance, Control, and Dynamics*, vol. 25, no. 6, pp. 1073–1080, November–December 2002.
- [30] J. A. Roberts and P. C. E. Roberts, “The Development of High Fidelity Linearized J_2 Models for Satellite Formation Flying Control,” in *AAS/AIAA Sapce Flight Mechanics Conference*, no. AAS 04-162, (Maui, Hawaii), February 8–12, 2004.

- [31] I. M. Ross, "Linearized Dynamic Equations for Spacecraft Subject to J2 Perturbations," *Journal of Guidance, Control, and Dynamics*, vol. 26, no. 4, pp. 657–659, July–August 2003.
- [32] T. A. Lovell, K. R. Horneman, S. G. Tragesser, and M. V. Tollefson, "A Guidance Algorithm for Formation Reconfiguration and Maintenance Based on the Perturbed Clohessy-Wiltshire Equations," in *AAS/AIAA Astrodynamics Specialists Conference*, no. AAS 03-649, (Big Sky, Montana), August 3–7, 2003.
- [33] D. Mishne, "Relative Formation Keeping of LEO Satellites Subject to Small Drag Differences," in *Proceedings of the AAS/AIAA Astrodynamics Specialists Conference*, no. AAS 01-455, (Quebec City, Quebec, Canada), July 30–August 2, 2001.
- [34] T. Carter and M. Humi, "Rendezvous Equations in a Central-Force Field with Linear Drag," *Journal of Guidance, Control, and Dynamics*, vol. 25, no. 1, pp. 74–79, January–February 2002.
- [35] T. Carter and M. Humi, "Clohessy-Wiltshire Equations Modified to Include Quadratic Drag," *Journal of Guidance, Control, and Dynamics*, vol. 25, no. 6, pp. 1058–1063, November–December 2002.
- [36] W. E. Wiesel, "Relative Satellite Motion About an Oblate Planet," *Journal of Guidance, Control, and Dynamics*, vol. 25, no. 4, pp. 776–785, July–August 2002.
- [37] T. E. Carter, "State Transition Matrices for Terminal Rendezvous Studies: Brief Survey and New Example," *Journal of Guidance, Control, and Dynamics*, vol. 21, no. 1, pp. 148–155, January–February 1998.
- [38] R. H. Battin, *An Introduction to the Mathematics and Methods of Astrodynamics, Revised Edition*. Reston, Virginia: American Institute of Aeronautics and Astronautics, 1999.
- [39] K. T. Alfriend, H. Schaub, and D.-W. Gim, "Gravitational Perturbations, Nonlinearity and Circular Orbit Assumption Effects on Formation Flying Control Strategies," in *Proceedings of the AAS Rocky Mountain Guidance and Control Conference*, no. AAS 00-012, (Breckenridge, Colorado), February 2–6, 2000.
- [40] J. L. Junkins, M. R. Akella, , and K. T. Alfriend, "Non-Gaussian Error Propagation in Orbital Mechanics," *Journal of the Astronautical Sciences*, vol. 44, no. 4, pp. 541–563, October–December 1996.

- [41] H. Schaub, S. R. Vadali, J. L. Junkins, and K. T. Alfriend, "Spacecraft Formation Flying Using Mean Orbit Elements," *Journal of the Astronautical Sciences*, vol. 48, no. 1, pp. 69–87, January–March 2000.
- [42] H. Schaub, "Spacecraft Relative Orbit Geometry Description Through Orbit Element Differences," in *Proceedings of the 14th U.S. National Congress of Theoretical and Applied Mechanics*, (Blacksburg, Virginia), June 23–28, 2002.
- [43] H. Schaub, "Incorporating Secular Drifts into the Orbit Element Difference Description of Relative Orbits," in *Proceedings of the 13th AAS/AIAA Spaceflight Mechanics Meeting*, no. AAS 03-115, (Ponce, Puerto Rico), February 9–13, 2003.
- [44] H. Schaub and K. T. Alfriend, "Hybrid Cartesian and Orbit Element Feedback Law for Formation Flying Spacecraft," *Journal of Guidance, Navigation and Control*, vol. 25, no. 2, pp. 387–393, March–April 2002.
- [45] D. A. Vallado, *Fundamentals of Astrodynamics and Applications*. El Segundo, California: Microcosm, Inc., 2001.
- [46] H. Schaub and K. T. Alfriend, " J_2 Invariant Relative Orbits for Spacecraft Formations," *Celestial Mechanics and Dynamical Astronomy*, vol. 79, pp. 77–95, 2001.
- [47] K. T. Alfriend and H. Schaub, "Dynamics and Control of Spacecraft Formations: Challenges and Some Solutions," *Journal of the Astronautical Sciences*, vol. 48, no. 2, pp. 249–267, April–September 2000.
- [48] S. R. Vadali, H. Schaub, and K. T. Alfriend, "Initial Conditions and Fuel-Optimal Control for Formation Flying of Satellites," in *Proceedings of the AIAA Guidance, Navigation and Control Conference*, no. AIAA 99-4265, (Portland, Oregon), August 9–12, 1999.
- [49] H. Schaub and K. T. Alfriend, "Impulsive Feedback Control to Establish Specific Mean Orbital Elements of Spacecraft Formations," *Journal of Guidance, Navigation and Control*, vol. 24, no. 4, pp. 739–745, August 2001.
- [50] S. S. Vaddi, K. T. Alfriend, and S. R. Vadali, "Sub-Optimal Formation Establishment and Reconfiguration Using Impulsive Thrust," in *Proceedings of the AAS/AIAA Astrodynamics Specialists Conference*, no. AAS 03-590, (Big Sky, Montana), August 3–7, 2003.
- [51] D.-W. Gim and K. T. Alfriend, "The State Transition Matrix of Relative Motion for the Perturbed Non-Circular Reference Orbit," in *Proceedings of the 12th*

- AAS/AIAA Spaceflight Mechanics Meeting*, no. AAS 01-222, (Santa Barbara, California), February 11–15, 2001.
- [52] M. E. Campbell, “Planning Algorithm for Large Satellite Clusters,” in *Proceedings of the AIAA Guidance, Navigation, and Control Conference*, no. AIAA 2002-4958, (Monterey, California), August 5–8, 2002.
 - [53] S. R. Vadali, S. S. Vaddi, and K. T. Alfriend, “An Intelligent Control Concept for Formation Flying Satellite Constellations,” *International Journal of Robust and Nonlinear Control*, vol. 12, no. 2-3, pp. 97–115, February–March 2002.
 - [54] R. W. Beard and F. Y. Hadaegh, “Fuel Optimization for Unconstrained Rotation of Spacecraft Formations,” *Journal of the Astronautical Sciences*, vol. 43, no. 3, pp. 259–273, July–December 1999.
 - [55] S. P. Hughes and C. D. Hall, “Optimal Configurations for Rotating Spacecraft Formations,” *Journal of the Astronautical Sciences*, vol. 48, no. 2–3, pp. 225–247, April–September 2000.
 - [56] S. P. Hughes and C. D. Hall, “Mission Performance Measures for Spacecraft Formation Flying,” in *Flight Mechanics Symposium*, (Greenbelt, Maryland), May 18–20, 1999.
 - [57] G. Inalhan, M. Tillerson, and J. P. How, “Relative Dynamics and Control of Spacecraft Formations in Eccentric Orbits,” *Journal of Guidance, Control, and Dynamics*, vol. 25, no. 1, pp. 48–59, January–February 2002.
 - [58] C. A. Bailey, T. W. McLain, and R. W. Beard, “Fuel-Saving Strategies for Dual Spacecraft Interferometry Missions,” *Journal of the Astronautical Sciences*, vol. 49, no. 3, pp. 469–488, July–September 2001.
 - [59] W. Kang and H.-H. Yeh, “Co-ordinated Attitude Control of Multi-Satellite Systems,” *International Journal of Robust and Nonlinear Control*, vol. 12, pp. 185–205, 2002.
 - [60] J. R. Lawton and R. W. Beard, “Synchronized Multiple Spacecraft Rotations,” *Automatica*, vol. 38, pp. 1359–1364, 2002.
 - [61] W. Rang, H.-H. Yeh, and A. Sparks, “Coordinated Control of Relative Attitude for Satellite Formation,” in *AIAA Guidance, Navigation, and Control Conference*, no. AIAA 2001-4093, (Montreal, Canada), August 6–9, 2001.

- [62] G. Q. Xing and S. A. Parvez, "Nonlinear Attitude State Tracking Control for Spacecraft," *Journal of Guidance, Control, and Dynamics*, vol. 24, no. 3, pp. 624–626, May–June 2001.
- [63] H. Pan and V. Kapila, "Adaptive Nonlinear Control for Spacecraft Formation Flying with Coupled Translational and Attitude Dynamics," in *Proceedings of the IEEE Conference on Decision and Control*, no. WeM11-6, (Orlando, Florida), pp. 2057–2062, December 2001.
- [64] M. C. VanDyke, "Decentralized Coordinated Attitude Control of a Formation of Spacecraft," Master's thesis, Virginia Polytechnic Institute and State University, Blacksburg, Virginia, 2004.
- [65] P. K. C. Wang and F. Y. Hadaegh, "Coordination and Control of Multiple Microspacecraft Moving in Formation," *Journal of the Astronautical Sciences*, vol. 44, no. 3, pp. 315–355, July–September 1996.
- [66] N. K. Philip and M. R. Ananthasayanam, "Relative Position and Attitude Estimation and Control Schemes for the Final Phase of an Autonomous Docking Mission of Spacecraft," *Acta Astronautica*, vol. 52, pp. 511–522, 2003.
- [67] D. Fragopoulos and M. Innocenti, "Autonomous Spacecraft 6DOF Relative Motion Control Using Quaternions and H-infinity Methods," in *Proceedings of the AIAA Guidance, Navigation and Control Conference*, no. AIAA 96-3725, (San Diego, California), July 29–31 1996.
- [68] D. C. Redding, B. A. Persson, and E. V. Bergmann, "Combined Solution of Spacecraft Rotational and Translational Maneuvers," in *Proceedings of the AIAA Guidance, Navigation, and Control Conference*, no. AIAA 86-2106, (Williamsburg, Virginia), pp. 441–451, August 18–20, 1986.
- [69] B. J. Naasz, M. M. Berry, H.-Y. Kim, and C. D. Hall, "Integrated Orbit and Attitude Control for a Nanosatellite with Power Constraints," in *Proceedings of the 13th AAS/AIAA Space Flight Mechanics Meeting*, (Ponce, Puerto Rico), February 9–12, 2003.
- [70] K. Yamanaka, "Simultaneous Translation and Rotation Control Law for Formation Flying Satellites," in *AIAA Guidance, Navigation, and Control Conference*, no. AIAA 2000-4440, (Denver, Colorado), August 14–17, 2000.
- [71] J. R. Carpenter, "A Preliminary Investigation of Decentralized Control for Satellite Formations," in *Proceedings of the IEEE Aerospace Conference*, (Big Sky, Montana), pp. 63–74, March 18–25, 2000.

- [72] J. R. Carpenter, "Decentralized Control of Satellite Formations," *International Journal of Robust and Nonlinear Control*, vol. 12, pp. 141–161, 2002.
- [73] J. R. Carpenter, "Partially Decentralized Control Architectures for Satellite Formations," in *Proceedings of the AIAA Guidance, Navigation and Control Conference*, no. AIAA 2002-4959, (Monterey, California), August 5–8, 2002.
- [74] J. R. T. Lawton, B. J. Young, and R. W. Beard, "A Decentralized Approach to Elementary Formation Maneuvers," in *Proceedings of the IEEE International Conference on Robotics and Automation*, (San Francisco, California), April 2000.
- [75] W. Ren and R. W. Beard, "Virtual Structure Based Spacecraft Formation Control with Formation Feedback," in *Proceedings of the AIAA Guidance, Navigation, and Control Conference*, no. AIAA 2002-4963, (Monterey, California), August 5–8, 2002.
- [76] R. W. Beard, J. Lawton, and F. Y. Hadaegh, "A Coordination Architecture for Spacecraft Formation Control," *IEEE Transactions on Control Systems Technology*, vol. 9, no. 6, pp. 777–790, November 2001.
- [77] W. Kang, A. Sparks, and S. Banda, "Coordinated Control of Multisatellite Systems," *Journal of Guidance, Control, and Dynamics*, vol. 24, no. 2, pp. 360–368, March–April 2001.
- [78] E. Nelson, A. Sparks, and W. Kang, "Coordinated Nonlinear Tracking Control for Satellite Formations," in *Proceedings of the AIAA Guidance, Navigation and Control Conference*, no. 2001-4025, (Montreal, Canada), August 6–9, 2001.
- [79] J. L. Schwartz, M. A. Peck, and C. D. Hall, "Historical Survey of Air-Bearing Spacecraft Simulators," *Journal of Guidance, Control, and Dynamics*, vol. 26, no. 4, pp. 513–522, July–August 2003.
- [80] K. E. Glover, "Development of a Large Support Surface for an Air-Bearing Type Zero-Gravity Simulator," Tech. Rep. NASA-TM-X-72780, April 1976.
- [81] H. Fornoff, "Final Report for Air Bearing Platform T50-2," Tech. Rep. NASA-CR-97588, October 1967.
- [82] S. Matunaga, K. Yoshihara, T. Takahashi, S. Tsurumi, and K. Ui, "Ground Experiment System for Dual-Manipulator-Based Capture of Damaged Satellites," in *Proceedings of the IEEE/RSJ International Conference on Intelligent Robots and Systems*, no. 92-4308, (Kagawa University, Takamatsu, Japan), pp. 1847–1852, October 30–November 5, 2000.

- [83] B. Pond and I. Sharf, "Experimental Demonstration of Flexible Manipulator Trajectory Optimization," in *Proceedings of the AIAA Guidance, Navigation, and Control Conference*, no. AIAA 99-4302, (Portland, Oregon), pp. 1869–1876, August 9–11, 1999.
- [84] J. L. Meyer, W. B. Harrington, B. N. Agrawal, and G. Song, "Application of piezoceramics to vibration suppression of a spacecraft flexible appendage," in *Proceedings of the AIAA Guidance, Navigation and Control Conference*, no. AIAA 96-3761, (San Diego, California), July 29–31, 1996.
- [85] M. G. Spencer, "Development of a Servicing Satellite Simulator," in *Proceedings of the AIAA Space Conference and Exposition*, no. AIAA 2001-4529, (Albuquerque, New Mexico), August 28–30, 2001.
- [86] H. Choset and D. Kortenkamp, "Path Planning and Control for Free-Flying Inspection Robot in Space," *Journal of Aerospace Engineering*, vol. 12, no. 2, pp. 74–81, April 1999.
- [87] Y. Toda, T. Iwata, K. Machida, A. Otuka, H. Toriu, Y. Shinomiya, Y. Fukuda, M. Asakura, and N. Matuhira, "Development of Free-Flying Space Telerobot, Ground Experiments on Two-Dimensional Flat Test Bed," in *Proceedings of the AIAA Guidance, Navigation and Control Conference*, no. AIAA 92-4308, (Hilton Head Island, South Carolina), pp. 33–39, August 10–12, 1992.
- [88] T. Corazzini, A. Robertson, J. C. Adams, A. Hassibi, and J. P. How, "Experimental Demonstration of GPS as a Relative Sensor for Formation Flying Spacecraft," *Navigation: Journal of the Institute of Navigation*, vol. 45, no. 3, pp. 195–207, Fall 1996.
- [89] M. O. Hilstad, "A Multi-Vehicle Testbed and Interface Framework for the Development and Verification of Separated Spacecraft Control Algorithms," Master's thesis, Massachusetts Institute of Technology, June 2002.
- [90] R. Kline-Schoder and J. D. Powell, "Experiments with the KITE Attitude Control Simulator," in *Proceedings of the 3rd International Conference on Tethers in Space-Toward Flight*, no. 89-1576, (San Francisco, California), pp. 205–214, May 17–19, 1989.
- [91] D. M. Meller, J. Reiter, M. Terry, K. F. Böhringer, and M. Campbell, "A Docking System for Microsatellites Based on MEMS Actuator Arrays," in *Proceedings of the AIAA/ASME/ASCE/AHS/ASC Structures, Structural Dynamics, and Materials Conference*, no. 2001-1504, (Seattle, Washington), April 16–19, 2001.

- [92] D. F. Wilcock, "Design and Performance of Gas Pressurized, Spherical Space-Simulator Bearings," *Journal of Basic Engineering (Transactions of the ASME)*, vol. 87, pp. 604–612, September 1965.
- [93] T. F. Yeh, "Viscous Torque in a Spherical Gas Bearing," *Journal of the Aerospace Sciences*, vol. 29, no. 2, pp. 160–161, February 1962.
- [94] J. S. White and J. S. Pappas, "General Considerations for Satellite Attitude Control Systems," in *Proceedings of the IAS 29th Annual Meeting*, no. 61-19, (New York, New York), January 23–25, 1961.
- [95] B. T. Bachofer and L. T. Seaman, "Air Bearing Dynamic Testing — One Arc Second Accuracy," in *Proceedings of the 1st AIAA Annual Meeting*, no. AIAA 64-205, (Washington, D.C.), June 29–July 2, 1964.
- [96] F. J. Moran and B. H. Dishman, "Air Bearing Table Mechanization and Verification of a Spacecraft Wide-Angle Attitude Control System," *Journal of Spacecraft*, vol. 7, no. 7, pp. 819–825, July 1970.
- [97] R. L. Peterson, "Air-Bearing Spin Facility for Measuring Energy Dissipation," Tech. Rep. NASA-TN-D-8346, October 1976.
- [98] S. S. F. de Cordova and D. B. DeBra, "Mass Center Estimation of a Drag-Free Satellite," in *Proceedings of the 6th Triennial World Congress of the International Federation of Automatic Control*, (Boston, Massachusetts), pp. 35.3 1–35.3 8, August 24–30, 1975.
- [99] G. A. Smith, "Dynamic Simulators for Test of Space Vehicle Attitude Control Systems," in *Proceedings of the Conference on the Role of Simulation in Space Technology, Part C*, (Blacksburg, Virginia), pp. XV-1–XV-30, August 17–21, 1964.
- [100] D. C. Fosth, "The Lunar Orbiter Attitude Control Simulator," *IEEE Transactions on Aerospace and Electronic Systems*, vol. AES-3, no. 3, pp. 417–423, May 1967.
- [101] W. A. Beaudry, "Simulation of a Flexible Spinning Vehicle," Tech. Rep. NASA-CR-123789, July 1972.
- [102] H. L. Mork and P. C. Wheeler, "Three-Axis Attitude Control System Air-Bearing Tests with Flexible Dynamics," in *Proceedings of the AIAA Guidance and Control Conference*, no. AIAA 73-866, (Key Biscane, Florida), August 20–22, 1973.
- [103] C. T. Cowen, "Precise Air Bearings Redesigned," *NASA Tech Briefs*, vol. 26, no. 11, pp. 48, 50, November 2002.

- [104] M. Romano and B. N. Agrawal, "Acquisition, tracking and pointing control of the Bifocal Relay Mirror spacecraft," in *Proceedings of the 53rd International Astronautical Congress of the International Astronautical Federation*, no. 02-A.4.05, (Houston, Texas), October 10–19, 2002.
- [105] B. N. Agrawal and R. E. Rasmussen, "Air Bearing Based Satellite Attitude Dynamics Simulator for Control Software Research and Development," in *Proceedings of the SPIE Conference on Technologies for Synthetic Environments: Hardware-in-the-Loop Testing VI*, (Orlando, Florida), pp. 204–214, April 16–18, 2001.
- [106] B. N. Agrawal, "Acquisition, Tracking, and Pointing of Bifocal Relay Mirror Spacecraft," in *Proceedings of the 13th AAS/AIAA Space Flight Mechanics Meeting*, no. AAS 03-151, (Ponce, Puerto Rico), February 9–13, 2003.
- [107] R. Thurber, "Dynamic Ground Simulation of Attitude Control Systems," in *Proceedings of the 35th AIAA Aerospace Sciences Meeting*, no. AIAA 97-0010, (Reno, Nevada), January 6–9, 1997.
- [108] R. R. Fullmer, "Dynamic ground testing of the Skipper Attitude Control System," in *Proceedings of the 34th AIAA Aerospace Sciences Meeting*, no. AIAA 96-0103, (Reno, Nevada), January 15–18, 1996.
- [109] C.-A. Brunet, J. de Lafontaine, and K. Schilling, *Engineering Education and Research 2002: A Chronicle of Worldwide Innovations*, ch. Tele-Education in Engineering Using a Virtual International Laboratory. iNEER (International Network for Engineering Education and Research), 2003 (to be published).
- [110] B. Kim, E. Velenis, P. Kriengsiri, and P. Tsiotras, "A Spacecraft Simulator for Research and Education," in *Proceedings of the AIAA/AAS Astrodynamics Specialists Conference*, no. AAS 01-367, (Quebec City, Quebec, Canada), pp. 897–914, July 30–August 2, 2001.
- [111] B. Kim, E. Velenis, P. Kriengsiri, and P. Tsiotras, "A Low-Cost Spacecraft Simulator for Research and Education," *IEEE Control Systems Magazine*, 2003 (to appear).
- [112] D. Jung and P. Tsiotras, "A 3-DoF Experimental Test-Bed for Integrated Attitude Dynamics and Control Research," in *Proceedings of the AIAA Guidance, Navigation and Control Conference*, (Austin, Texas), 2003.

- [113] D. M. Halsmer, A. R. Fetter, and M. C. Chidebelu-Eze, “Simulation Accuracy of an Apparatus to Test the Stability of Spinning Spacecraft Under Thrust,” in *Proceedings of the NASA Goddard Space Flight Center Flight Mechanics Symposium*, (Greenbelt, Maryland), May 19–21, 1997.
- [114] P. J. Richards, “A Liquid-Filled Projectile Simulator,” *Journal of Physics E: Scientific Instrumentation*, vol. 16, pp. 236–240, 1983.
- [115] A. Das, J. L. Berg, G. A. Norris, D. F. Cossey, T. J. Strange III, and W. T. Schlaegel, “ASTREX — A Unique Test Bed for CSI Research,” in *Proceedings of the 29th Conference on Decision and Control*, (Honolulu, Hawaii), pp. 2018–2023, December 1990.
- [116] F. Li, P. M. Bainum, N. G. Creamer, and S. Fisher, “Rapid Reorientation Maneuvers of Experimental Spacecraft with a Pendulum Appendage,” *Journal of Guidance, Control, and Dynamics*, vol. 21, no. 1, pp. 164–171, January–February 1998.
- [117] N. G. Creamer, G. Kirby, R. Weber, A. Bosse, and S. Fisher, “An Integrated GPS / Gyro / Smart Structures Architecture for Attitude Determination and Baseline Metrology,” in *Proceedings of the AIAA Guidance, Navigation, and Control Conference*, no. AIAA 98-4513, (Boston, Massachusetts), pp. 1945–1955, August 10–12, 1998.
- [118] R. E. Rasmussen, “Dynamic Test Platforms and Air Bearings.” <http://home.earthlink.net/~rermussen/dyntestab.htm>.
- [119] I. Rizos, J. Arbes, and J. C. Raoult, “A Spherical Air Bearing Supported Test Facility for Performance Testing of Satellite Attitude Control Systems,” in *Proceedings of the 4th International Federation of Automatic Control Symposium on Automatic Control in Space*, pp. 3.41–3.48, September 1971.
- [120] R. Unterberger and L. Schmieder, “Air-Bearing Facility for the Simulation of Spin-Stabilized Satellites,” in *Proceedings of the 6th International Gas Bearing Symposium*, (University of Southampton, England), pp. B2–9–B2–23, March 27–29, 1974.
- [121] S. W. Tonkin and W. J. Shackcloth, “Practical Test Behaviour of a Counterspun Compliant Flywheel Nutation Damper on a Spinning Prolate Body,” in *Proceedings of the AIAA Guidance and Control Conference*, no. AIAA 78-1312, pp. 490–497, 1978.

- [122] J. Prado and G. Bisacchi, "Dynamic Balancing for a Satellite Attitude Control Simulator," *Journal of the Mexican Society of Instrumentation*, vol. 4, no. 5, pp. 76–81, 1998.
- [123] W. C. Leite Filho, L. M. R. Mallaco, and D. S. Carrijo, "Hardware in the Loop Simulation of an Attitude Control System," in *Proceedings of the AIAA Modeling and Simulation Technologies Conference*, no. AIAA 99-4323, (Portland, Oregon), pp. 423–426, August 9–11, 1999.
- [124] J. Shen, N. H. McClamroch, and A. M. Bloch, "Local Equilibrium Controllability of the Triaxial Attitude Control Testbed," in *Proceedings of the 41st IEEE Conference on Decision and Control*, (Las Vegas, Nevada), pp. 528–533, December 2002.
- [125] S. Cho, J. Shen, N. H. McClamroch, and D. S. Bernstein, "Equations of Motion for the Triaxial Attitude Control Testbed," in *Proceedings of the 40th IEEE Conference on Decision and Control*, (Orlando, Florida), pp. 3429–3434, December 2001.
- [126] J. E. Colebank, R. D. Jones, G. R. Nagy, R. D. Pollak, and D. R. Mannebach, "SIMSAT: A Satellite Simulator and Experimental Test Bed for Air Force Research," in *Proceedings of the AIAA Space Technology Conference and Exposition*, no. AIAA 99-4428, (Albuquerque, New Mexico), September 28–30, 1999.
- [127] F. D. Roe, D. W. Mitchell, B. M. Linner, and D. L. Kelley, "Simulation Techniques for Avionics Systems — An Introduction to a World Class Facility," in *Proceedings of the AIAA Flight Simulation Technologies Conference*, no. AIAA 96-3535, (San Diego, California), pp. 535–543, July 29–31, 1996.
- [128] A. G. Ledebuhr, L. C. Ng, M. S. Jones, B. A. Wilson, R. J. Gaughan, E. F. Breitfeller, W. G. Taylor, J. A. Robinson, D. R. Antelman, and D. P. Neilsen, "Micro-Satellite Ground Test Vehicle for Proximity and Docking Operations Development," in *Proceedings of the IEEE Aerospace Conference*, (Big Sky, Montana), pp. 2493–2504, March 10–17, 2001.
- [129] C. A. Lindensmith, "Technology Plan for the Terrestrial Planet Finder," Tech. Rep. 03-007, Rev A, Jet Propulsion Laboratory, Pasadena, CA, March 7, 2003.
- [130] G. E. Riccio, "Understanding Skill in EVA Mass Handling Volume III: Empirical developments and conclusions," Tech. Rep. NASA-TP-3684, 1998.
- [131] J. Leitner, "A Hardware-in-the-Loop Testbed for Spacecraft Formation Flying Applications," in *Proceedings of the IEEE Aerospace Conference*, (Big Sky, Montana), pp. 2–615–2–620, March 10–17, 2001.

- [132] J. Leitner, F. Bauer, D. Folta, M. Moreau, R. Carpenter, and J. How, "Distributed Spacecraft Systems Develop New GPS Capabilities," *GPS World*, February 1, 2002.
- [133] F. Busse and J. How, "Real-time Experimental Demonstration of Precise Decentralized Relative Navigation for Formation Flying Spacecraft," in *AIAA Guidance, Navigation, and Control Conference*, (Monterey, California), August 5–8, 2002.
- [134] E. Gill, B. J. Naasz, and T. Ebinuma, "First Results from a Hardware-in-the-Loop Demonstration of Close-Loop Autonomous Formation Flying," in *AAS/AIAA Spaceflight Mechanics Conference*, no. AAS 03-040, (Breckenridge, Colorado), February 5–9, 2003.
- [135] J. R. Carpenter and E. R. Schiesser, "Semimajor Axis Knowledge and GPS Orbit Determination," *Navigation: The Journal of The Institute of Navigation*, vol. 48, no. 1, pp. 57–68, Spring 2001.
- [136] M. C. Moreau, P. Axelrad, J. L. Garrison, and A. Long, "GPS Receiver Architecture and Expected Performance for Autonomous Navigation in High Earth Orbits," *Navigation: The Journal of The Institute of Navigation*, vol. 47, no. 3, pp. 191–204, Fall 2000.
- [137] E. A. Olsen, C.-W. Park, and J. P. How, "3D Formation Flight Using Differential Carrier-Phase GPS Sensors," *Navigation: The Journal of The Institute of Navigation*, vol. 48, no. 1, pp. 35–48, Spring 1999.
- [138] F. D. Busse, J. P. How, and J. Simpson, "Demonstration of Adaptive Extended Kalman Filter for Low Earth Orbit Formation Estimation Using CDGPS," in *Proceedings of the Institute of Navigation GPS Meeting*, (Portland, Oregon), September 2002.
- [139] C. A. McLaughlin, C. Sabol, A. Swank, R. D. Burns, and K. Luu, "Modeling Relative Position, Relative Velocity, and Range Rate for Formation Flying," in *Proceedings of the AAS/AIAA Astrodynamics Specialists Conference*, no. AAS 01-457, (Quebec City, Quebec, Canada), July 30–August 2, 2001.
- [140] C.-W. Park, J. P. How, and L. Capots, "Sensing Technologies for Formation-Flying Spacecraft in LEO Using CDGPS and an Interspacecraft Communications System," *Navigation: The Journal of The Institute of Navigation*, vol. 49, no. 1, pp. 45–60, Spring 2002.

- [141] F. H. Bauer, K. Hartman, J. P. How, J. Bristow, D. Weidow, and F. Busse, "Enabling Spacecraft Formation Flying Through Spaceborne GPS and Enhanced Automation Technologies," in *Proceedings of the ION-GPS Conference*, (Nashville, Tennessee), September 15, 1999.
- [142] P. A. Stadter, A. A. Chacos, R. J. Heins, G. T. Moore, E. A. Olsen, M. S. Asher, and J. O. Bristow, "Confluence of Navigation, Communication, and Control in Distributed Spacecraft Systems," *AESS*, pp. 26–32, May 2002.
- [143] P. A. Stadter, G. R. Barrett, D. P. Watson, T. C. Esposito, and J. O. Bristow, "Autonomous Command and Control for Distributed Spacecraft Systems," in *NanoTech 2002 — At the Edge of Revolution*, no. AIAA 2002-5725, (Houston, Texas), September 9–12, 2002.
- [144] L. Meirovitch, *Methods of Analytical Dynamics*. McGraw-Hill Book Company, 1988. Originally published in 1970.
- [145] P. C. Hughes, *Spacecraft Attitude Dynamics*. John Wiley and Sons, 1986.
- [146] C. D. Hall, "AOE 4140 Spacecraft Dynamics and Control Lecture Notes." 2004.
- [147] W. T. Thompson, *Introduction to Space Dynamics*. Dover Publications, 1986. Originally published by John Wiley and Sons in 1961 and 1963.
- [148] S. Sastry, *Nonlinear Systems: Analysis, Stability, and Control*. New York: Springer-Verlag, 1999.
- [149] M. E. Pittelkau, "Kalman Filtering for Spacecraft System Alignment Calibration," *Journal of Guidance, Control, and Dynamics*, vol. 24, no. 6, pp. 1187–1195, November–December 2001.
- [150] M. D. Shuster, "A Survey of Attitude Representations," *The Journal of the Astronautical Sciences*, vol. 41, no. 4, pp. 439–517, October–December 1993.
- [151] Systron Donner Inertial Division, BEI Technologies, Inc., Concord, California, *MotionPak II Operating Manual*.
- [152] J. S. Bendat and A. G. Piersol, *Random Data: Analysis and Measurement Procedures*. Hoboken, New Jersey: Wiley-Interscience, April 1986.
- [153] D. C. Montgomery, G. C. Runger, and N. F. Hubele, *Engineering Statistics*. New York: John Wiley and Sons, 2001.

- [154] R. F. Stengel, *Optimal Control and Estimation*. New York, New York: Dover Publications, Inc., September 1994.
- [155] J. L. Crassidis and J. L. Junkins, *Optimal Estimation of Dynamic Systems*. Boca Raton, Florida: CRC Press, to be published 2004.
- [156] A. Gelb, ed., *Applied Optimal Estimation*. Cambridge, Massachusetts: The MIT Press, 1974.
- [157] E. J. Lefferts, F. L. Markley, and M. D. Shuster, “Kalman Filtering for Spacecraft Estimation,” *Journal of Guidance*, vol. 5, no. 5, pp. 417–427, September–October 1982.
- [158] M. D. Shuster, “The Quaternion in the Kalman Filter,” in *AAS*, no. AAS 93-553, pp. 25–37, 1993.
- [159] F. L. Markley, “Attitude Representations for Kalman Filtering,” in *AAS/AIAA Astrodynamics Specialists Conference*, no. AAS 01-309, (Quebec City, Quebec, Canada), July 30–August 2, 2001.
- [160] M. E. Pittelkau, “An Analysis of the Quaternion Attitude Determination Filter,” in *AAS/AIAA Space Flight Mechanics Meeting*, no. AAS 03-194, (Ponce, Puerto Rico), February 9–13, 2003.
- [161] M. D. Shuster, “Maximum Likelihood Estimation of Spacecraft Attitude,” *Journal of the Astronautical Sciences*, vol. 37, no. 1, pp. 79–88, January–March 1989.
- [162] M. D. Shuster, “A Simple Kalman Filter and Smoother for Spacecraft Attitude,” *Journal of the Astronautical Sciences*, vol. 37, no. 1, pp. 79–88, January–March 1989.
- [163] M. D. Shuster, “Kalman Filtering of Spacecraft Attitude and the QUEST Model,” *Journal of the Astronautical Sciences*, vol. 38, no. 3, pp. 377–393, July–September 1990.
- [164] F. L. Markley, “Attitude Error Representations for Kalman Filtering,” *Journal of Guidance, Control, and Dynamics*, vol. 26, no. 2, pp. 311–317, March 2003.
- [165] R. L. Farrenkopf, “Analytic Steady-State Accuracy Solutions for Two Common Spacecraft Attitude Estimators,” *Journal of Guidance*, vol. 1, no. 4, pp. 282–284, July–August 1978.

- [166] G. S. Agnes and J. Fulton, "Design and Testing of SIMSAT — A Three-Axis Satellite Dynamics Simulator," in *Proceedings of the 42nd AIAA/ASME/ASCE/AHS/ASC Structures, Structural Dynamics, and Materials Conference*, no. AIAA 01-1591, (Seattle, Washington), April 16–19, 2001.
- [167] V. J. Dabrowski and R. G. Cobb, "Experimental Demonstration of an Algorithm to Detect the Presence of a Parasitic Satellite," in *Proceedings of the AAS/AIAA Astrodynamics Specialists Conference*, no. AAS 03-610, (Big Sky, Montana), August 3–7, 2003.
- [168] M. G. Spencer, V. Chernesky, J. Baker, and M. Romano, "Bifocal Relay Mirror Experiments on the NPS Three Axis Spacecraft Simulator," in *Proceedings of the AIAA Guidance, Navigation, and Control Conference*, no. AIAA 02-5031, (Monterey, California), August 5–8, 2002.
- [169] J. Ahmed, V. T. Coppola, and D. S. Bernstein, "Adaptive Asymptotic Tracking of Spacecraft Attitude Motion with Inertia Matrix Identification," *Journal of Guidance, Control, and Dynamics*, vol. 21, no. 5, September/October 1998.
- [170] S. Tanygin and T. Williams, "Mass Property Estimation Using Coasting Maneuvers," *Journal of Guidance, Control, and Dynamics*, vol. 20, no. 4, pp. 625–632, July–August 1997.
- [171] M. A. Peck, "Estimation of Inertia Parameters for Gyrostats Subject to Gravity-Gradient Torques," in *Proceedings of the AAS/AIAA Astrodynamics Specialist Conference*, no. AAS 01-308, (Quebec City, Quebec, Cananda), July 30–August 2, 2001.
- [172] M. T. Carter, S. R. Vadali, and G. E. Chamitoff, "Parameter Identification for the International Space Station Using Nonlinear Momentum Management Control," in *Proceedings of the AIAA Guidance, Navigation, and Control Conference*, no. AIAA 97-3524, (New Orleans, Lousiana), pp. 252–262, August 11–13, 1997.
- [173] A. Y. Lee and J. A. Wertz, "In-Flight Estimation of the Cassini Spacecraft's Inertia Tensor," *Journal of Spacecraft and Rockets*, vol. 39, no. 1, pp. 153–154, January–February 2002.
- [174] C. Clemen, "New Method for On-Orbit-Determination of Parameters for Guidance, Navigation and Control," *Acta Astronautica*, vol. 51, no. 1–9, pp. 457–465, July 2002.

- [175] M. L. Psiaki, "Estimation of the Parameters of a Spacecraft's Attitude Dynamics Model Using Flight Data," in *Goddard Space Flight Center Flight Mechanics Symposium*, no. 36, (Greenbelt, Maryland), October 28–30, 2003.
- [176] M. A. Peck, "Uncertainty Models for Physically Realizable Inertia Dyadics," in *Goddard Space Flight Center Flight Mechanics Symposium*, no. 34, (Greenbelt, Maryland), October 28–30, 2003.
- [177] M. R. Akella, "Adaptive Control — A Departure from the Certainty-Equivalence Paradigm," in *Proceedings of the John L. Junkins Astrodynamics Symposium*, no. AAS 03-279, (College Station, Texas), May 23–24, 2003.
- [178] P. Ekyhoff, "Process Parameter and State Estimation," *Automatica*, vol. 4, pp. 205–233, 1968.
- [179] J. L. Schwartz and C. D. Hall, "Comparison of System Identification Techniques for a Spherical Air-Bearing Spacecraft Simulator," in *Proceedings of the AAS/AIAA Astrodynamics Specialist Conference*, no. AAS 03-611, (Big Sky, Montana), August 3–7, 2003.
- [180] J. L. Schwartz and C. D. Hall, "System Identification of a Spherical Air-Bearing Spacecraft Simulator," in *Proceedings of the AAS/AIAA Space Flight Mechanics Conference*, no. AAS 04-122, (Maui, Hawaii), February 8–12, 2004.
- [181] M. C. VanDyke, J. L. Schwartz, and C. D. Hall, "Unscented Kalman Filtering for Spacecraft Attitude State and Parameter Estimation," in *Proceedings of the AAS/AIAA Space Flight Mechanics Conference*, no. AAS 04-115, (Maui, Hawaii), February 8–12, 2004.
- [182] R. E. Kalman, "A New Approach to Linear Filtering and Prediction Problems," *Transactions of the ASME — Journal of Basic Engineering, D*, vol. 82, pp. 35–45, 1960.
- [183] R. E. Kalman and R. S. Bucy, "New Results in Linear Filtering and Prediction Theory," *Transactions of the ASME — Journal of Basic Engineering, D*, vol. 83, pp. 95–108, March 1961.
- [184] R. S. Bucy, "Nonlinear Filtering Theory," *IEEE Transactions on Automatic Control*, vol. AC-10, no. 2, p. 198, April 1965.
- [185] M. Athans, R. P. Wishner, and A. Bertolini, "Suboptimal State Estimation for Continuous-Time Nonlinear Systems from Discrete Noisy Measurements," *IEEE Transactions on Automatic Control*, vol. 13, no. 5, pp. 504–514, October 1968.

- [186] R. W. Bass, V. D. Norum, and L. Schwartz, “Optimal Multichannel Nonlinear Filtering,” *Journal of Mathematical Analysis and Applications*, vol. 16, pp. 152–164, 1966.
- [187] H. J. Kushner, “Dynamical Equations for Optimal Nonlinear Filtering,” *Journal of Differential Equations*, vol. 3, pp. 179–190, 1967.
- [188] H. J. Kushner, “Approximations to Optimal Non-Linear Filters,” in *Proceedings of the IEEE Joint Automatic Control Conference*, pp. 613–623, June 1967.
- [189] T. Lefebvre, H. Bruyninckx, and J. D. Schutter, “Kalman Filters for Nonlinear Systems: A Comparison of Performance,” Tech. Rep. 01R033, Department of Mechanical Engineering, Katholieke Universiteit, Leuven, Belgium, October 2001. Submitted as Regular Paper to IEEE Transactions on Automatic Control, October 2001.
- [190] S. J. Julier, J. K. Uhlmann, and H. F. Durrant-Whyte, “A New Approach for Filtering Nonlinear Systems,” in *Proceedings of the American Control Conference*, vol. 3, pp. 1628–1632, June 21–23 1995.
- [191] S. J. Julier and J. K. Uhlmann, “A General Method for Approximating Nonlinear Transformations of Probability Distributions,” tech. rep., Robotics Research Group, Department of Engineering Science, University of Oxford, 1994.
- [192] S. J. Julier and J. K. Uhlmann, “A New Extension of the Kalman Filter to Nonlinear Systems,” in *Proceedings of the SPIE AeroSense International Symposium on Aerospace/Defense Sensing, Simulation and Controls*, (Orlando, Florida), April 20–25, 1997.
- [193] S. J. Julier and J. K. Uhlmann, “A Non-divergent Estimation Algorithm in the Presence of Unknown Correlations,” in *Proceedings of the American Control Conference*, vol. 4, (Albuquerque, New Mexico), pp. 2369–2373, June 4–6, 1997.
- [194] S. J. Julier, “The Scaled Unscented Transformation,” in *Proceedings of the American Control Conference*, vol. 6, pp. 4555–4559, 2002.
- [195] T. Lefebvre, H. Bruyninckx, and J. D. Schutter, “A Non-Minimal State Kalman Filter for Nonlinear Parameter Estimation Applied to Autonomous Compliant Motion,” in *Proceedings of the IEEE International Conference on Robotics and Automation*, (Taipei, Taiwan), May 12–17, 2003.
- [196] M. Nørgaard, N. K. Poulsen, and O. Ravn, “Advances in Derivative-Free State Estimation for Nonlinear Systems,” Tech. Rep. IMM-REP-1998-15, Technical University of Denmark, 2800 Lyngby, Denmark, April 7, 2000.

- [197] M. Nørgaard, N. K. Poulsen, and O. Ravn, “New Developments in State Estimation for Nonlinear Systems,” *Automatica*, vol. 36, pp. 1627–1638, 2000.
- [198] T. S. Schei, “A Finite-Difference Method for Linearization in Nonlinear Estimation Algorithms,” *Automatica*, vol. 33, no. 11, pp. 2053–2058, 1997.
- [199] E. A. Wan and R. van der Merwe, “The Unscented Kalman Filter for Nonlinear Estimation,” in *Proceedings of the IEEE Symposium 2000: Adaptive Systems for Signal Processing, Communications, and Control*, (Lake Louise, Alberta, Canada), October 1–4, 2000.
- [200] E. A. Wan, R. van der Merwe, and A. T. Nelson, *Advances in Neural Information Processing Systems 12*, ch. Dual Estimation and the Unscented Transformation, pp. 666–672. Cambridge, Massachusetts: MIT Press, 2000.
- [201] R. van der Merwe and E. A. Wan, “Efficient Derivative-Free Kalman Filters for Online Learning,” in *Proceedings of European Symposium on Artificial Neural Networks*, (Bruges, Belgium), April 2001.
- [202] E. A. Wan and R. van der Merwe, *Kalman Filtering and Neural Networks*, ch. 7, The Unscented Kalman Filter. New York, New York: John Wiley and Sons, Inc., September 2001.
- [203] R. L. Bellaire, E. W. Kamen, and S. M. Zabin, “A New Nonlinear Iterated Filter with Applications to Target Tracking,” in *Proceedings of the International Society for Optical Engineering (SPIE) Conference on Signal and Data Processing of Small Targets*, vol. 2561, pp. 240–251, 1995.
- [204] D.-J. Lee and K. T. Alfriend, “Precise Real-Time Orbit Estimation Using the Unscented Kalman Filter,” in *Proceedings of the 13th AAS/AIAA Space Flight Mechanics Winter Meeting*, no. AAS 03-230, (Ponce, Puerto Rico), February 9–13, 2003.
- [205] J. L. Crassidis and F. L. Markley, “Unscented Filtering for Spacecraft Attitude Estimation,” *Journal of Guidance, Control, and Dynamics*, vol. 26, no. 4, July–August 2003.
- [206] A. T. Nelson, “Nonlinear Estimation and Modeling of Noisy Time-Series by Dual Kalman Filtering Methods,” Master’s thesis, Oregon Graduate Institute of Science and Technology, Department of Electrical and Computer Engineering, Beaverton, Oregon, September 2000.

- [207] E. A. Wan and A. T. Nelson, *Kalman Filtering and Neural Networks*, ch. 5, Dual Extended Kalman Filter Methods. New York, New York: John Wiley and Sons, Inc., September 2001.
- [208] S. Haykin, ed., *Kalman Filtering and Neural Networks*. New York, New York: John Wiley and Sons, Inc., 2001.
- [209] A. T. Nelson and E. A. Wan, “A Two-Observation Kalman Framework for Maximum-Likelihood Modelling of Noisy Time Series,” in *Proceedings of the IEEE International Joint Conference on Neural Networks*, pp. 2489–2494, 1998.
- [210] L. W. Nelson and E. Stear, “The Simultaneous On-Line Estimation of Parameters and States in Linear Systems,” *IEEE Transactions on Automatic Control*, vol. AC-21, no. 2, pp. 94–98, 1976.
- [211] E. A. Wan and A. T. Nelson, “Neural Dual Extended Kalman Filtering: Applications in Speech Enhancement and Monaural Blind Signal Separation,” in *Proceedings of the IEEE Workshop on Neural Networks for Signal Processing VII*, (Florida), September 1997.
- [212] E. A. Wan and A. T. Nelson, *Advances in Neural Information Processing Systems 9*, ch. Dual Kalman Filtering Methods for Nonlinear Prediction, Smoothing, and Estimation, pp. 793–799. MIT Press, 1997.
- [213] J. Genin, J. Hong, and W. Xu, “Accelerometer Placement for Angular Velocity Determination,” *Journal of Dynamics Systems, Measurement and Control*, vol. 119, no. 3, pp. 474–477, 1997.
- [214] G. S. Nusholtz, “Geometric Methods in Determining Rigid Body Dynamics,” *Experimental Mechanics*, vol. 33, no. 2, pp. 153–158, 1993.

Vita

Jana Lyn Schwartz was born to Sam and Lisa Schwartz on January 2, 1977 in Lafayette, Indiana. As is the case with many military brats, ninth grade was her eighth school. Jana graduated from the Thomas Jefferson High School for Science and Technology in 1995 and began her college education as an Archaeology major at Boston University. At that time, she had grand dreams of growing up to be Indiana Jones.

Jana transferred to Virginia Tech after just one semester, now pursuing Physics. However, after several semesters of assuming chickens to be spherical, she was again in need of a change. Jana transferred into the Department of Aerospace and Ocean Engineering and (finally) found her niche.

Jana earned her Bachelor's Degree in December 1999. She earned her Master's Degree in May 2002 and defended her PhD on July 7, 2004.

After graduation Jana is returning to Boston. She will be joining the Systems Engineering and Evaluation Directorate of The Charles Stark Draper Laboratory.

In her free time, Jana enjoys running, scuba diving, digital photography, and brewing her own beer.